

Design, development, and validation of a soft wearable robotic suit to assist human walking

Enrica Tricomi



UNIVERSITÄT
HEIDELBERG
ZUKUNFT
SEIT 1386

Design, development, and validation of a soft wearable robotic suit to assist human walking

Doctoral Dissertation

Faculty of Engineering Sciences

Heidelberg University, Germany

Degree of Doctor of Engineering (Dr.-Ing)

Author: M.Sc. Enrica Tricomi

Supervisor: Prof. Dr. Lorenzo Masia

Year: 2025

Design, development, and validation of a soft wearable robotic suit to assist human walking

Author: Enrica Tricomi

Supervisor: Prof. Dr. Lorenzo Masia

Declaration

I hereby declare that I have written the submitted dissertation "Design, development, and validation of a soft wearable robotic suit to assist human walking" myself and have not used any sources or assistance other than those expressly designated by me. I declare that I have not applied for an examination procedure at any other institution or that I have already used the dissertation in this or any other form elsewhere as an examination paper or submitted it to another faculty as a dissertation.

Heidelberg, 06/12/2024
Place and date



Enrica Tricomi

List of awards, scientific publications, and patent applications

Awards

- **IEEE Robotics and Automation Society 2024 Distinguished Student Leadership Award**, awarded to **Enrica Tricomi** at the IEEE RAS International Conference on Robotics and Automation 40th Anniversary (ICRA40), Rotterdam, The Netherlands, September 2024, for the outstanding contributions as the Student Activities Committee Chair and the Administrative Committee Student Representative of IEEE RAS.

- **Best Late Breaking Result Award**, at the TUM Geriatronics Summit, Garmisch Partenkirchen, Germany, June 2024.
  Paper **Tricomi** et al. "*Enhancing Walking Efficiency in Older Adults with a Soft Wearable Hip Exosuit.*"

- **Best Late Breaking Result Award**, at the 16th International Workshop on Human-Friendly Robotics, Munich, Germany, September 2023.
  Paper **Tricomi** et al. "*Environment-based Assistance Modulation for a Hip Exosuit via Computer Vision.*"

- **Best Paper Award**, at the Workshop on Computer Vision for Wearable Robotics, IEEE RAS International Conference on Robotics and Automation (ICRA), London, UK, April 2023.
  Paper **Tricomi** et al. "*Adapting Walking Assistance in Soft Exosuits According to Path Recognition via Computer Vision.*"

- **Finalist for the Best IEEE Robotics and Automation Letter (RAL) Paper Award**, at the IEEE 9th International Conference on Biomedical Robotics and Biomechatronics (Biorob), Seoul, South Korea, August 2022.
  Paper **Tricomi**† and Zhang† et al. "*Enhancing gait assistance control robustness of a hip exosuit by means of machine learning.*"

Journal papers (first author contributions)

- **E. Tricomi**, G. Piccolo[†1], F. Russo[†1], X. Zhang, F. Missiroli, S. Ferrari, L. Gionfrida, F. Ficuciello, M. Xiloyannis and L. Masia, "*Leveraging geometric modeling-based computer vision for context aware control in a hip exosuit*", **accepted at IEEE Transactions on Robotics**, 2024.
- **E. Tricomi**, F. Missiroli[†1], M. Xiloyannis[†1], N. Lotti, X. Zhang, M. Stefanakis, M. Theisen, J. Bauer, C. Becker, and L. Masia. "*Soft robotic shorts improve outdoor walking efficiency in older adults*", **Nature Machine Intelligence**, 2024.
- **E. Tricomi**, M. Mossini, F. Missiroli, N. Lotti, X. Zhang, M. Xiloyannis, L. Roveda, and L. Masia, "*Environment-based assistance modulation for a hip exosuit via computer vision*", **IEEE Robotics and Automation Letters**, 2023.
- **E. Tricomi**[†1], X. Zhang[†1], F. Missiroli, N. Lotti, C. Bokranz, D. Nicklas, and L. Masia, "*Enhancing gait assistance control robustness of a hip exosuit by means of machine learning*", **IEEE Robotics and Automation Letters**, 2022.
- **E. Tricomi**, N. Lotti, F. Missiroli, X. Zhang, M. Xiloyannis, T. Müller, S. Crea, E. Papp, J. Krzywinski, N. Vitiello, and L. Masia "*Underactuated soft hip exosuit based on adaptive oscillators to assist human locomotion*", **IEEE Robotics and Automation Letters**, 2021.

[1]These authors contributed equally to this work.

Journal papers (other)

- A. Ciaramella[†1], T. Bagneschi[†1], **E. Tricomi**, F. Missiroli, X. Zhang, A. Frisoli, and L. Masia, "*Design and Overground Testing of a Portable Hip Exosuit for Enhancing Running Efficiency*". **IEEE Transactions on Medical Robotics and Bionics**, 2024.

- X. Zhang, **E. Tricomi**, X. Ma, M.G. Correa, A. Ciaramella, F. Missiroli, L. Mišković, H. Su, and L. Masia, "*A lower limb wearable hip exosuit for improved sitting, standing, and walking efficiency*". **IEEE Transactions on Robotics**, 2024.

- L. Mišković, **E. Tricomi**, X. Zhang, F. Missiroli, K. Krstanović, T. Petrič, L. Masia, "*Hybrid Rigid-Soft and Pneumatic-Electromechanical Exoskeleton for Multi-joint Lower Limb Assistance*". **IEEE Transactions on Medical Robotics and Bionics**, 2024.

- N. Lotti[†1], F Missiroli[†1], E. Galofaro, **E. Tricomi**, D. Di Domenico, M. Semprini, M. Casadio, G. Brichetto, L. De Michieli, A. Tacchino, and L. Masia "*Soft robotics to enhance upper limb endurance in individuals with multiple sclerosis*". **Soft Robotics**, vol. 11, no. 2, pp. 338-346, 2024.

- F. Missiroli, P. Mazzoni, N. Lotti, **E. Tricomi**, F. Braghin, L. Roveda, and L. Masia. "*Integrating Computer Vision in Exosuits for Adaptive Support and Reduced Muscle Strain in Industrial Environments*". **IEEE Robotics and Automation Letters**, 2023.

- X. Zhang, **E. Tricomi**, F. Missiroli, N. Lotti, C. Bokranz, D. Nicklas, and L. Masia, "*Real-time assistive control via IMU locomotion mode detection in a soft exosuit: an effective approach to enhance walking metabolic efficiency*", **IEEE/ASME Transactions on Mechatronics**, 2024

- F. Missiroli, N. Lotti, **E. Tricomi**, C. Bokranz, R. Alicea, M. Xiloyannis, J. Krzywinski, S. Crea, N. Vitiello, and L. Masia. "*Rigid, soft, passive, and active: A hybrid occupational exoskeleton for bimanual multijoint assistance*", **IEEE Robotics and Automation Letters**, 2022.

[1]These authors contributed equally to this work.

Conference proceedings

- L. Mišković, **E. Tricomi**, X. Zhang, F. Missiroli, K. Krstanović, T. Petrič, L. Masia, Coupling Rigid Pneumatic Knee Exoskeleton with Soft Tendon-Driven Hip Exosuit: First Insights, 2024 10th IEEE RAS/EMBS International Conference for Biomedical Robotics and Biomechatronics (BioRob), Heidelberg, Germany, Sept 2024.

- V. Gerhard, L. Mišković, A. Nanni, **E. Tricomi**, F. Missiroli, L. Palmerini, L. Chiari, L. Masia, Design of a High Bandwidth Actuation for Seamless Assistance in Walking and Running, 2024 10th IEEE RAS/EMBS International Conference for Biomedical Robotics and Biomechatronics (BioRob), Heidelberg, Germany, Sept 2024.

- **E. Tricomi**, X. Zhang, F. Missiroli, and L. Masia, "*Enhancing Walking Efficiency in Older Adults with a Soft Wearable Hip Exosuit*", TUM Geriatronics Summit, Garmisch Partenkirchen, Germany, June 2024. (**Best Late Breaking Result Award**)

- **E. Tricomi**, M. Mossini, F. Missiroli, N. Lotti, **X. Zhang**, M. Xiloyannis, L. Roveda, and L. Masia, "*Environment-based assistance modulation for a hip exosuit via computer vision*", 16th International Workshop on Human-Friendly Robotics, Munich, Germany, Sept. 2023. (**Best Late Breaking Result Poster Award**)

- X. Zhang, **E. Tricomi**, F. Missiroli, N. Lotti, and L. Masia, "*Improving walking assistance efficiency in real-world scenarios with soft exosuits using locomotion mode detection*", 2023 IEEE International Conference on Rehabilitation Robotics (ICORR), Singapore, Sept. 2023. (**1st Best Student Paper Award**)

- **E. Tricomi**, M. Mossini, F. Missiroli, N. Lotti, X. Zhang, M. Xiloyannis, L. Roveda, and L. Masia, "*Adapting walking assistance in soft exosuits according to path recognition via computer vision*", Workshop on Computer Vision for Wearable Robotics, 2023 IEEE RAS International Conference on Robotics and Automation (ICRA), London, UK, May, 2023. (**Best Paper Award**)

- N. Lotti, **E. Tricomi**, F. Missiroli, X. Zhang, and L. Masia, "*Machine learning techniques in soft robotic suits for whole body assistance*", In 2022

IEEE Intl Conf on Dependable, Autonomic and Secure Computing, Intl Conf on Pervasive Intelligence and Computing, Intl Conf on Cloud and Big Data Computing, Intl Conf on Cyber Science and Technology Congress (DASC/PiCom/CBDCom/CyberSciTech), Sept. 2022.

- **E. Tricomi**[†1], X. Zhang[†1], F. Missiroli, N. Lotti, C. Bokranz, D. Nicklas, and L. Masia, "*Enhancing gait assistance control robustness of a hip exosuit by means of machine learning*", 2022 9th IEEE RAS/EMBS International Conference on Biomedical Robotics and Biomechatronics (BioRob), Seoul, Korea, Aug. 2022. (**Finalist of the Best IEEE RAL Paper Award**)

[1]These authors contributed equally to this work.

Patent applications

- **E. Tricomi**, L. Masia, F. Missiroli, L. Lotti, "*Assistance system for walking assistance, computer-implemented method for controlling an assistance system, and corresponding non-transitory computer readable storage medium*", WO 2024/160839 A1, 2024.

Authorship attribution statement

This thesis includes contents from five manuscripts and one patent application, all published in peer-reviewed journals where I am the first and corresponding author.

The research presented in this work was conducted at the Institute of Computer Engineering (ZITI) at Heidelberg University, under the technical supervision of Prof. Dr. Lorenzo Masia.

Chapter 3 is based on the contents related to the hardware design of the soft robotic suits, as detailed on the patent application and the five journal papers.

Chapter 4 is based on the following manuscripts:

- **E. Tricomi**, N. Lotti, F. Missiroli, X. Zhang, M. Xiloyannis, T. Müller, S. Crea, E. Papp, J. Krzywinski, N. Vitiello, and L. Masia "*Underactuated soft hip exosuit based on adaptive oscillators to assist human locomotion*", **IEEE Robotics and Automation Letters**, 2021.

  Authors' contribution:

  – Design of the soft robotic suit — ET, XZ, FM, NL, and LM
  – Implementation of the controller — ET and LM
  – Experimental study and data analysis — ET, FM, NL, XZ, and LM
  – Manuscript preparation — ET, and LM
  – Results interpretation, review and feedback all authors

- **E. Tricomi**[†] and X. Zhang[†], F. Missiroli, N. Lotti, C. Bokranz, D. Nicklas, and L. Masia, "*Enhancing gait assistance control robustness of a hip exosuit by means of machine learning*", **IEEE Robotics and Automation Letters**, 2022.

  Authors' contribution:

  – Design of the soft robotic suit — ET, XZ, FM, NL, and LM
  – Implementation of the Adaptive Oscillators controller — ET, and LM
  – Implementation of the Machine Learning controller — XZ, ET and LM
  – Experimental study and data analysis — ET and XZ, DN, and LM
  – Manuscript preparation — ET and XZ, and LM
  – Results interpretation, review and feedback all authors

Chapter 5 is based on the following manuscripts:

- **E. Tricomi**, M. Mossini, F. Missiroli, N. Lotti, X. Zhang, M. Xiloyannis, L. Roveda, and L. Masia, "*Environment-based assistance modulation for a hip*

exosuit via computer vision", **IEEE Robotics and Automation Letters**, 2023.

Authors' contribution:

– Design of the soft robotic suit	– ET, XZ, FM, and LM
– Implementation of the vision-based controller	– ET, MM, and LM
– Experimental study and data analysis	– ET, MM, and LM
– Manuscript preparation	– ET and LM
– Results interpretation, review and feedback	all authors

- **E. Tricomi**, G. Piccolo†, F. Russo†, X. Zhang, F. Missiroli, S. Ferrari, L. Gionfrida, F. Ficuciello, M. Xiloyannis and L. Masia, "*Leveraging geometric modeling-based computer vision for context aware control in a hip exosuit*", **Accepted at IEEE Transactions on Robotics**, 2024.

  Authors' contribution:

– Design of the soft robotic suit	– ET, XZ, FM, and LM
– Implementation of the vision-based controller	– ET, GP, FR, and LM
– Experimental study and data analysis	– ET, GP, FR, and LM
– Manuscript preparation	– ET and LM
– Results interpretation, review and feedback	all authors

Chapter 6 and **Chapter 7** are based on the following manuscript:

- **E. Tricomi**, F. Missiroli†, M. Xiloyannis†, N. Lotti, X. Zhang, M. Stefanakis, M. Theisen, J. Bauer, C. Becker, and L. Masia. "*Soft robotic shorts improve outdoor walking efficiency in older adults*". **Nature Machine Intelligence** pp. 1-11, 2024.

  Authors' contribution:

– Design of the soft robotic suit	– ET, XZ, FM, and LM
– Implementation of the controller	– ET, NL and LM
– Experimental study and data analysis	– ET, FM, MS, MX, MT, and LM
– Manuscript preparation	– ET and LM
– Results interpretation, review and feedback	all authors

Heidelberg, 06/12/2024 — Enrica Tricomi

Place and date

"*Cu nesci, arrinesci.*" [1]

A Papà, Mamma, Virginia, e Pietro
A Nonna Tina

[1]Old Sicilian proverb conveying the idea that stepping outside one's comfort zone and taking risks often brings rewarding results. Literally translated: "He who leaves, succeeds."

Abstract

The 21st century witnesses significant advancements in wearable assistive robotics, shifting from rigid exoskeletons to flexible, soft robotic suits. These suits, being clothing-like devices, better align with the body's natural biomechanics, offering enhanced comfort, efficiency, and adaptability. However, challenges remain in balancing support, energy efficiency, and real-world readiness.

This thesis aims to address these challenges by developing a wearable soft robotic suit designed to assist walking for both healthy individuals and those with mobility decline, with older adults as a key use case. The research has two objectives: (1) Technological development: designing a lightweight, portable device that minimizes sensory input and calibration, providing a simple, plug-and-play solution. The focus is on hip flexion assistance, a critical movement for walking, especially for frail individuals with weakened hip flexors due to aging; and (2) Real-world assessment: evaluating the device's effectiveness in healthy individuals and later in frail older adults, to assess its potential in dynamic, everyday environments.

The thesis hypothesizes that a tendon-driven, lightweight design can balance efficiency, portability, and comfort across diverse users. Two actuation configurations are explored: an underactuated single-motor system and a fully actuated dual-motor system for bilateral assistance. The research also posits that a control system using minimal sensory input, such as inertial sensors, can adapt dynamically to gait cadence and, as an add-on, leveraging computer vision for context-aware control can effectively modulate assistance across environments. Ultimately, it is hypothesized that this soft robotic suit can enhance metabolic efficiency, maintain natural gait patterns, and support user autonomy.

Beyond the hardware design, a significant contribution of this thesis is the development of advanced control strategies to ensure synchronization with the user's natural gait.

Initial development focuses on laboratory testing, exploring dynamic gait phase estimation using an Adaptive Oscillator (AOs)-based controller relying on inertial sensors. This approach works well in controlled settings but faces limitations related to delayed responses during abrupt gait transitions, such as cadence changes or starting from a standstill. To improve performance, a machine learning (ML)-augmented AOs controller is introduced in a sub-study, enabling dynamic adjustments during transitions.

A key innovation of this thesis, beyond gait cadence adaptation, is the integration of computer vision for context-aware modulation. While most current assistive devices are optimized for level walking, the controller of the device can integrate computer vision to analyze environmental features, such as terrain variations (e.g., slopes, stairs, or flat ground), to dynamically adjust the level of assistance. This contextual awareness enables the system to more effectively respond to real-world challenges, significantly enhancing its adaptability, versatility, and efficiency, marking a major advancement in wearable assistive robotics.

The transition from laboratory testing to real-world applications highlights, however, the need for a more streamlined control strategy. The complexities of dynamic environments informs the development of a simplified, high-performance control system that eliminates the need for dynamic models or machine learning. The improved controller employs a phase portrait-based approach, estimating gait phases from raw motion data, computing the angular separation between position and velocity vectors in the hip phase portrait. This refinement enhances the system's effectiveness in outdoor settings and sets the stage for trials with both fit and frail individuals.

The real-world applicability of the soft robotic suit is assessed through field tests, starting with young, fit individuals hiking outdoor. The suit demonstrates an average 17.79% reduction in metabolic cost of transport, improving efficiency without disrupting natural gait. These results are indicative of the suit's ability to augment walking in physically demanding activities in unstructured environments, a challenge for many systems designed for controlled settings. The suit also preserves the user's sense of agency, being both effective and intuitive to use.

Finally, the soft robotic suit is tested in older adults, showing an average 10.48% reduction in metabolic cost of transport during outdoor walking tasks on flat ground. This is particularly significant for frail individuals, who often experience reduced walking efficiency and increased fatigue with age.

The overall results demonstrate the suit's potential to effectively assist walking while maintaining natural gait patterns. These findings suggest the possibility of improving mobility and reducing fatigue for both fit and frail users.

Zusammenfassung

Das 21. Jahrhundert ist Zeuge bedeutender Fortschritte in der tragbaren Hilfsrobotik, die sich von starren Exoskeletten zu flexiblen, weichen Roboteranzügen entwickelt hat. Diese Anzüge, die wie Kleidung aussehen, passen sich besser an die natürliche Biomechanik des Körpers an und bieten mehr Komfort, Effizienz und Anpassungsfähigkeit. Es bleibt jedoch eine Herausforderung, ein Gleichgewicht zwischen Unterstützung, Energieeffizienz und Praxistauglichkeit herzustellen.

Diese Arbeit zielt darauf ab, diese Herausforderungen zu bewältigen, indem ein tragbarer weicher Roboteranzug entwickelt wird, der sowohl gesunde Personen als auch Personen mit eingeschränkter Mobilität beim Gehen unterstützen soll, wobei ältere Erwachsene einen wichtigen Anwendungsfall darstellen. Die Forschung verfolgt zwei Ziele: (1) Technologische Entwicklung: Entwurf eines leichten, tragbaren Geräts, das den sensorischen Input und die Kalibrierung minimiert und eine einfache Plug-and-Play-Lösung bietet. Der Schwerpunkt liegt auf der Unterstützung der Hüftbeugung, einer entscheidenden Bewegung beim Gehen, insbesondere für gebrechliche Personen mit altersbedingt geschwächten Hüftbeugern; und (2) Bewertung in der realen Welt: Bewertung der Wirksamkeit des Geräts bei gesunden Personen und später bei gebrechlichen älteren Erwachsenen, um sein Potenzial in dynamischen, alltäglichen Umgebungen zu bewerten.

Die These lautet, dass ein sehnengetriebenes, leichtes Design Effizienz, Tragbarkeit und Komfort für verschiedene Benutzer in Einklang bringen kann. Es werden zwei Antriebskonfigurationen untersucht: ein untermotorisiertes einmotoriges System und ein vollständig angetriebenes zweimotoriges System für bilaterale Unterstützung. Die Forschung geht auch davon aus, dass sich ein Steuerungssystem mit minimalen sensorischen Eingaben, wie z. B. Trägheitssensoren, dynamisch an die Gangkadenz anpassen kann, und dass die Nutzung von Computer Vision für eine kontextbezogene Steuerung die Unterstützung in verschiedenen Umgebungen effektiv modulieren kann. Letztendlich wird angenommen, dass dieser weiche Roboteranzug die Stoffwechseleffizienz verbessern, natürliche Gangmuster beibehalten und die Autonomie des Benutzers unterstützen kann.

Über das Hardware-Design hinaus besteht ein wesentlicher Beitrag dieser Arbeit in der Entwicklung fortschrittlicher Kontrollstrategien, um die Synchronisation mit dem natürlichen Gang des Benutzers zu gewährleisten.

Die anfängliche Entwicklung konzentriert sich auf Labortests, bei denen die dy-

namische Gangphasenschätzung mit einem auf Trägheitssensoren basierenden Controller auf der Grundlage eines adaptiven Oszillators (AOs) untersucht wird. Dieser Ansatz funktioniert in kontrollierten Umgebungen gut, stößt aber bei abrupten Gangwechseln, wie z. B. bei Trittfrequenzänderungen oder beim Starten aus dem Stand, auf Einschränkungen, die mit verzögerten Reaktionen zusammenhängen. Um die Leistung zu verbessern, wird in einer Teilstudie ein AOs-Controller mit maschinellem Lernen (ML) eingeführt, der dynamische Anpassungen bei Übergängen ermöglicht.

Eine Schlüsselinnovation dieser Arbeit, die über die Anpassung der Schrittfrequenz hinausgeht, ist die Integration von Computer Vision für eine kontextabhängige Modulation. Während die meisten aktuellen Hilfsmittel für gleichmäßiges Gehen optimiert sind, kann der Controller des Geräts Computer Vision integrieren, um Umgebungsmerkmale wie Geländevariationen (z. B. Steigungen, Treppen oder flacher Boden) zu analysieren und den Grad der Unterstützung dynamisch anzupassen. Durch dieses kontextbezogene Bewusstsein kann das System effektiver auf reale Herausforderungen reagieren, was seine Anpassungsfähigkeit, Vielseitigkeit und Effizienz erheblich steigert und einen wichtigen Fortschritt in der tragbaren Hilfsrobotik darstellt.

Der Übergang von Labortests zu realen Anwendungen macht jedoch deutlich, dass eine schlankere Kontrollstrategie erforderlich ist. Die Komplexität dynamischer Umgebungen hat zur Entwicklung eines vereinfachten Steuerungssystems geführt, das dynamische Modelle oder maschinelles Lernen überflüssig macht.

Die verbesserte Steuerung verwendet einen auf dem Phasenporträt basierenden Ansatz, bei dem die Gangphasen aus den rohen Bewegungsdaten geschätzt werden und der Winkelabstand zwischen Positions- und Geschwindigkeitsvektoren im Hüftphasenporträt berechnet wird. Diese Verfeinerung erhöht die Effektivität des Systems im Freien für Versuche mit fitten und gebrechlichen Personen.

Die reale Anwendbarkeit des weichen Roboteranzugs wird durch Feldtests bewertet, beginnend mit jungen, fitten Personen, die im Freien wandern. Der Anzug zeigt eine durchschnittliche Reduzierung der metabolischen Transportkosten um 17.79% und verbessert die Effizienz, ohne den natürlichen Gang zu beeinträchtigen. Diese Ergebnisse zeigen, dass der Anzug das Gehen bei körperlich anspruchsvollen Aktivitäten in unstrukturierten Umgebungen unterstützen kann - eine Herausforderung für viele Systeme, die für kontrollierte Umgebungen entwickelt wurden. Der Anzug bewahrt auch die Selbstständigkeit des Benutzers und ist sowohl effek-

tiv als auch intuitiv zu bedienen.

Schließlich wurde der weiche Roboteranzug an älteren Erwachsenen getestet und zeigte eine durchschnittliche Verringerung der metabolischen Transportkosten beim Gehen im Freien auf flachem Boden um 10.48%. Dies ist vor allem für gebrechliche Personen von Bedeutung, die mit zunehmendem Alter oft eine geringere Gehleistung und zunehmende Ermüdung aufweisen.

Die Gesamtergebnisse zeigen, dass der Anzug das Gehen wirksam unterstützen kann, wobei das natürliche Gangbild erhalten bleibt. Diese Ergebnisse deuten auf die Möglichkeit hin, die Mobilität zu verbessern und Ermüdungserscheinungen sowohl bei fitten als auch bei gebrechlichen Nutzern zu verringern.

Contents

Declaration **I**

List of awards, scientific publications, and patent applications **III**

Authorship attribution statement **IX**

Abstract **XIII**

Zusammenfassung **XV**

List of Figures **XXIII**

List of Tables **XXV**

Notations **XXVII**

1 Introduction **1**

1.1 Gait in aging and disease 2

1.2 Research motivation and aims 4

1.2.1 General hypotheses 4

1.3 Thesis outline 5

2 On the evolution of wearable assistive robotics **7**

2.1 The origin and early developments 7

2.2 The 21st century: walking with robotics 10

2.2.1 From rigid exoskeletons to soft robotic suits 12

2.3 Research gap and open challenges 14

3 Suit design motivation and principles **17**

3.1 The hip joint 17

3.1.1 The impact of aging 18

3.2 Design requirements 19

3.2.1 Motivations behind a tendon-driven design 20

3.3 Hardware design of the soft robotic suit . . . 21
3.3.1 Textile interface . . . 23
3.3.2 Actuation . . . 25
3.3.3 Control unit and sensing . . . 27
3.4 Outline of the control framework: requirements and generalizability 28
3.4.1 Generalizability of the control framework . . . 31

4 Adaptive controller to support leg swinging 35

4.1 The leg as a dynamic oscillator . . . 36
4.2 AOs-based real-time control framework . . . 37
4.2.1 High-level controller: gait phase estimator . . . 38
4.2.2 Mid-level controller . . . 40
4.2.3 Low-level controller . . . 40
4.3 Evaluation and effects on human movements . . . 41
4.3.1 Experimental protocol and data collection . . . 41
4.3.2 Data analysis . . . 42
4.3.3 Results . . . 43
4.4 Discussion . . . 47
4.5 Increasing controller robustness via learning . . . 49
4.5.1 ML-augmented controller . . . 50
4.5.2 Experimental assessment . . . 53
4.5.3 Results . . . 56
4.5.4 Discussion . . . 58
4.6 Conclusions . . . 60

5 Introducing context awareness to wearable assistive robotics 61

5.1 Exploring the surroundings through vision . . . 62
5.2 Context-aware controller . . . 64
5.2.1 High-level controller . . . 64
5.2.2 Mid-level controller . . . 76
5.2.3 Low-level controller . . . 77
5.3 Performance evaluation and human experiments . . . 78
5.3.1 Experimental protocol . . . 78
5.3.2 Data analysis . . . 79
5.3.3 Results . . . 82

5.4 Discussion 87

6 From the laboratory to the real-world: a hiking study 93

6.1 Out of the lab, into the field 94

6.2 Phase portrait-based control framework 95

6.2.1 High-level controller 96

6.2.2 Mid-level controller 99

6.2.3 Low-level controller 100

6.3 Technology assessment on hiking trail 100

6.3.1 Experimental Protocol 100

6.3.2 Data analysis 102

6.4 Results 104

6.5 Discussion 105

7 Enhancing walking efficiency in older adults 111

7.1 The age of aging 112

7.2 Efficacy study with older adults 113

7.2.1 Experimental protocol 113

7.2.2 Data analysis and statistics 116

7.3 Results 117

7.4 Discussion 118

8 Conclusion 123

8.1 General overview 123

8.1.1 Major contributions of the thesis 123

8.2 Current limitations and future work 125

Appendix 134

Bibliography 135

List of Figures

2.1 Early concepts and first prototypes. 8
2.2 Walking assistive robotics timeline. 11

3.1 Design overview. 22
3.2 Textile interface. 24
3.3 Actuation configurations. 26
3.4 Control unit and sensing. 27
3.5 Outlook of the general control framework. 29
3.6 Control framework generalizability across hardware configurations. . 32

4.1 Soft robotic suit and AOs-based control framework. 38
4.2 Controller performance. 44
4.3 Motor torque and power. 45
4.4 Kinematics and muscle activity. 46
4.5 ML-augmented controller. 50
4.6 Performance comparison on human motion estimation. 57
4.7 Metabolic cost. 58

5.1 Hardware design. 65
5.2 Context aware control framework. 66
5.3 Graphical overview of the key steps. 69
5.4 Experimental protocol. 80
5.5 Classification accuracy. 83
5.6 Motor reference modulation. 84
5.7 Kinematics. 85
5.8 Metabolic cost with CNN-based computer vision. 85
5.9 Metabolic cost with GM-based computer vision. 87

6.1 Phase portrait-based controller. 96
6.2 Representation of the phase portrait-based control framework. . . . 97
6.3 Uphill outdoor walking task. 103

6.4 Metabolic cost. 105
6.5 Kinematics. 106
6.6 Sense of agency. 107

7.1 An older adult wearing the soft robotic suit. 114
7.2 Outdoor walking task. 116
7.3 Metabolic cost. 117
7.4 Kinematics. 118
7.5 Sense of agency. 119

A.1 Hiking study. 128
A.2 Uphill hiking results. 129
A.3 Downhill hiking results. 130
A.4 Sense of agency. 131
A.5 Cost of transport results for five young adults. 133
A.6 Cost of transport results for four older adults. 134

List of Tables

3.1 Design requirements. 20
3.2 Hardware components of the soft robotic suit. 23

4.1 Participants demographic. 41
4.2 Participants demographic. 54

5.1 Participants demographic. 79
5.2 Computational load of the two computer vision methods. 84

6.1 Participants demographic. 101

7.1 Participants demographic 115

Notations

Acronym

ANOVA	ANalysis Of VAriance
AOs	Adaptive Oscillators
AS	Ascending Stairs
BLE	Bluetooth Low Energy
bpm	Beats per minute
CAN	Controller Area Network
CART	Classification and regression trees
CNN	Convolutional Neural Network
CoT	Cost of transport
CV	Computer Vision
DS	Descending Stairs
EMG	Electromyography
FA	Fully-actuated design
GL	Gastroctemius Lateralis
GM	Geometric modeling
GP	Gait Phase
I2C	Inter-Integrated Circuit
IMU	lnertial Measurement Unit
LG	Level Ground
LSBoost	Least Squares Gradient Boosting
ML	Machine Learning
MVC	Maximum Voluntary Contraction
PCA	Principal Component Analysis
PID	Proportional-Integral-Derivative
RMS	Root Mean Square
RMSE	Root Mean Square Error

ROM	Range of Motion
s.e.m	Standard Error of the Mean
SD	Standard Deviation
ST	Semitendinosus
TA	Tibilias Anterior
TFL	Tensor Fasciae Latae
UA	Underactuated design
WHO	World Health Organization

List of Symbols

$\alpha_0(t)$	Offset
$\alpha_n(t)$	Amplitude of n^{th} harmonic component
$\dot{\theta}(t)$	hip velocity
η	Amplitude gain
η_1	Learning rate
$\hat{\theta}_r$	Estimated reference position trajectory
$\hat{\dot{\theta}}(t)$	Normalized and centered hip velocity
$\hat{\theta}(t)$	Normalized and centered hip angle
$\hat{\theta}_{IL}(t)$	Estimated inter-limb hip flexion angle
ν_ω	Frequency gain
ν_φ	Phase gain
$\omega(t)$	Fundamental frequency
ω_{AOs}	Estimated walking frequency from AOs
ω_{ML}	Estimated walking frequency from ML
ω_{stride}	Actual walking frequency from IMUs
$\overline{v}$	Average walking speed
ϕ	Gait phase
$\theta(t)$	hip angle
$\theta_{IL}(t)$	Inter-limb hip flexion angle
θ_m	Actual motor position
θ_{ref}	Reference position trajectory after interpolation
θ_r	Reference position trajectory
φ_e	Corrective factor
φ_{GP}	Gait phase variable from Adaptive Oscillators
$\varphi_n(t)$	Phase of n^{th} harmonic component
C	Context surrounding the user

$C_{U/A}$	Magnitude-squared coherence
$F(t)$	Difference between $\theta_{IL}(t)$ and $\widehat{\theta}_{IL}(t)$
g	Gravitational acceleration
$G_{\theta_{IL}\theta_{ref}}$	Cross-spectral density
$G_{\theta_{IL}}$	Autospectral density of inter-limb hip flexion angle
$G_{\theta_{ref}}$	Autospectral density of actuator reference motion
P	Net metabolic power
r^2	Coefficient of determination
t_{start}	Stride start
T_i	Period of the i_{th} stride
w	Body weight

Chapter 1

Introduction

"Walking is man's best medicine." — Hippocrates

Few achievements in life are as universally celebrated as a child's first steps. This moment marks not only the beginning of independent mobility but also the start of a deeper connection with the world around us. The significance of walking extends far beyond those early steps; it is a fundamental activity that underpins both our physical and social development. Walking is essential to maintaining our independence, well-being, and overall quality of life throughout adulthood and into old age.

From a biomechanical perspective, walking is a highly coordinated process that balances motion, stability, and energy efficiency [1]. The process is defined by the *gait cycle*, which consists of two main phases: *stance* and *swing*. During stance, one foot remains in contact with the ground, providing support and propulsion, while during swing the opposite foot advances in preparation for the next step. Within these phases, specific events such as heel strike, mid-stance, toe-off, and the various swing stages contribute to efficient motion [1, 2].

The mechanics of walking depend on the integration of muscular, skeletal, and neural systems. Central pattern generators in the spinal cord produce the rhythmic alternation between flexor and extensor muscle activation necessary for basic locomotion. This rhythmic activity establishes the timing and intensity of muscle contractions that drive the legs' movements. These fundamental patterns are continuously refined by sensory feedback from peripheral receptors, enabling adaptive responses to variations in terrain, speed, and direction [2].

The synchronized action of muscles ensures efficient joint movement at the hips,

knees, and ankles, while the central nervous system regulates balance and posture dynamically. Walking efficiency is further optimized by the pendulum-like motion of the lower limbs and the elastic properties of tendons, which store and release energy at each step [3, 4].

Research has extensively demonstrated that the benefits of walking extend well beyond locomotion [5]. Regular walking promotes cardiovascular health, improves metabolic efficiency, and reduces the risk of chronic diseases such as diabetes, hypertension, and obesity [5–7]. Additionally, walking has a profound impact on mental health, helping to reduce stress, alleviate anxiety and depression, and enhance cognitive function [7].

1.1 Gait in aging and disease

Walking ability is often compromised by both the aging process and various health conditions. These impairments can significantly hinder an individual's mobility, making it more difficult to perform daily tasks, engage in social activities, and maintain an active lifestyle. As a result, the loss of walking ability can lead to broader consequences, including physical decline, psychological distress, and a diminished quality of life [8].

Age-related physiological changes, for instance, have a profound impact on walking efficiency. The musculoskeletal system undergoes a gradual decline, with a notable reduction in muscle mass and strength, decreased joint flexibility, and diminished bone density. These changes directly affect the mechanics of walking, making it less efficient and more prone to injury. Additionally, proprioception, the body's ability to sense its position and movement in space, declines with age, contributing to balance problems and an increased risk of falls. Slower reaction times and decreased cardiovascular fitness further limit walking speed and endurance, making it increasingly challenging to navigate everyday environments and engage in physical activity [8–10].

Neurological conditions, such as Parkinson's disease, multiple sclerosis, and the aftermath of a stroke, present additional barriers to normal walking patterns. These disorders disrupt the brain's ability to coordinate lower-limb movement, resulting in gait abnormalities such as rigidity, instability, and tremors. In many cases, individuals with neurological conditions may develop compensatory gait strategies that, while allowing for some degree of movement, often lead to further inefficien-

cies and discomfort [11].

The cumulative effects of these physiological and neurological impairments can be debilitating. As walking ability declines, individuals tend to engage in less physical activity, which in turn amplifies the physical and psychological effects of reduced mobility. This negative feedback loop can lead to a decline in fitness, increased social isolation, and a decrease in overall health. Older adults are particularly vulnerable to these changes, often facing a loss of confidence, independence, and self-esteem [8].

With the global population rapidly aging [12], and considering that this natural process affects each and every individual, addressing mobility challenges has become an urgent and essential healthcare priority. Impaired walking profoundly impacts daily life, making it crucial to implement solutions that improve mobility and support both physical health and mental well-being.

Advances in assistive technologies, particularly wearable assistive robotics, hold significant promise for helping individuals regain or maintain their walking ability. Over the years, numerous wearable devices have been developed to address mobility impairments, enhance physical capabilities, and support human augmentation. These systems, designed to be worn on the body, offer tailored support to improve mobility, stabilize gait, reduce the risk of falls, and promote greater independence [13–15]. Chapter 2 of this dissertation offers a detailed overview of these technologies, emphasizing the key challenges currently faced by the field, challenges that this thesis aims to address in the subsequent chapters.

However, despite their potential, most of these devices remain confined to laboratory settings and have yet to be fully integrated into everyday life. This is primarily due to technological constraints, as many of these systems are not yet ready for real-world application, as well as the lack of thorough validation outside of controlled environments. Additionally, only a few devices have been proven effective in addressing mobility challenges related to aging [16–18], an area that remains underexplored, yet increasingly important given its widespread impact on the global population.

1.2 Research motivation and aims

To address mobility challenges associated with aging or conditions that impair walking ability, there is a need for the development of wearable systems that are lightweight, adaptable, and effective in real-world environments.

Current assistive robotic devices often struggle with issues related to portability, user comfort, and their ability to adapt to dynamic environments and individual needs. Many of these systems depend on complex sensory networks that are primarily suited for controlled laboratory settings, which restricts their practical application. There is a pressing need for innovative designs and control strategies that can overcome these challenges, facilitating integration into everyday life.

This thesis aims to tackle the mentioned challenges in wearable assistive robotics, with a focus on both technical advancements and real-world assessment.

The thesis is centered around **two main objectives:**

1. **Technological development:** To design and develop a fully portable and lightweight soft robotic suit that assists walking, incorporating a minimal sensory network and requiring little to no calibration. The system needs to be a plug-and-play solution.
2. **Real-world assessment:** To evaluate the suit's effectiveness in the real-world, initially with fit individuals for walking augmentation, and subsequently to assess its potential in frail users, focusing on older adults as a specific use case for demonstration.

1.2.1 General hypotheses

The following main hypotheses guide the development and evaluation of the soft robotic suit presented in this dissertation, focusing on three key areas: (1) design, (2) control, and (3) practical application:

Hypothesis 1 A tendon-driven design can provide an optimal balance between efficiency, portability, and user comfort. Additionally, assisting the hip joint, particularly during flexion, can offer valuable support to counteract the early weakness of hip flexors caused by aging or frailty, while also assisting fit individuals in demanding walking tasks.

Hypothesis 2 A minimal sensory network, relying solely on inertial sensors, can enable the soft robotic suit to adapt to walking cadence in real time, accommodating varying gait patterns. Furthermore, environmental sensing through computer vision can facilitate context-aware modulation of assistance.

Hypothesis 3 In real-world settings, the soft robotic suit can enhance metabolic efficiency, maintain natural gait patterns, and preserve user agency during outdoor and challenging walking tasks, while providing effective support for both fit and frail individuals.

Each chapter of this dissertation explores specific subhypotheses related to these overarching hypotheses, contributing to a deeper understanding of the suit's design, control mechanisms, and real-world performance.

1.3 Thesis outline

This dissertation is organized into the following chapters, each designed to address the thesis objectives and test the general hypotheses. The structure takes the reader through the entire research process, starting with the motivation and background of the study, progressing through the detailed technical development and in-lab iterations, and concluding with the validation of the system in real-world settings.

Chapter 2 provides an overview of the evolution of wearable assistive robotics devices for human locomotion, highlighting the transition from rigid exoskeletons to soft robotic suits. It identifies key limitations in current systems setting the stage for the research gaps this thesis addresses.

Chapter 3 details the hardware design of the soft robotic suit, highlighting its lightweight, textile-based composition and tendon-driven actuation system. Two configurations, underactuated and fully actuated, are presented. The targeted joint is the hip, focusing specifically on flexion, due to its critical role in providing meaningful support during demanding walking tasks, such as uphill or stair climbing. This focus is particularly relevant as the hip flexor muscles are among the first to weaken with aging and conditions associated with frailty.

Chapter 4 discusses the initial implementation of control systems that synchronize robotic assistance with the user's natural gait, relying solely on inertial sensors. The chapter explores an Adaptive Oscillator (AO)-based controller, enabling

effective assistance across varying walking conditions. A substudy introduces a methodology based on learning to improve control robustness during abrupt transitions in walking cadence.

Chapter 5 presents the incorporation of computer vision into the control system disclosed in the previous Chapter. It serves at the purpose of enabling context-aware assistance modulation, allowing the suit to recognize environmental features, such as stairs or flat ground, and dynamically adjust its assistance. The chapter evaluates two approaches: data-driven and physics-informed computer vision.

Chapter 6 demonstrates the performance of the soft robotic suit in an outdoor, real-world setting, specifically during uphill hiking with healthy young adults. Building upon the limitations identified on control strategies explored in Chapters 4 and 5, a revised control framework is here presented to improve robustness in unstructured walking with the aim to enhance energy efficiency and preserve natural gait.

Chapter 7 extends the evaluation to frail individuals, focusing on older adults as a case study. This chapter demonstrates the suit's potential to increase energy efficiency and improve mobility for this target population.

Chapter 2

On the evolution of wearable assistive robotics

This chapter examines the historical development and current landscape of wearable robotics, focusing on systems designed to enhance human locomotion. It traces the evolution of wearable robots from early concepts in the late 19th century through the key milestones of the 20th and 21st centuries. A central theme of the discussion is the transition from rigid exoskeletons to soft robotic suits, which offer a more flexible and comfortable solution through the use of soft materials and clothing-like designs. Despite significant progress, the chapter highlights ongoing research gaps, such as the need for lightweight, portable, and robust devices suitable for daily use. It concludes by outlining the specific challenges that this thesis will address in subsequent chapters.

2.1 The origin and early developments

The idea of augmenting human strength and mobility through wearable robotic systems dates back over a century, with various attempts to create machines capable of assisting with human movement.

The earliest known designs for wearable robots can be traced to the late 19th and early 20th centuries. In 1890, Nicholas Yagn, a Russian engineer, filed a patent proposing a system using springs to assist in walking, running, and jumping [19]. It was a passive device that worked in parallel with the user's legs, incorporating a locking mechanism that engaged during the stance phase of walking, while al-

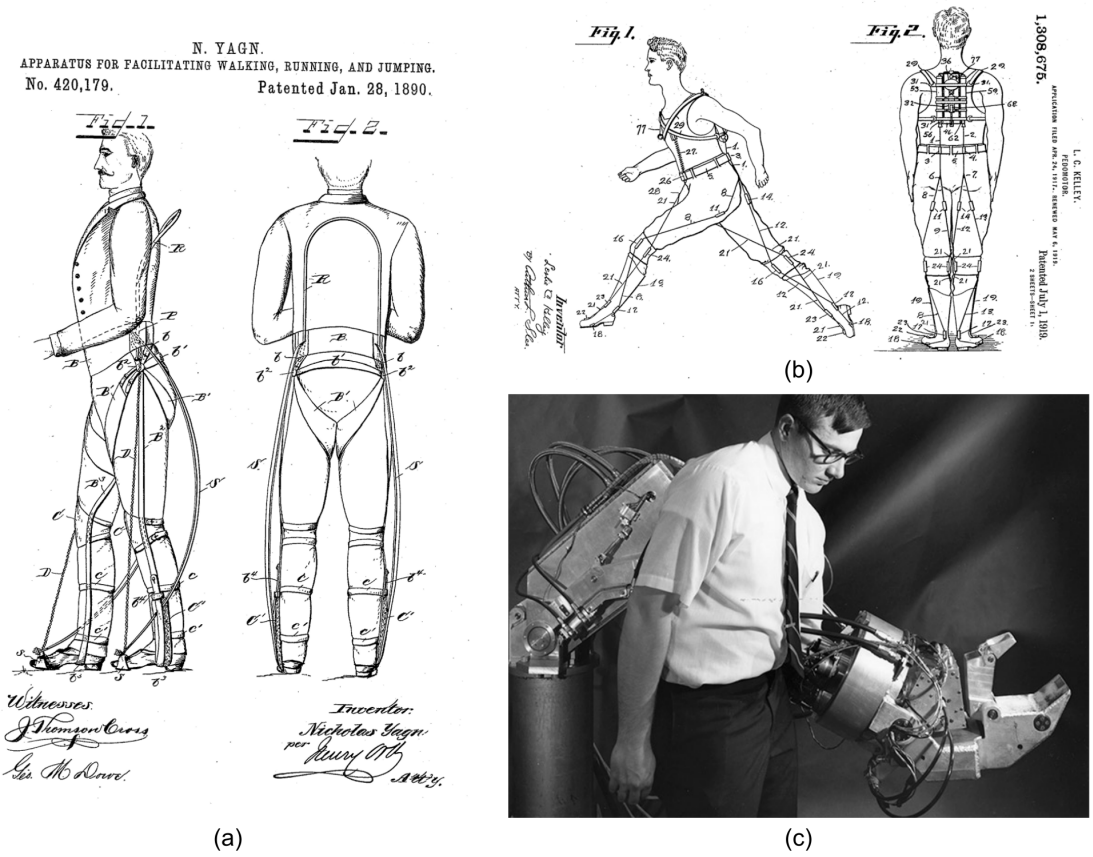


Figure 2.1. Early concepts and first prototypes. (a) Yagn's spring-like concept [19]. (b) The "Pedomotor" [20]. (c) The Mosher's Hardiman [21]. Pictures are adapted from [19], [20], and [21]

lowing the leg to move freely during the swing phase. Although it was only in a conceptual phase, this design foreshadowed the potential of external systems to augment human locomotion (Fig. 2.1-(a)).

Similarly, in 1917, U.S. inventor Leslie C. Kelley developed a "pedomotor" (Fig. 2.1-(b)), which, according to one of its patent claims, was designed *"to relieve the muscles utilized during the running operation of the anatomy from strain and fatigue"* [20]. This system, powered by steam, incorporated artificial ligaments to assist the wearer's movements, representing another early effort to combine mechanical support with human motion.

These early forays, however, were limited by the technology of their time. Most of these designs remained theoretical or never moved beyond conceptual drawings. The first truly ambitious attempt to create a wearable robotic exoskeleton emerged in the 1960s with the creation of the "Hardiman" [21], shown in Fig. 2.1-(c). Designed by Ralph Mosher and developed by General Electric in collaboration

with the U.S. Armed Forces, the Hardiman was conceived as a wearable device capable of amplifying the wearer's strength by 25 times. The device, powered by hydraulics and electricity, could make lifting 110 kilograms feel like lifting only 4.5 kilograms. Despite its bold vision, the Hardiman faced significant issues, most notably its enormous weight, over 680 kilograms, making it impractical for everyday use. Furthermore, the system suffered from slow response times and erratic motion due to technological limitations of the time. These issues ultimately led to the project's unsuccess, highlighting the complexity of designing a human-robot interface capable of amplifying human strength without compromising mobility.

Around the same time, in 1963, a paper by Zarodney from the U.S. Army Exterior Ballistics Laboratory highlighted some of the fundamental challenges faced by powered exoskeletons [22]. Although it remained a conceptual study, Zarodney's work laid the foundation for addressing critical issues, such as the need for a portable power supply, the complexities of interfacing with human biomechanics, and the development of sophisticated control systems for effective operation.

Interestingly, as far back as the 1990s, wearable robots began to capture the public imagination, not just in military and industrial contexts but also in popular culture. One example is the 1993 animated film "The Wrong Trousers", co-written and directed by Nick Park [23]. This stop-motion movie, presented a humorous yet thought-provoking take on exoskeleton-like technology. In the story, one of the main characters, Wallace dons a robotic suit designed to enhance mobility, but it ultimately becomes a tool for a villainous scheme. This playful portrayal reflected the growing public interest in wearable robots, showing both their possibilities and potential challenges. While purely fictional, the film hinted at the transformative possibilities of such technology and contributed to the wider interest in its future.

In the years that followed, wearable robotics progressed rapidly, propelled by the dual demands of defense applications and the increasing need for medical and rehabilitation solutions. The 21st century witnessed a surge in these technologies, marked by significant advancements.

A brief overview of these developments is provided in the following sections. However, from this point onward, this chapter will focus specifically on the evaluation and progress of wearable robotics designed to assist human locomotion. This shift in focus aligns with the central theme of this thesis, which is dedicated to lower limb assistive technologies for walking. It is important to note, though, that significant strides have also been made in the development of wearable robotics for

upper limb assistance. These contributions have been essential in advancing the broader field of wearable robotics and continue to be a key area of research and innovation.

While this chapter aims to provide a comprehensive overview of walking assistive robotics, it does not attempt to cover the entire breadth of research in this rapidly advancing field. Instead, the focus is on offering a representative analysis of the most significant and impactful developments and to highlight the currently open challenges.

2.2 The 21st century: walking with robotics

The 2000s and beyond marked a significant expansion in wearable assistive robotics. As illustrated in the timeline of Figure 2.2, this period saw the development of key designs that continue to influence the field today.

At the start of the 21st century, wearable assistive devices were predominantly rigid exoskeletons relying on heavy, inflexible structures to assist with load-bearing, which allowed for substantial mobility enhancement but also introduced significant challenges [24].

Early progress in exoskeleton technology was propelled by initiatives like the DARPA Exoskeletons for Human Performance Augmentation (EHPA) program, which began in 2001 [25]. This program was instrumental in advancing the field, leading to the development of groundbreaking systems such as the BLEEX (Berkeley Lower Extremity Exoskeleton) [26, 27]. BLEEX was among the first devices to achieve energetic autonomy, enabling it to function independently without the need for external power sources. However, despite these innovations, BLEEX required over 1300 watts of power, significantly more than the 165 watts typically used by a human during walking, underscoring the substantial energy demands of such systems.

A critical turning point in walking assistive robotics emerged with the development of the MIT exoskeleton [46–48]. This system adopted a novel approach by incorporating passive elements such as springs and dampers to reduce power consumption dramatically. Weighing only 11 kilograms and requiring just 2 watts of power, the MIT exoskeleton represented a significant step forward in energy-efficient design. However, despite its reduced energy demands, the device inadvertently introduced

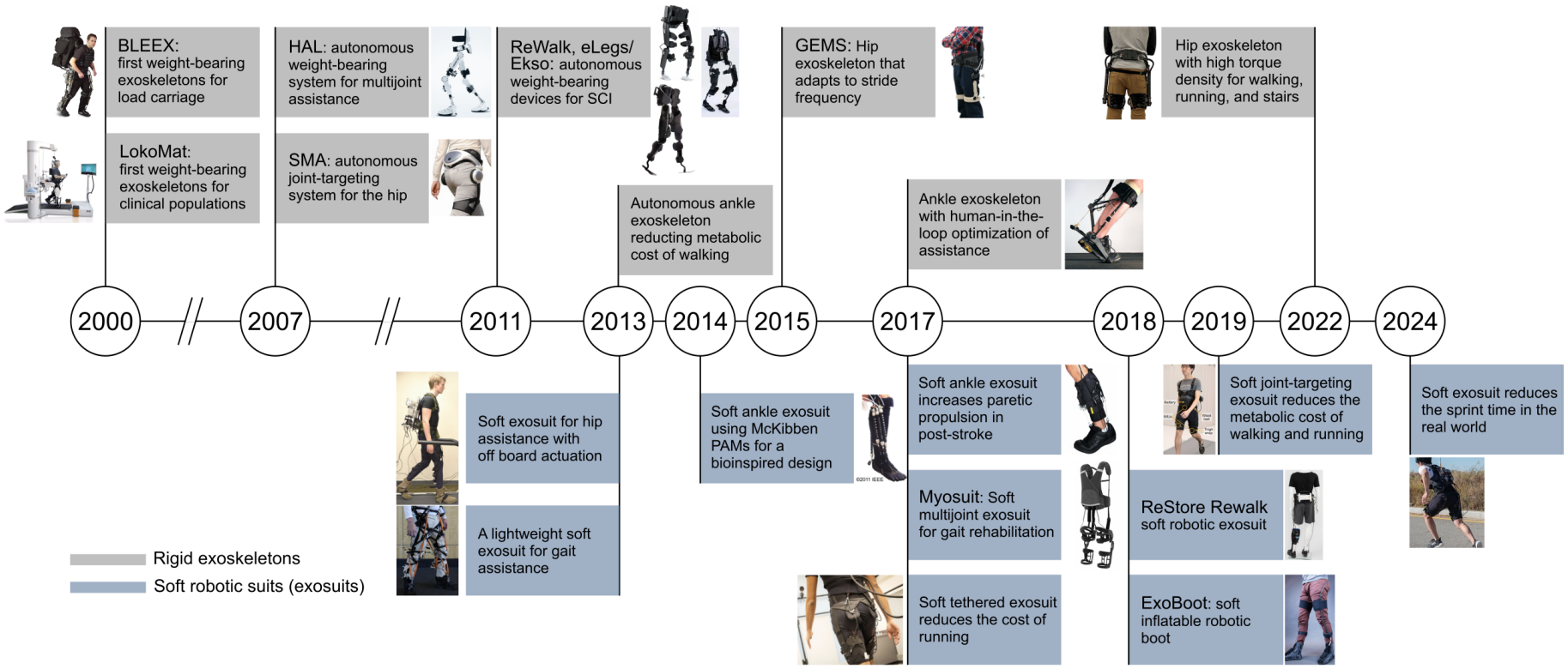


Figure 2.2. Walking assistive robotics timeline. Significant advancements in exoskeletons (gray, upper row) and soft robotic suits (navy, lower row) for gait assistance from 2000 to the present. The figure is adapted from references [28] and [24]. Cited rigid exoskeletons (from left to right) are: BLEEX [26, 27], LokoMat [29], HAL [30], SMA [31], ReWalk [32], eLegs/Ekso [33], autonomous ankle exoskeleton [15], GEMS [34], ankle exoskeleton with human-in-the-loop optimization of assistance [35], and hip exoskeleton with high torque density [36]. Cited soft robotic suits (from left to right) are: soft exosuit for hip assistance with off-board actuation [37], a lightweight soft exosuit for hip assistance [38], soft ankle exosuit using McKibben PAMs [39], soft ankle exosuit to increase paretic propulsion post-stroke [40], Myosuit [41], soft tethered exosuit [42], ReStore Rewalk [43], ExoBoot [44], soft joint-targeting exosuit [14], soft exosuit reducing sprint time [45].

kinematic constraints, which altered the user's natural walking pattern. This alteration increased the metabolic cost of walking by approximately 10%, underscoring a key challenge in wearable robotics: providing effective assistance without interfering with the body's natural biomechanics.

Along the years, the development of exoskeletons has advanced beyond load-enhancing devices to encompass a range of applications, including mechanized physical therapy and mobility restoration for individuals with walking impairments. Notable examples include the Lokomat [29], which automates gait training for individuals recovering from spinal cord injuries or strokes, and high-power, weight-bearing exoskeletons like the Hybrid Limb Assist (HAL) [30], ReWalk [32], and eLegs/Ekso [33]. Originally designed for individuals with paraplegia, these devices have also been employed as tools for gait rehabilitation in patients with partial walking ability.

In parallel, joint-targeting exoskeletons have emerged, mainly focusing on reducing the metabolic cost of walking in unimpaired individuals by providing powered assistance at specific joints, such as the ankle [15, 35]. Unlike weight-bearing systems, these devices avoid large rigid structures, though rigid components still offer benefits for efficiently transferring torque. This is evident in ankle-targeting devices, that improve walking efficiency under both loaded and unloaded conditions [15]. This approach has facilitated the development of autonomous exoskeletons for various applications, including the Stride Management Assist (SMA) [31] and the Gait Enhancing and Motivation System (GEMS) [34], which serve industrial, recreational, and clinical purposes. Furthermore, exoskeletons designed to assist running are expanding the scope of these technologies, exemplifying their versatility in enhancing human mobility [36].

While these systems marked significant progress in assistive robotics, their rigid designs often came with issues such as misalignment, discomfort, and high energy consumption, all of which hindered broader adoption. Over time, however, this led to the exploration of more adaptable and efficient technologies, laying the groundwork for the diverse range of devices we see today.

2.2.1 From rigid exoskeletons to soft robotic suits

Rigid exoskeletons, despite their impressive capabilities, are primarily confined to research labs or high-cost rehabilitation centers, making them largely inaccessible

to the general public. This limited availability is mainly due to their complexity, which results in high costs, heavy designs, and bulky systems [49]. Much of this complexity stems from the requirement for rigid structures to accurately align with the joint movements of the human body. When the joints of the exoskeleton does not match up perfectly with the user's joints, it can cause unwanted forces that make movement harder, less efficient, and even uncomfortable. These issues make it clear that wearable robots need to be simpler, more adaptable, and easier to use [24].

The need for more adaptable solutions has driven the field to shift away from rigid designs in favor of softer, more flexible systems that better mimic the natural movements of the human body. Advances in soft materials and control system engineering have enabled the creation of wearable devices known as "soft exoskeletons", "exosuits", or "soft robotic suits", terms often used interchangeably. For consistency, we will refer to them as "soft robotic suits" in the following sections. By definition, soft robotic suits are wearable robotic devices designed to fit like clothing, working alongside a person's muscles to provide support. They actively transmit power to the human body via either cables powered by electric motors or soft pneumatic actuators. Unlike traditional exoskeletons, soft robotic suits leverage the body's natural structure to transmit forces across body segments, eliminating the need for a rigid, load-bearing frame. This design allows them to act more like an additional layer of muscles rather than an external skeleton, enhancing flexibility and comfort while providing effective assistance [24].

The first major advancements in soft assistive robotics were pioneered by Harvard's Biodesign Lab, led by Professor Conor J. Walsh, and have continued to evolve from there (Fig. 2.2). Early developments, dating back to 2013 and supported by DARPA's Warrior Web program, demonstrated the potential of using tensile elements and various actuator systems to create more flexible and adaptable assistive devices. For example, Wehner et al. designed a device featuring a network of soft webbing bands, actuated by pneumatic artificial muscles (McKibben PAMs), to assist movements at the hip, knee, and ankle joints [38]. On the other hand, Asbeck et al.'s approach used Bowden cables powered by electric motors to route artificial tendons, providing assistance at the ankle and hip [37]. These initial models highlighted the ability of soft robotic suits to apply precise forces during assistive phases, while also becoming "transparent" during non-assistive phases, thus reducing interference with natural gait. Furthermore, strategically placing actuators near the wearer's center of mass helped mitigate the metabolic

cost of carrying the additional weight, making these systems more energy efficient and user-friendly [37].

Subsequent innovations broadened the scope of soft robotic suits in rehabilitation. Devices powered by McKibben pneumatic artificial muscles (PAMs) showed promise in enhancing ankle–foot function [39], while later models focused on improving mobility for stroke patients, increasing walking symmetry and efficiency for individuals with hemiparesis [40, 43, 44].

Commercial products like the Myosuit by MyoSwiss AG [41] have made significant advancements in mobility support and rehabilitation by incorporating soft, lightweight components. The flexible design of the Myosuit allows the accommodation of a wide range of users, demonstrating positive outcomes in individuals with spinal cord injury (SCI) [50], stroke hemiparesis [51], and muscular dystrophy [51], as well as healthy individuals.

Recent developments have expanded the capabilities of soft wearable robotics, with designs aimed at facilitating transitions between walking and running, or even supporting sprinting. Studies by Lee et al. [42], Kim et al. [14], and Moon et al. [45] have explored these dynamic functionalities, signaling the growing potential of wearable robotics in a variety of movement contexts.

2.3 Research gap and open challenges

Despite substantial advancements in walking assistive robotic technologies, several critical challenges remain in developing lightweight, portable, and user-friendly devices that can effectively assist individuals across a variety of real-world environments. Many current devices for the lower limbs rely on complex calibration processes or sophisticated sensory networks [52, 53], which hinder their portability and adaptability in dynamic settings. Furthermore, most existing systems have primarily been tested in controlled laboratory environments, with limited investigation into their performance under unstructured walking conditions.

This work seeks to address these gaps by designing and developing a lightweight soft robotic suit that assists locomotion with minimal sensory network and minimal calibration to increase robustness and practicality, while providing effective support across a range of walking tasks and environments. A key focus is facilitating the transition from laboratory testing to real-world applications, demonstrating the

suit's ability to enhance walking in healthy young adults, and exploring its use in frail individuals, particularly older adults, as a specific use case.

The following open challenges in the field are tackled in the next chapters:

Challenge 1: control robustness and adaptability across tasks with minimal sensory framework Current wearable assistive devices for the lower limbs predominantly rely on gait-event detection using a combination of sensors such as foot switches, pressure sensors [39, 54], Elecromyography (EMG) [55], and Inertial Measurement Units (IMUs) placed on the legs to monitor key gait phases [14, 40]. In addition to relying on multiple sensors, current control systems often struggle to adjust timely the level of assistance based on changing conditions, such as variations in walking speed, cadence, or terrain [24]. While some progress has been made in adapting the timing of assistance to walking cadence, systems that can dynamically adjust both the timing and magnitude of assistance based on real-time conditions remain underdeveloped. For instance, Asbeck et al. [56] propose adjusting the assistive profile's gait period based on the average period of the last five steps. Although this approach synchronizes the assistance with the user's cadence, it can limit responsiveness, particularly in dynamic walking situations where gait changes abruptly or becomes inconsistent. Furthermore, most existing controllers are unable to modulate walking assistance according to the external context, such as varying walking tasks like stair climbing or traversing uneven terrain. Chapters 4, 5, and 6 will address this issue by presenting control strategies for the designed soft robotic suit, relying solely on IMU sensors to provide real-time, accurate assistance. This will involve improving the system's ability to estimate gait phases and tailor assistance to a wider range of tasks and environmental conditions, with the ultimate goal of creating a plug-and-play solution through iterative refinements of the control framework and both laboratory and field testing.

Challenge 2: transition from laboratory testing to real-world deployment for fit and frail users While laboratory-based studies have demonstrated the potential of soft robotic suits in controlled environments, applying these results to real-world settings remains a significant challenge. Real-world environments present complex variables, such as uneven terrain and unpredictable gait patterns, that many current systems struggle to accommodate effectively [24]. Chapters 6 will address this gap by evaluating the performance of the soft robotic suit in a hiking outdoor walking task with healthy young adults. The focus will be on assessing

the suit's impact on metabolic efficiency, gait patterns, and user agency during a strenuous outdoor activity. Additionally, chapter 7 will finally explore the suit's applicability outdoor for frail individuals, with a specific use case focused on older adults, a population that stands to benefit significantly from robotic assistance, but has received limited attention and only in few lab-based studies [17, 42].

Chapter 3

Suit design motivation and principles

The contents of this chapter are adapted mainly from the patent application:
E. Tricomi, L. Masia, F. Missiroli, L. Lotti, "*Assistance system for walking assistance, computer-implemented method for controlling an assistance system, and corresponding non-transitory computer readable storage medium*", WO 2024/160839 A1, 2024.

This chapter presents the hardware design of the soft robotic suit tailored to assist hip flexion during walking. It begins with a brief overview of the anatomy and biomechanics of the hip joint later focusing on the motivations for targeting hip flexion, emphasizing its critical role in mobility and the potential benefits of augmenting this phase of the motion, particularly for frail individuals. The subsequent sections describe the design, including the textile structure, transmission system and actuation mechanisms, as well as an outline of the control framework for delivering effective assistive forces. Two distinct actuation configurations are explored: an underactuated design employing a single motor and a double-layer pulley to symmetrically drive both legs, and a fully actuated design with independent motors for each leg.

3.1 The hip joint

The hip joint plays a critical role in human locomotion, providing the stability and mobility required for activities such as walking, running, and climbing [1]. Structurally, it is a ball-and-socket joint formed by the articulation of the femoral head with the acetabulum of the pelvis, reinforced by a robust capsule and surrounding ligaments. This configuration enables a wide range of motion across multiple

planes, including flexion-extension, abduction-adduction, and internal-external rotation [57].

During walking, the hip joint has critical action both in stance and swing.

In the stance phase, the hip provides stability, bearing the weight of the body while facilitating force transmission between the trunk and the lower limbs. The hip extensors, including the gluteus maximus and hamstrings, play a central role in this phase, ensuring upright posture and controlling the deceleration of the forward motion of the trunk. The adductor muscles contribute by stabilizing the pelvis, preventing excessive lateral tilt, while the abductors, such as the gluteus medius and minimus, maintain balance by counteracting gravitational forces.

In the swing phase, the hip shifts its role from stability to mobility, advancing the limb forward to prepare for the next step. This phase relies heavily on the hip flexor muscles, with the iliopsoas (a composite of the iliacus and psoas major) being the primary contributor. It generates the torque necessary to initiate hip flexion, lifting the thigh and ensuring adequate ground clearance. The rectus femoris, part of the quadriceps group, assists in flexion while stabilizing the joint, while secondary muscles like the sartorius and tensor fasciae latae fine-tune leg movement. These coordinated muscular actions enable the hip to overcome gravitational and inertial forces, facilitating efficient and fluid limb advancement [57].

Although the pendulum model of gait suggests that the swing phase has minimal energy demands [4], studies show that the transition from stance to swing contributes to up to one-third of the total energy expenditure during walking [58]. Ground incline further impacts energy costs, with walking on steeper gradients resulting in higher energy demands for the hip joint [59]. In such cases, the limb advancement phase becomes more strenuous, requiring increased effort from the hip flexors to lift the swinging leg against gravity [60]. This is due to the muscular effort needed to overcome gravitational and inertial forces, as well as to stabilize the advancing limb's trajectory [58, 61, 62].

3.1.1 The impact of aging

As individuals age, the biomechanical demands on the hip joint become more pronounced, with aging significantly affecting the muscles of the lower extremities. Strength declines at an annual rate of approximately 1–4% starting around the age of 50 [63], with the hip flexors being the first muscles to experience weakness.

These muscles are often the first to exhibit substantial deterioration, reducing the torque-generating capacity necessary for efficient leg advancement [8].

During the swing phase, this decline compromises the ability to lift and advance the leg, leading to compensatory mechanisms such as increased co-activation of antagonistic muscles around the hip joint. While this strategy enhances joint stability, it imposes a significant metabolic cost, resulting in higher energy expenditure during walking [9, 60, 64, 65].

Research shows that older adults exhibit altered hip kinetics, particularly during the push-off phase, where higher mechanical work and energy expenditure are required to maintain mobility [9].

These biomechanical considerations underscore the importance of developing targeted interventions to address the age-related decline in hip function, particularly the weakening of hip flexors. Given its critical role in advancing the limb, ensuring ground clearance, and maintaining stride efficiency, supporting hip flexion emerges as a pivotal strategy for mitigating potential gait inefficiencies with age.

To this end, the design of the soft robotic suit presented in this dissertation specifically targets hip flexion assistance, with the goal of reducing the metabolic burden of walking and preserving mobility. By focusing on the hip flexors, which are among the first muscles to weaken with age, this approach aims to support mobility in frail individuals. Additionally, enhancing hip function can also benefit fit individuals, improving walking efficiency, reducing fatigue, and boosting performance in more demanding physical tasks.

3.2 Design requirements

The design of the soft robotic suit is informed by several key requirements to ensure that it effectively assists the hip joint during locomotion. These requirements focus on the functional needs of hip flexion assistance, user comfort, and practicality.

The main design considerations are as follows:

- *Range of motion:* The suit must assist hip flexion within the range typically observed during the swing phase of walking, which is approximately -15° to 30° of hip flexion in the sagittal plane.
- *Lightweight design:* To minimize energy expenditure and avoid user fatigue,

the suit must be lightweight, with a design that does not impose a significant additional load on the body and most of the weight focused around the user's center of mass. A tendon-driven design is well-motivated and merits exploration, as discussed in Section 3.2.1.

- *Comfort and fit:* The interface between the suit and the user must be comfortable to wear for extended periods. This includes the use of soft, flexible materials that provide support without causing discomfort. The design should accommodate a wide range of body shapes and sizes through adjustable components to ensure a secure and customized fit.
- *Scalability and adaptability:* The actuation unit should dynamically adjust assistance based on the user's movement and anthropometry, ensuring that assistive torque is tailored to the individual user's needs without manual calibration.
- *Robust performance across walking conditions:* The design should be versatile enough to assist users across different walking environments, including flat surfaces, uphill, or stairs.

The main requirements to inform the design of the soft robotic suit are summarized in Table 3.1 below.

Requirement	**Characteristics**
Hip range of motion	-15 / +30 °
Hip peak velocity (swing)	150 - 200 °/s
Suit weight	$<$ 3 kg
Suit size	one size fits all
Force at the tendon	100 - 150 N
Motor power	60 - 90 W
Friction	low

Table 3.1. Design requirements.

3.2.1 Motivations behind a tendon-driven design

Considering the need to match the biomechanical demands of the hip joint for assistance with the requirements for a lightweight and unobtrusive design, a tendon-

driven actuated assistive system emerged as an ideal choice. The selection of a tendon-driven design for the robotic suit to assist hip flexion is motivated by its ability to provide practical engineering benefits while addressing critical biomechanical requirements. By drawing inspiration from biological systems, this approach ensures efficient force transmission, portability, and user comfort, making it well-suited for wearable applications.

From an engineering standpoint, tendon-driven mechanisms excel in portability and flexibility compared to fluid-driven or direct-drive alternatives. On one hand, fluid-driven systems, like pneumatic actuators, while capable of high force output, require bulky pressure sources and complex plumbing, which are incompatible with mobile and lightweight designs. On the other hand, direct-drive systems, which involve placing actuators directly at the joint, increase the mass and inertia of the limb, negatively affecting efficiency and comfort. Tendon-driven systems, instead, enable the actuators, such as compact electric motors powered by high-energy-density lithium-polymer batteries, to be positioned remotely, such as near the torso or in a backpack [24]. This arrangement minimizes the mechanical burden on the limbs, reduces metabolic costs, and ensures portability [66].

Biomechanically, the tendon-driven approach mirrors the efficiency of natural tendons, which transmit force from proximal muscles to distal joints with minimal added mass. This design is particularly advantageous for assisting hip flexion during the swing phase of gait, where the hip flexors generate torque to advance the leg and clear the ground. By decoupling the actuator from the hip joint, the system avoids interference with the natural dynamics of gait, ensuring smooth and efficient motion.

3.3 Hardware design of the soft robotic suit

This section describes the hardware design of the soft robotic suit. It covers the materials and structure of the textile base, the two actuation configurations that were explored, and the electronic components that enable real-time monitoring and control. **The core idea is to develop a fully portable and lightweight device that assist with leg swinging requiring minimal calibration.**

Figure 3.1 offers a comprehensive overview of the design, while Table 3.2 enumerates the specific chosen hardware components. The following sections detail each unit composing the suit.

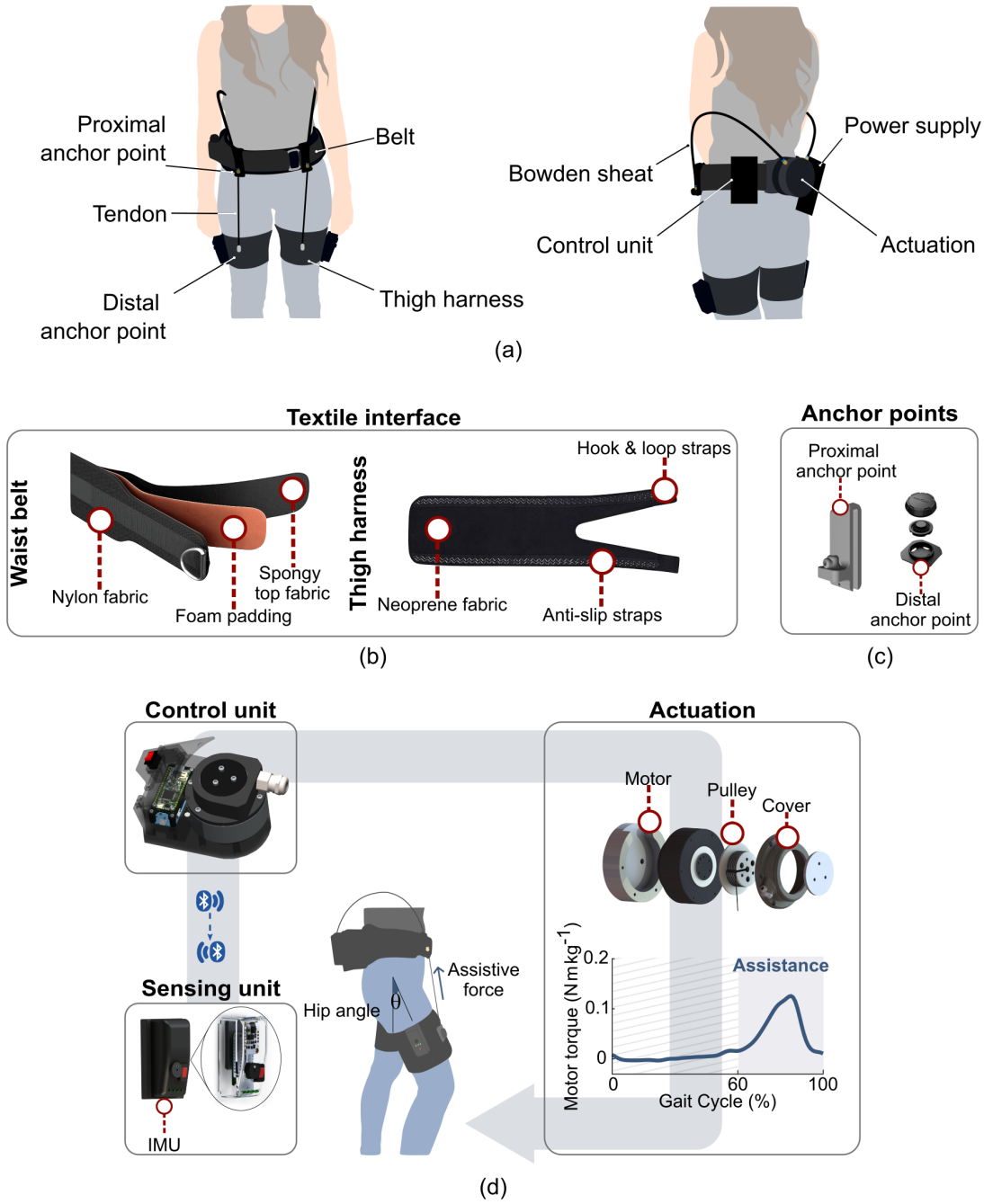


Figure 3.1. Design overview. (a) Soft robotic suit design sketch. (b) Textile interface. (c) Anchor points located on the belt and thigh harness to direct the artificial tendons. (d) Control unit, sensing unit, and actuation. The blue arrow indicates information flow to actuate the suit: the sensing unit streams thigh motion signal to the microcontroller, which then process and converts them into commands for the motor(s).

	Component	Model
Textile interface	Waist belt	(-)
	Thigh harness	(-)
Actuation	Brushless DC motor	T-motor AK series
	Bowden Cables	Shimano SLR
	Artificial tendons	Black braided kevlar fiber
Control unit	Microcontroller	Arduino MKR 1010 WiFi
	Can Bus shield	Arduino CAN bus shield
	Bluetooth Low Energy board	Feather nRF52832
Sensing unit	IMU sensor	Bosch BNO055
	Bluetooth Low Energy board	Feather nrf52832
	Lithium Polimer Battery	EEMB 3.7V, 800mAh
Power supply	Lithium Polimer Battery	Tattu 14.8V, 3700mAh

Table 3.2. Hardware components of the soft robotic suit.

3.3.1 Textile interface

The textile interface of the soft robotic suit serves as the primary connection between the system and the human body. It is designed to ensure both comfort and stability while holding the actuation and electronic components. A blueprint of the textile components is shown in Fig. 3.2, illustrating the layout.

The interface consists of an adjustable waist belt, worn at the user's iliac crest level, and two thigh fabric harnesses (Fig. 3.1-(b)). These components provide a secure attachment point for the suit, ensuring it remains in place during movement and assists with the proper transmission of forces.

Both the waist belt and thigh harnesses feature an inner layer of neoprene, chosen for its tensile strength, durability, and soft contact with the skin. Neoprene's properties allow for a firm yet comfortable fit, making it ideal for use in wearable systems that require both flexibility and stability.

To accommodate a wide range of body sizes and shapes, Velcro strips are incorporated into the design of the belt and harnesses, offering a custom fit and ensuring ease of adjustment.

The textile interface also functions as a base for the anchor points, the actuation stage and electronic components. It helps guide the tendon-driven transmission, which is crucial for delivering the desired assistance in hip flexion.

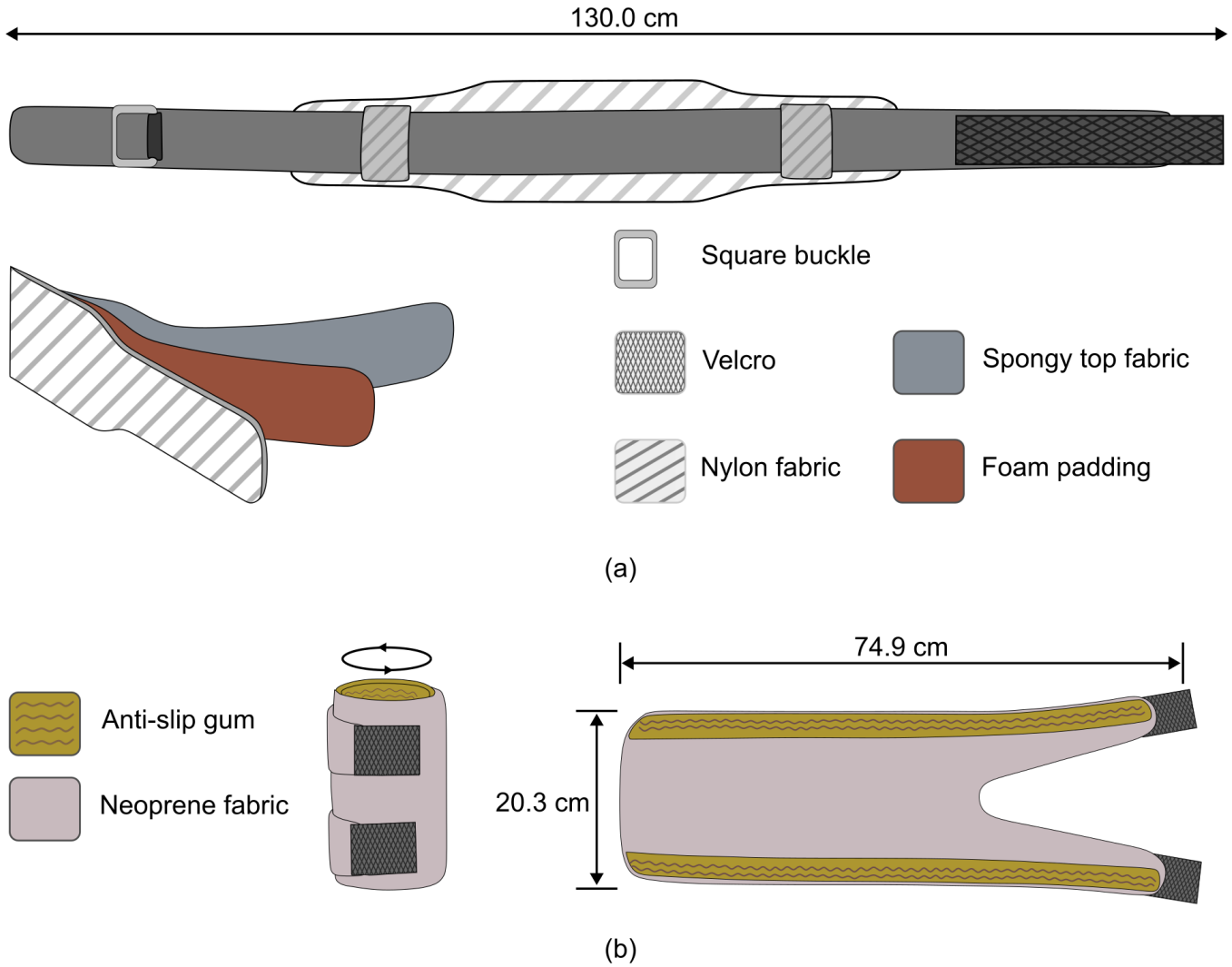


Figure 3.2. Textile interface. (a) Composition of the waist belt and its layers. (b) Inner view of the thigh textile harness and its closed configuration.

3.3.2 Actuation

The primary design requirements for the suit focus on achieving a lightweight, energy-efficient system that provides effective assistance while ensuring user comfort. In this context, two widely debated approaches in the field of wearable assistive robotics exist: underactuated systems, which use fewer motors to assist multiple degrees of freedom, and fully-actuated systems, where each joint has its own dedicated motor [49].

Underactuated systems feature a simpler and lighter design, thanks to a reduced number of motors. This makes them more energy-efficient and better able to harness the natural synergy of human movements [51,67]. Typically, these systems use a single motor to assist multiple joints or degrees of freedom simultaneously, which helps decrease weight and complexity. However, this approach may limit control and adaptability, as fewer motors result in less ability to adjust assistance for each individual joint.

In contrast, fully-actuated systems provide greater precision and independence in controlling each joint. With one motor per degree of freedom, these systems offer more adaptable and customizable assistance profiles that can better meet individual user needs, particularly in varying and dynamic environments. Fully-actuated systems enable greater flexibility in terms of movement and range of motion. However, they come at the cost of increased system weight and power consumption [14, 56, 68].

To investigate which approach best assists hip flexion during locomotion, these two mechanical configurations were explored in the context of this dissertation: an underactuated actuation stage (UA) and a fully-actuated actuation stage (FA). Figure 3.3 presents the two actuation designs. The performance of these configurations in assisting walking in the real world is compared and results are reported in the Appendix of the present thesis.

The two designs share similar components but differ in their actuation methods. Both configurations utilize a transmission system with artificial tendons made of black braided Kevlar fiber (KT5703-06, max load 2.2 kN, USA). Each tendon is enclosed in a Bowden sheath (Shimano SLR, 5 mm, Sakai, Ōsaka, Japan), running from the motor to the proximal anchor points. These anchor points are hook-shaped, 3D-printed parts positioned on the front of the belt near the iliac crest (Fig. 3.1-(c)). The exposed tendons extend along the user's thighs, connecting to the distal anchor points, which are also 3D-printed components securely attached

to the thigh harnesses. When the actuator pulls the anchor points together, it creates tension in the tendons, generating a flexion moment at the hip joint to provide assistance.

Underactuated configuration (UA) The UA configuration (Fig. 3.3-(a)) employs a single brushless DC motor (AK80-6, 12Nm peak torque, T-MOTOR, China) to symmetrically drive both legs through artificial tendons. These tendons are wrapped around a double-layer pulley (diameter 78 mm) in opposite directions. The motor alternately pulls one tendon while releasing the other by an equal amount, in sync with the natural alternation of the swing phases of the legs. By minimizing the number of motors and simplifying the actuation mechanism, this configuration adheres to the underactuated design philosophy, focusing on reduced complexity and lower weight.

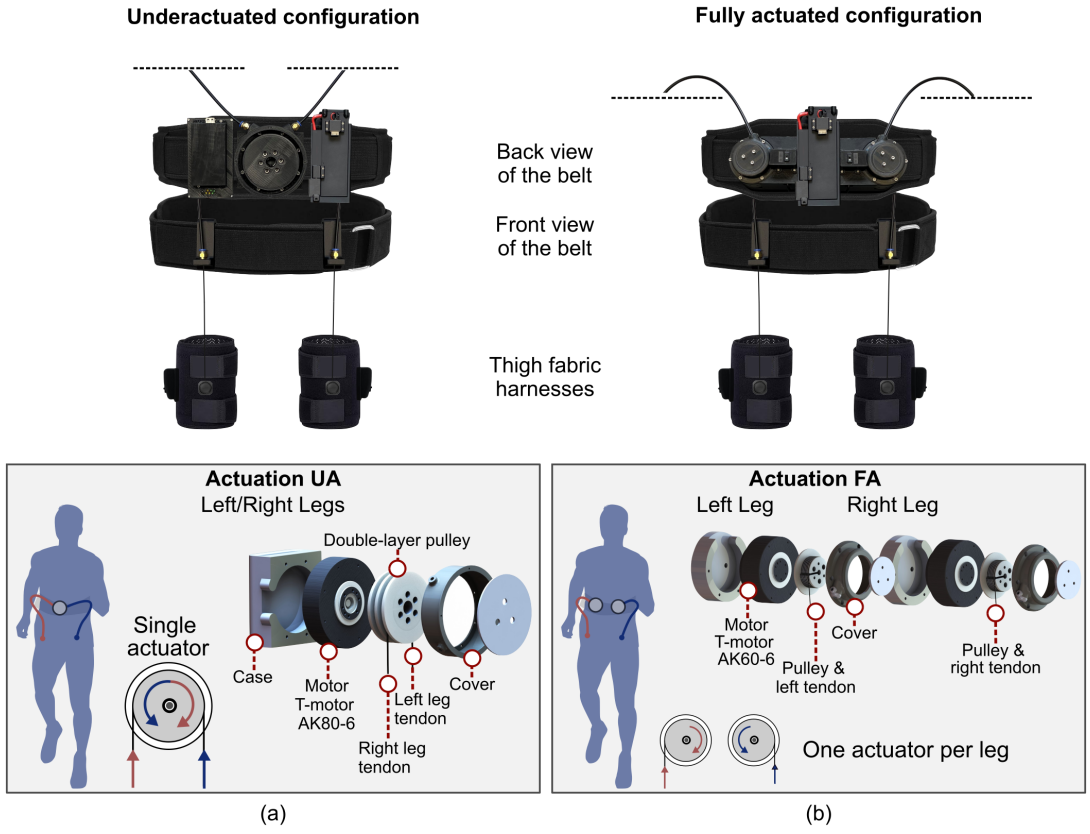


Figure 3.3. Actuation configurations. (a) The underactuated configuration (UA) utilizes a single, centrally positioned motor along with a double-layer pulley system that wraps the two artificial assistive tendons in opposite directions. (b) The fully-actuated configuration (FA) employs one actuator for each leg, ensuring that the two artificial assistive tendons operate independently.

Fully-actuated configuration (FA) The FA configuration (Fig. 3.3-(b)) utilizes two independent motors (AK60-6, 9Nm peak torque, T-MOTOR, China), with one motor dedicated to each leg. In this setup, the tendons are wrapped around different pulleys mounted directly on each motor (diameter 35 mm). This independent control enables greater flexibility and precision, as each tendon can be adjusted separately to assist flexion during the swing phase and release tension during extension. The FA configuration provides enhanced adaptability, allowing the system to accommodate more complex and individualized movement patterns, resulting in more customizable and precise assistance for each leg.

These whole suit in these configurations weigh 2.77 kg and 2.93 kg, respectively.

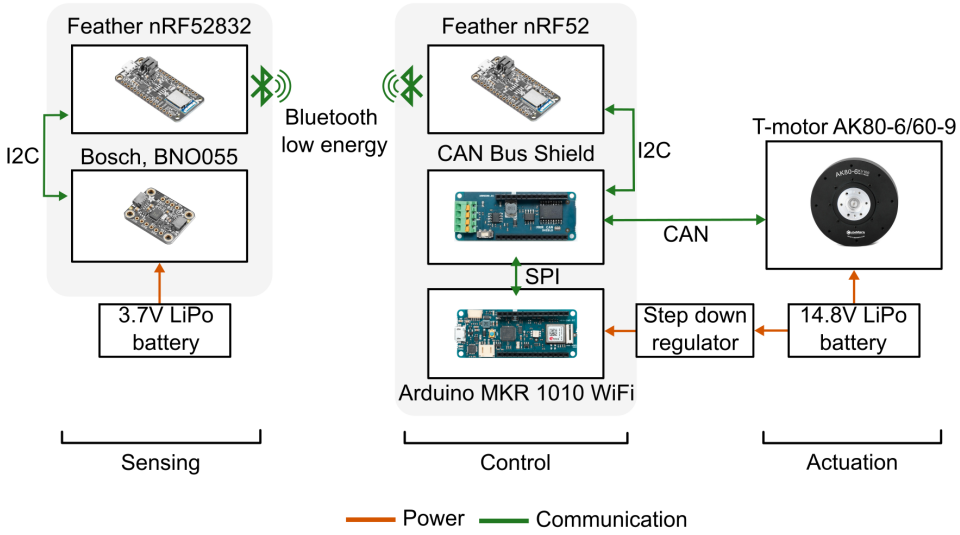


Figure 3.4. Control unit and sensing. Overview of the control and sensing system: the microcontroller communicates with motors via CAN bus and sensors via Bluetooth Low Energy (BLE). IMU sensors on the thigh monitor hip motion.

3.3.3 Control unit and sensing

The control unit is based on a microcontroller (Arduino MKR 1010 WiFi, Arduino, Italy), operating at a frequency of 100 Hz, which communicates with the motors through the CAN bus protocol.

For real-time movement monitoring, the sensor unit is equipped with two Inertial Measurement Unit (IMU) sensors (BNO055, Bosch, Germany), positioned laterally on the thigh harnesses. These sensors continuously track hip flexion angles and velocities in the sagittal plane, sending the data to the microcontroller via Bluetooth Low Energy (BLE).

Each sensor module is independently powered by a lithium-polymer battery (EEMB, 15.5g, 3.7V, 800mAh) and includes an IMU that communicates with a Feather nRF52832 board (Bluefruit, Adafruit) using the Inter-Integrated Circuit (I2C) protocol. This Feather board serves as the transmitter, while a corresponding board in the control unit acts as the BLE receiver for data transfer.

The entire suit is powered by a lithium-polymer battery (Tattu, 400g, 14.8V, 3700mAh), which provides the necessary energy for operation while ensuring portability. The battery, along with the other electronic components and actuators, is housed in custom 3D-printed enclosures made from PLA material. These housings are placed on the back of the waist to optimize weight distribution and minimize interference with natural movement.

3.4 Outline of the control framework: requirements and generalizability

The control framework for the soft robotic suit should be designed to provide assistive forces during human locomotion by actuating tendon displacement based on the kinematics of the hip joint (Fig. 3.1-(d)). This section outlines the core principles and overarching design requirements of the framework, while detailed implementation specifics are presented in subsequent chapters.

A key goal of this framework (objective 1, "Technological development", outlined in Chapter 1) is to establish a control scheme that minimizes the need for external calibration and generates accurate motor commands using only a single sensory input. This approach contrasts with many existing methods in the literature, where systems often rely on multiple sensors, such as force sensors [14, 69], EMG [55, 70, 71], or combinations of sensing modalities [72], to estimate user intent and deliver assistance. While such systems can achieve precise control, they typically require labor-intensive calibration procedures to adapt to individual differences in anthropometry, gait patterns, and walking conditions, which limits scalability and increases setup time [49].

The proposed framework aims therefore to rely on a single sensor to measure hip motion, simplifying system setup and eliminating the need for anthropometric scaling or extensive calibration. In this sense, motion sensor data can drive a position-based closed-loop control system, dynamically adapting tendon displace-

ment - and, consequently, assistive torque - based on the user's natural gait dynamics and leg weight. Such a streamlined control strategy simplifies operation and supports broad compatibility across diverse user populations.

The control framework can be organized into three hierarchical levels (Fig. 3.5):

- **High-level controller:** aims to estimate the user's gait phase in real-time based on hip kinematic data, such as angle and velocity. The high-level controller can be enhanced with a module to detect the environmental context, enabling it to differentiate between ground and stairs.

- **Mid-level controller:** aims to generate actuator reference position trajectories according to the user's gait phase (and context).

- **Low-level controller:** translates these trajectories into precise tendon displacement by commanding the actuators with a closed-loop control trying to minimize the error between the desired position trajectory and the actual motor position.

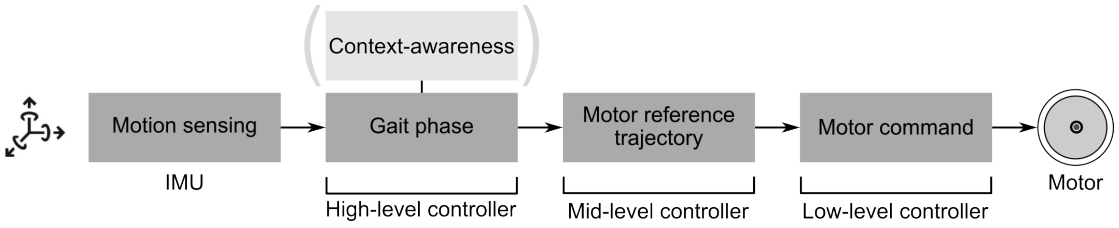


Figure 3.5. Outlook of the general control framework.

The pseudocode below provides an overview of the general control framework, detailing the key processes managed by its three layers and outlining the flow of information from sensors to actuators. This includes determining the gait phase (ϕ) using hip angle and velocity measurements ($\theta, \dot{\theta}$) from the sensors, which are then used to compute a motor reference position trajectory (θ_{ref}). The system compares this reference trajectory with the actual motor position (θ_m) to minimize error. Chapters 4, 5, and 6 delve into the specific algorithms and methods developed for each component. Additionally, the framework can incorporate advanced sensing techniques to estimate the environmental context (C), allowing modulation of the motor reference position trajectory's amplitude based on walking conditions. Chapter 5 introduces a novel computer vision approach to achieve this adaptation.

Algorithm 1 General control framework pseudocode

function HIGH_LEVEL_CONTROLLER($\theta, \dot{\theta}$)
    $\phi \leftarrow$ ESTIMATE_GAIT_PHASE($\theta, \dot{\theta}$)
    $C \leftarrow$ ESTIMATE_CONTEXT
    return ϕ, C
end function

function MID_LEVEL_CONTROLLER(ϕ, C)
    $\theta_r \leftarrow A(C)\sin(\phi)$
    $\theta_{\text{ref}} \leftarrow$ CUBIC_SPLINE_INTERPOLATION(θ_r)
    return θ_{ref}
end function

function LOW_LEVEL_CONTROLLER($\theta_{\text{ref}}, \theta_{\text{m}}$)
    motor_command $\leftarrow$ PID_CONTROLLER($\theta_{\text{ref}} - \theta_{\text{m}}$)
    return motor_command
end function

function MAIN_CONTROLLER($\theta, \dot{\theta}, \theta_{\text{m}}$)
    $\phi, C \leftarrow$ HIGH_LEVEL_CONTROLLER($\theta, \dot{\theta}$)
    $\theta_{\text{ref}} \leftarrow$ MID_LEVEL_CONTROLLER(ϕ, C)
    motor_command $\leftarrow$ LOW_LEVEL_CONTROLLER($\theta_{\text{ref}}, \theta_{\text{m}}$)
    return motor_command
end function

function STOP_CONDITION($\theta, \dot{\theta}$, stop_threshold)
    if speed_gait < stop_threshold **then**
        return True
    else
        return False
    end if
end function

MAIN CODE
while True **do**
    $\theta, \dot{\theta} \leftarrow$ READ_SENSORS
    if not STOP_CONDITION() **then**
        motor_command $\leftarrow$ MAIN_CONTROLLER($\theta, \dot{\theta}, \theta_{\text{m}}$)
        ACTUATE_MOTOR(motor_command)
    else
        STOP_MOTOR
    end if
end while

3.4.1 Generalizability of the control framework

A central aspect of the proposed control framework is its *generalizability*, designed to adapt across different users and hardware configurations. This feature directly addresses objective 1 outlined in Chapter 1.

Generalizability across users

By deriving an reference position trajectory for the actuator based on the user's movements, the system dynamically adjusts the assistive torque in real-time to accommodate the user's leg weight. This is achieved by commanding the actuator to reach specific angular positions, which are translated into tendon displacements. Consequently, the exerted motor torque naturally adapts to the load (i.e., the weight of the user's leg). This approach eliminates the downside of torque-controlled systems that needs to be manually scaled to the anthropometry of the user, offering a more intuitive, adaptable, and plug-and-play solution.

Generalizability across hardware configurations

The general framework outlined here can be easily adapted to a variety of hardware configurations, including both underactuated (UA) and fully-actuated (FA) versions of the soft robotic suit. This flexibility allows for a unified approach to tendon-driven actuation, preserving the core of the control framework and providing adjustments only to the input and output signals to accommodate the specific mechanical characteristics.

In the context of this dissertation, the two actuation configurations explored, underactuated (UA) and fully-actuated (FA), differ in the way they manage tendon displacement. The following paragraphs describe how the control framework is adapted for each configuration (Fig. 3.6):

Underactuated configuration (UA) In the UA configuration (Fig. 3.6-(a)), the control strategy can leverage the inter-limb flexion angle as input, calculated as the difference between the flexion angles of the left and right hips. The two artificial tendons are wound in opposite directions on a double-layer pulley mounted atop the motor. This arrangement allows the input signal to drive a symmetrical motor trajectory, where the motor alternately pulls one tendon while releasing the other by an equal amount, in sync with the alternating swing phases of the legs.

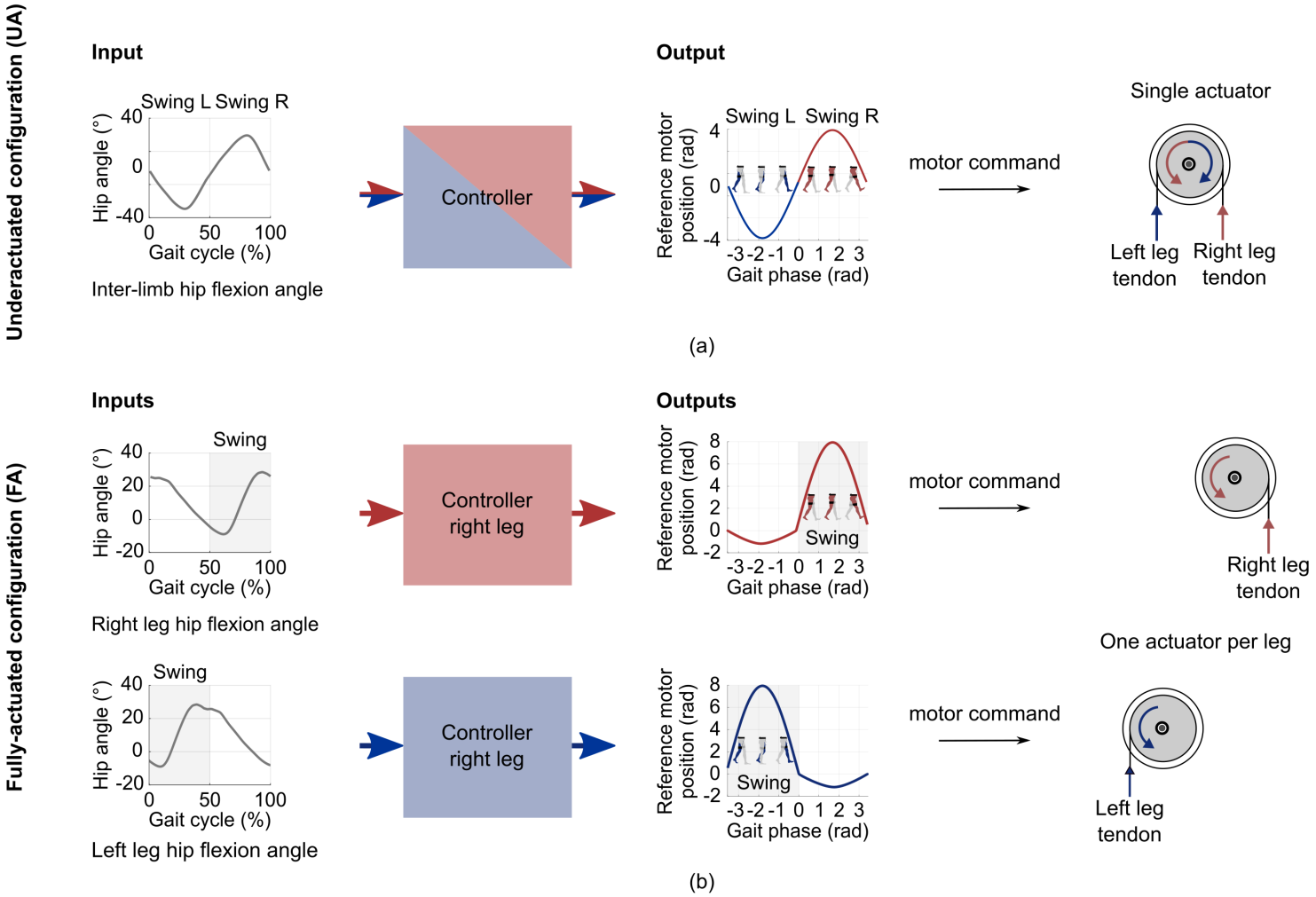


Figure 3.6. Control framework generalizability across hardware configurations. (a) Underactuated (UA) configuration. (b) Fully-actuated (FA) configuration.

Fully-actuated configuration (FA) In the FA configuration (Fig. 3.6-(b)), each leg is equipped with an independent motor, allowing the system to process the flexion angle of each hip independently. This can enable the generation of separate motor trajectories for each leg, providing independent control over tendon displacement for each side. During the swing phase, the actuators assist hip flexion by pulling on the respective tendons, while releasing them of a lower amount during hip extension.

Chapter 4

Adaptive controller to support leg swinging

The contents of this chapter are adapted from the journal papers:

E. Tricomi, N. Lotti, F. Missiroli, X. Zhang, M. Xiloyannis, T. Müller, S. Crea, E. Papp, J. Krzywinski, N. Vitiello, and L. Masia "*Underactuated soft hip exosuit based on adaptive oscillators to assist human locomotion*", **IEEE Robotics and Automation Letters**, vol. 7, no. 2, pp. 936–943, 2021.

E. Tricomi† and X. Zhang†, F. Missiroli, N. Lotti, C. Bokranz, D. Nicklas, and L. Masia, "*Enhancing gait assistance control robustness of a hip exosuit by means of machine learning*", **IEEE Robotics and Automation Letters**, vol. 7, no. 3, pp. 7566–7573, 2022.

This chapter presents a control strategy for gait phase estimation in the soft robotic suit, utilizing an Adaptive Oscillator (AOs)-based controller to enable real-time estimation by treating the hip joint as a dynamic oscillator. This approach leverages the sinusoidal motion patterns inherent in human walking, allowing the system to adapt to changes in walking cadence and synchronize robotic assistance with the user's natural gait. The AOs-based controller demonstrates effective performance in controlled treadmill walking but exhibits delays when transitioning between cadences (couple of steps) or initiating movement from a standstill (up to eight steps). To overcome these limitations, the chapter introduces in its final part an ML-augmented AOs controller, designed to enhance robustness in unstructured environments such as overground walking. This layered approach integrates the adaptability of AOs with the noise rejection and predictive capabilities of ensemble learning, enabling real-time refinement of gait phase estimates during complex tasks, including ramps and u-turns. Comparative evaluations revealed that while both controllers performed similarly in treadmill walking, the ML-augmented system significantly reduced gait estimation errors and improved performance during overground walking, providing greater benefits to the user.

4.1 The leg as a dynamic oscillator

In the realm of assistive robotics, particularly for human locomotion, achieving effective synchronization between the robotic system and the user's gait phase is essential for providing natural and intuitive assistance. Over the years, gait phase estimation techniques have evolved to address this challenge, employing various methods to track user movement patterns and ensure that robotic assistance aligns with the natural walking cycle [73].

These techniques often rely on a combination of sensors to analyze joint motion and include strategies such as modeling joint trajectories as phase-dependent variables [74], classifying gait cycle phases via inertial sensors [75], detecting sub-phases using ground reaction force data [76], and monitoring muscle activity through EMG signals [77, 78]. The critical aim of these approaches is to track gait phases reliably and dynamically, ensuring that the system can adapt to variations in walking speed, stride length, and cadence.

Walking, by nature, is a rhythmic activity where the trajectories of certain lower-limb joints, such as the hip, can be closely approximated by sinusoidal waveforms. The leg, particularly the hip joint, can be modeled effectively as a dynamic oscillator since the motion resembles a sinusoidal oscillation that can be decomposed into a fundamental frequency and its harmonics. Specifically for the hip joint, in the sagittal plane, this motion can be represented as the sum of three harmonics, capturing the fundamental rhythm and higher-order dynamics that arise from complex muscle-tendon interactions and gravitational forces [79]. This sinusoidal representation provides a natural framework for estimating the gait phase, as the joint angle can be directly mapped to the phase extracted from the periodic signal. Such a model offers a simplified yet accurate representation of human locomotion.

To dynamically track the key components of this oscillatory motion, namely frequency and phase, a promising approach involves leveraging Adaptive Oscillators (AOs). First introduced by Righetti et al. in the early 2000s [80, 81], AOs are nonlinear mathematical tools designed to capture and track the essential features of periodic signals, such as frequency, amplitude, phase, and offset.

From a mathematical perspective, AOs are modeled as oscillators that can dynamically adjust their internal parameters to synchronize with an external periodic signal given as input. While classic non linear oscillators have finite entrainment region, meaning they can synchronize only within certain bounds of frequency and

phase, AOs incorporate instead adaptive mechanisms to overcome these limitations. Specifically, by introducing dynamics into the parameters of the oscillator, it becomes possible for the system to "learn" the frequency of an input signal, adapting continuously to changes in the periodic input. This adaptation is akin to dynamic Hebbian learning, a mechanism often seen in neural networks, where the system learns and encodes the frequency of the input signal even after the signal disappears. This adaptation process goes beyond mere entrainment, allowing the oscillator to operate independently of initial conditions, making it suitable for a wide range of dynamic systems [80, 81].

This chapter explores the application of Adaptive Oscillators (AOs) theory to the real-time control of the soft robotic suit presented in Chapter 3, designed to assist hip flexion during walking. An AOs-based gait phase estimator was integrated into the high-level controller, using only sagittal plane hip flexion angles recorded by inertial measurement unit (IMU) sensors as input. The estimator dynamically adjusts to changes in the user's walking cadence, autonomously learning the frequency, amplitude, and phase of the hip flexion trajectory. This adaptability ensures precise synchronization with the user's natural motion, facilitating effective and intuitive assistance by the robotic suit.

Hypothesis An AOs-based controller for the soft robotic suit can enable user-adaptive assistance by accurately synchronizing with the wearer's natural gait patterns.

4.2 AOs-based real-time control framework

The real-time control system was evaluated using the underactuated configuration of the soft robotic suit (Fig. 4.1-(a)) and implemented in MATLAB/Simulink. The framework consists of three layers: a high-level controller that estimates the gait phase by monitoring the hip flexion angle with Adaptive Oscillators (AOs) [80], a mid-level controller that generates the desired motor reference trajectory based on the gait phase, and a low-level controller that delivers the required assistance to both legs according to their motion.

The three layers are described in details henceforth and schematically shown in Figure 4.1-(b).

4.2.1 High-level controller: gait phase estimator

The high-level controller is tasked with estimating the gait phase in real-time using kinematic data, specifically the hip flexion angles, through an AOs-based approach. This model, adapted from Yan et al. [79], serves as the *gait phase estimator*.

The *gait phase estimator* consists of three main components: (1) the AOs dynamic system, (2) the gait event detection module, and (3) the phase error correction module. These components are explained in more detail in the following sections. The structure, initially proposed by Yan et al. [79], has been modified for an underactuated system, where the driving signal is the inter-limb angle, $\theta_{\mathrm{IL}}(t)$, representing the difference between the angular displacements of the right and left hips. Assistance is provided to each leg only during the swing phase, with no assistive forces applied during the stance phase.

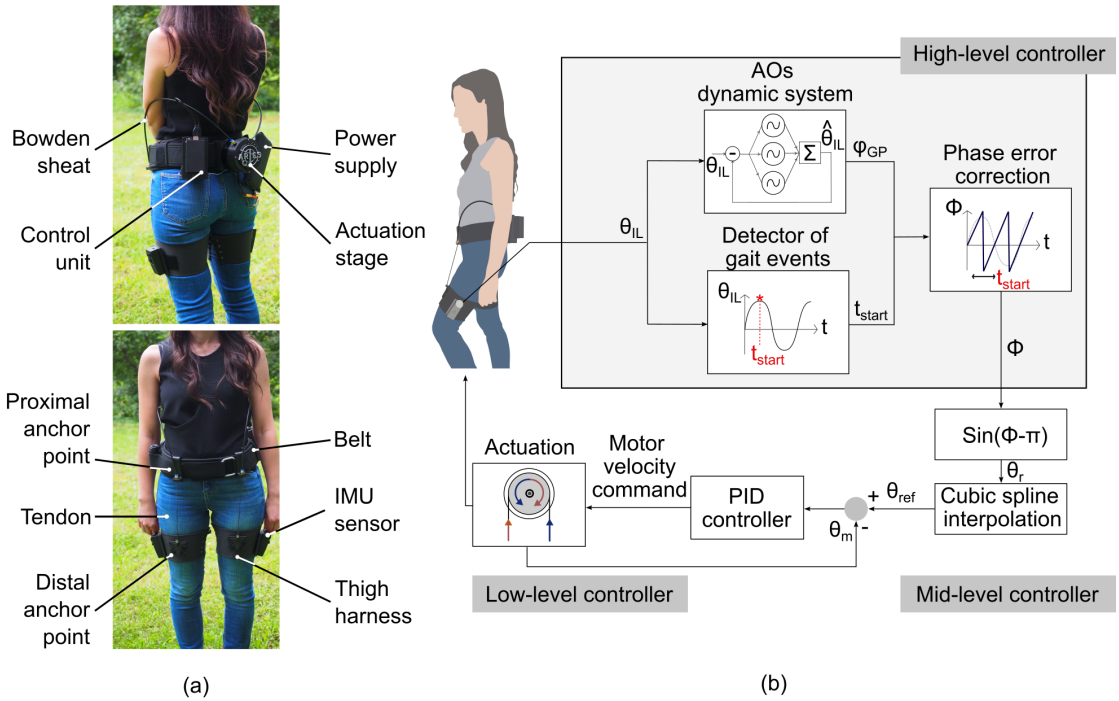


Figure 4.1. Soft robotic suit and AOs-based control framework. (a) Underactuated soft robotic suit. (b) The real-time control system based on Adaptive Oscillators (AOs) employs the AOs dynamic system module in the high-level controller to estimate the gait phase $\varphi_{\mathrm{GP}}(t)$ by tracking the inter-limb hip flexion angle $\theta_{\mathrm{IL}}(t)$. The gait phase $\varphi_{\mathrm{GP}}(t)$ is updated dynamically at the beginning of each stride. The mid-level controller then converts the corrected gait phase $\phi(t)$ into a motor reference trajectory $\theta_{\mathrm{ref}}(t)$ using cubic spline interpolation. Finally, the PID controller processes the position error between the motor reference trajectory and the actual motor position $(\theta_{\mathrm{ref}} - \theta_{\mathrm{m}})$ to generate the motor's angular velocity command.

AOs dynamic system The AOs dynamic system serves as the core of the gait phase estimation strategy, reconstructing the inter-limb flexion angle $\theta_{\mathrm{IL}}(t)$ as the sum of sinusoidal functions:

$$\hat{\theta}_{\mathrm{IL}}(t) = \alpha_0(t) + \sum_{n=1}^{N} \alpha_{\mathrm{n}}(t) \sin(\varphi_{\mathrm{n}}(t)) \tag{4.1}$$

where $\hat{\theta}_{\mathrm{IL}}(t)$ is the reconstructed input signal, $\alpha_{\mathrm{n}}(t)$ and $\varphi_{\mathrm{n}}(t)$ represent the amplitude and phase of each harmonic, and $\alpha_0(t)$ is the offset. The number of harmonics was set to $N = 3$ as suggested in [79] to effectively track human walking biomechanics.

Equations below describe how the signal features are dynamically extracted [80]:

$$\dot{\varphi}_{\mathrm{n}}(t) = \omega(t) \cdot n + \nu_{\varphi} \frac{F(t)}{\sum \alpha_{\mathrm{n}}} \cos(\varphi_{\mathrm{n}}(t)) \tag{4.2}$$

$$\dot{\omega}(t) = \nu_{\omega} \frac{F(t)}{\sum \alpha_{\mathrm{n}}} \cos(\varphi_1(t)) \tag{4.3}$$

$$\dot{\alpha}_{\mathrm{n}}(t) = \eta F(t) \sin(\varphi_{\mathrm{n}}(t)) \tag{4.4}$$

$$\dot{\alpha}_0(t) = \eta F(t) \tag{4.5}$$

where $F(t) = \theta_{\mathrm{IL}}(t) - \hat{\theta}_{\mathrm{IL}}(t)$ is the driving signal that ensures convergence, $\omega(t)$ is the fundamental frequency, $\nu_{\varphi}, \nu_{\omega}$, and η are the learning gains for phase, frequency, and amplitude, respectively. Through offline preliminary tests, the gains were tuned to $\nu_{\varphi} = 20$, $\nu_{\omega} = 20$, and $\eta = 5$.

The fundamental phase, $\varphi_1(t)$, is normalized within the interval $[0, 2\pi)$ to define a continuous gait phase variable, $\varphi_{\mathrm{GP}}(t)$, that evolves through a complete stride:

$$\varphi_{\mathrm{GP}}(t) = \mathrm{mod}(\varphi_1(t), 2\pi) \tag{4.6}$$

Detector of gait events This module detects the beginning of each gait cycle by identifying gait events. From $\theta_{\mathrm{IL}}(t)$, the start of a stride is marked as the instant of maximum hip flexion, which corresponds to the moment when the hip angular velocity crosses zero.

To eliminate erroneous detections, a selected time t_{i} is accepted as a valid stride start (t_{start}) only if it is at least $0.7 \times T(t)$ apart from the previous detection, where $T(t)$ is the stride period computed as $T(t) = 2\pi/\omega(t)$.

Phase error correction The phase error correction module aligns the gait phase variable $\varphi_{\mathrm{GP}}(t)$ with each detected gait event, t_{start}. The alignment is performed by adjusting the error in the phase variable using the following equation:

$$\dot{\varphi}_{\mathrm{e}} = C_{\mathrm{e}}\omega(t)e^{-\omega(t)(t-t_{\mathrm{start}})} \tag{4.7}$$

where $C_{\mathrm{e}} = k_{\mathrm{e}}(P_{\mathrm{e}}(t_{\mathrm{start}}) - \varphi_{\mathrm{e}}(t_{\mathrm{start}}))$ is a proportional gain, and $P_{\mathrm{e}}(t_{\mathrm{start}})$ represents the initial mismatch:

$$P_{\mathrm{e}}(t_{\mathrm{start}}) = \begin{cases} -\varphi_{\mathrm{GP}}(t_{\mathrm{start}}), & 0 \leq \varphi_{\mathrm{GP}}(t_{\mathrm{start}}) < \pi, \\ 2\pi - \varphi_{\mathrm{GP}}(t_{\mathrm{start}}), & \pi \leq \varphi_{\mathrm{GP}}(t_{\mathrm{start}}) < 2\pi. \end{cases} \tag{4.8}$$

Finally, the corrected gait phase $\phi(t)$ is obtained as:

$$\phi(t) = \mathrm{mod}(\varphi_{\mathrm{GP}}(t) + \varphi_{\mathrm{e}}(t), 2\pi) \tag{4.9}$$

4.2.2 Mid-level controller

The high-level controller provides the estimated gait phase $\phi(t)$ as input to the mid-level controller, which generates a desired motor reference position trajectory. This reference position, $\theta_{\mathrm{ref}}(t)$, is computed by first shifting the gait phase by π and then applying a sinusoidal function:

$$\theta_{\mathrm{r}}(t) = \sin(\phi(t) - \pi) \tag{4.10}$$

The final reference $\theta_{\mathrm{ref}}(t)$ is determined using cubic spline interpolation of $\theta_{\mathrm{r}}(t)$.

4.2.3 Low-level controller

A feedback position loop compares the actual motor position $\theta_{\mathrm{m}}(t)$ with the reference position $\theta_{\mathrm{ref}}(t)$. A PID controller then converts the position error $(\theta_{\mathrm{ref}} - \theta_{\mathrm{m}})$ into motor velocity, governed by the following transfer function:

$$Y(s) = \frac{K_p + K_i \cdot \frac{1}{s}}{1 + K_d \cdot s} \tag{4.11}$$

where the gains K_p, K_i, and K_d were tuned in preliminary trials for accurate tracking of $\theta_{\mathrm{ref}}(t)$.

4.3 Evaluation and effects on human movements

An experimental evaluation was conducted with healthy individuals aimed to assess the performance of the controller and the effects of the soft robotic suit on muscular effort and walking kinematics.

4.3.1 Experimental protocol and data collection

Six healthy individuals participated in the study (Table 4.1), comprising four females and two males with an average age of 27.14 ± 1.86 years, a mean weight of 67.29 ± 15.37 kg, and an average height of 172.14 ± 12.40 cm. None of the participants reported any history of musculoskeletal or neurological conditions. Prior to the experiments, all participants provided written informed consent. The study adhered to the principles outlined in the Declaration of Helsinki and received approval from the Ethical Committee of Heidelberg University (resolution S-313/2020).

Participant	Age (year)	Weight (kg)	Height (cm)	Sex (-)
①	29	90	185	M
②	28	54	163	F
③	26	85	193	M
④	26	48	158	F
⑤	29	62	168	F
⑥	28	64	173	F

Table 4.1. Participants demographic.

Participants performed two tasks while walking on an actuated treadmill (Merax, G500): variable speed walking and constant speed walking.

Variable speed walking To assess the controller's ability to adapt to changing walking patterns, participants performed a variable speed walking task. Over a duration of five minutes, the treadmill speed alternated between 0.4 m/s, 0.7 m/s, and 1.0 m/s, with each speed maintained for one minute.

Constant speed walking A constant speed walking task was conducted to evaluate the impact of assistance on hip kinematics and muscle activity. Participants walked at three fixed speeds (0.4 m/s, 0.7 m/s, and 1.0 m/s), completing a five-minute trial at each speed.

Trials were conducted under two conditions: (1) *assistance on*, where the robotic suit actively delivered assistance, and (2) *assistance off*, in which participants wore the suit with the power supply switched off and tendons untied. To avoid the effect of fatigue, participants rested for 10 min between trials, and the order of tasks, speeds, and conditions was randomized.

Data were collected to assess the performance of the controller and to examine the effects of the robotic suit on both walking kinematics and muscle activity. Surface electromyography (sEMG) signals were acquired using a Trigno wireless multi-channel system (Delsys, Natick, MA, USA), with electrode placement following SENIAM guidelines [82]. The monitored muscles included the Tensor Fasciae Latae (TFL) and Semitendinosus (ST), which are involved in hip flexion and extension, as well as the Tibialis Anterior (TA) and Gastrocnemius Lateralis (GL) to evaluate any impact on unassisted joints. Electromyographic data were sampled at 1 kHz using a Quanser QPIDe data acquisition board (Markham, Ontario, Canada). Before the experiments, maximum voluntary contractions (MVCs) were recorded for each muscle to enable normalization of the sEMG data during analysis.

4.3.2 Data analysis

Controller performance For the variable walking speed task, the primary focus was on the controller's ability to track the user's walking intention. The walking angular frequency estimated by the AOs-based controller, ω_{AOs}, was compared to the angular frequency measured at the hip joint via inertial measurement units (IMUs), ω_{stride}. Kinematic data from the IMUs were low-pass filtered at 10 Hz using a fourth-order Butterworth filter and segmented into strides. The stride angular frequency was computed as $\omega_{\text{stride}_i} = 2\pi/T_i$, where T_i is the period of the i-th stride. Tracking performance was assessed by calculating the root mean square error (RMSE) between ω_{AOs} and ω_{stride}, and the coefficient of determination (r^2) between the two signals.

Motor torque and power Motor torque data were low-pass filtered at 10 Hz (fourth-order Butterworth filter), normalized to each participant's weight, and segmented into swing phases for each leg. Motor power was calculated as the product of normalized torque and motor angular velocity.

Kinematics Hip kinematics was analyzed by segmenting IMU data into steps, following low-pass filtering at 10 Hz (Butterworth filter, fourth order). Step ini-

tiation and termination were determined based on hip angular velocity. Mean peak velocities in stance (negative peak) and swing (positive peak) were compared between the *assistance on* and *assistance off* conditions.

Muscle activity Muscle activity analysis involved band-pass filtering sEMG signals between 20 Hz and 400 Hz (fourth-order Butterworth filter), full-wave rectification, and low-pass filtering at 6 Hz to derive the sEMG envelope. Signals were normalized to the MVC for each muscle and segmented into steps using kinematic data. The root mean square (RMS) of the sEMG signal was computed for each step and averaged across steps for each trial.

Statistics Data distributions were tested for normality using the Shapiro-Wilk test ($\alpha = 0.05$). A two-way repeated measures ANOVA was performed to examine the effects of condition (*assistance on* vs. *assistance off*) and walking speed (0.4 m/s, 0.7 m/s, and 1.0 m/s) on kinematic and muscle activity metrics for both legs. Post-hoc pairwise comparisons were conducted using Fisher's LSD test when significant interactions were found. Results are presented as mean values with standard error of the mean (s.e.m) or standard deviation (SD) when specified.

4.3.3 Results

Controller performance An example of the gait phase estimated by the AOs-based controller is provided in Figure 4.2-(a) for a representative participant during few seconds of walking in the variable walking speed task. Figure 4.2-(b) illustrates the angular frequency estimated by AOs (ω_{AOs}) alongside the measured angular frequency (ω_{stride}) for a representative participant during the variable speed walking task. The RMSE values calculated between these two frequencies, aggregated across cycles for all participants, are presented in the histogram in Fig. 4.2-(c). The average RMSE, computed across all strides and subjects, was 0.26 ± 0.29 rad/s (mean $\pm$ SD). Figure 4.2-(d, e) highlight the correlation between measured and estimated angular frequencies for a representative participant, demonstrating strong agreement. The mean coefficient of determination (r^2) across subjects was 0.70 ± 0.22.

Motor torque and power Figure 4.3-(a) displays the average motor torque and power profiles throughout a stride for the 0.7 m/s trial. Negative torque values correspond to assistance during the left leg swing, while positive values represent assistance during the right leg swing. The mean motor torque profiles for each

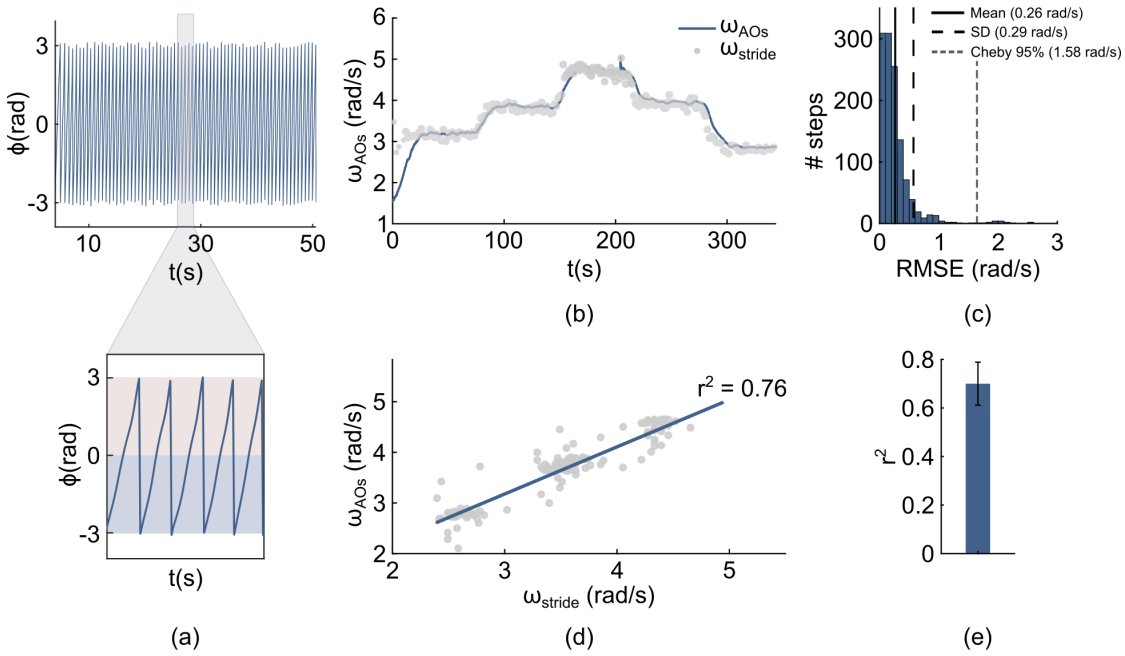


Figure 4.2. Controller performance. (a) Gait phase estimated by Adaptive Oscillators (AOs) during a segment of the variable speed walking task for a representative participant, with a detailed view of several steps. (b) Comparison of walking angular frequency estimated by AOs (ω_{AOs}) and measured stride angular frequency (ω_{stride}) during the variable speed task for a representative participant. (c) Root Mean Square Error (RMSE) between ω_{AOs} and ω_{stride} for each gait cycle across all participants. (d) Angular frequency tracking performance for a representative participant. (e) Mean coefficient of determination (r^2) for angular frequency tracking across all participants.

subject across different constant speed trials, separated by leg, are shown in Fig. 4.3-(b). Peak motor torque values, averaged across participants, were recorded as -0.042 ± 0.004 and 0.042 ± 0.004 Nm/kg (left and right, respectively) for the 0.4 m/s trial; -0.037 ± 0.004 and 0.044 ± 0.002 Nm/kg for the 0.7 m/s trial; and -0.029 ± 0.003 and 0.030 ± 0.002 Nm/kg for the 1.0 m/s trial.

Kinematics Figure 4.4-(a) presents hip velocity profiles at 0.7 m/s for a representative participant in both the *assistance off* and *assistance on* conditions. The solid line represents the mean across steps during 3 min of walking, with shaded areas indicating the standard deviation (SD). Bar plots represent averaged data across participants. When comparing peak velocities during swing (positive peak) and stance phases (negative peak) across the three constant speed trials, a slight increase was observed in swing peak velocities and a reduction in stance peak velocities under the *assistance on* condition. Significant differences, however, were found only at 0.4 m/s. Specifically, for the left leg during the swing phase, the

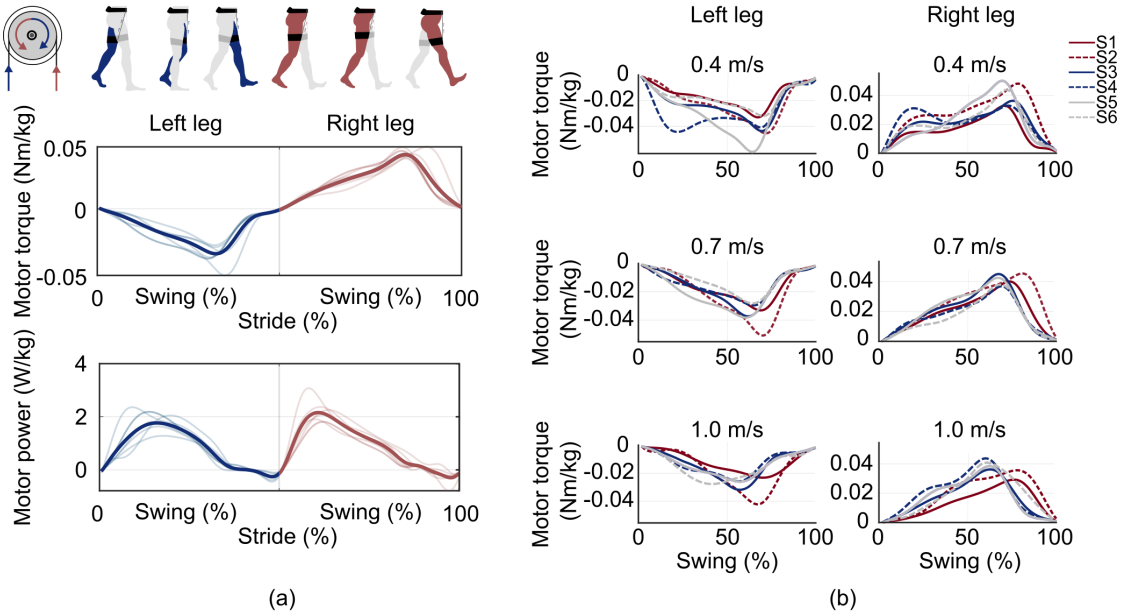


Figure 4.3. Motor torque and power. (a) Motor torque and power profiles during walking at 0.7 m/s across a complete gait cycle. Negative torque values indicate assistance to the left leg (blue), while positive values represent assistance to the right leg (red). Thin transparent lines show the average gait cycle for each subject over 3 minutes of walking, and the thick line represents the overall mean across all participants. (b) Motor torque profiles for constant-speed walking trials (0.4 m/s, 0.7 m/s, 1.0 m/s), presented separately for the left and right legs. Each line reflects the mean gait cycle for individual subjects over 3-min walking.

average peak velocities were 67.61 ± 7.63 and 85.20 ± 6.50 °/s for the *assistance off* and *assistance on* conditions, respectively ($p = 0.004$). For the stance phase at the same speed, significant differences were observed for both legs ($p < 0.005$).

Muscle activity The impact of the suit on muscle activation is depicted in Fig. 4.4-(b) for the Tensor Fasciae Latae (TFL) and Semitendinosus (ST) muscles. EMG envelopes are shown for a representative participant at 0.7 m/s, comparing the *assistance off* and *assistance on* conditions. Solid lines is the mean among steps in 3 min walking; shaded areas is the SD. Data are presented in percentage of step duration. Bar plots summarize the normalized RMS values averaged across all participants for each trial. The TFL activation showed a significant reduction at 0.4 m/s during *assistance on*. For the left leg, the RMS values were $4.54 \pm 0.50\%$ MVC (*assistance off*) and $3.72 \pm 0.68\%$ MVC (*assistance on*) ($p = 0.02$). For the right leg, the values were $6.85 \pm 1.70\%$ MVC (*assistance off*) and $5.42 \pm 1.28\%$ MVC (*assistance on*) ($p = 0.03$). At 0.7 m/s, a similar reduction in TFL activation was observed. For the left leg, RMS values decreased from $5.21 \pm 1.70\%$ MVC

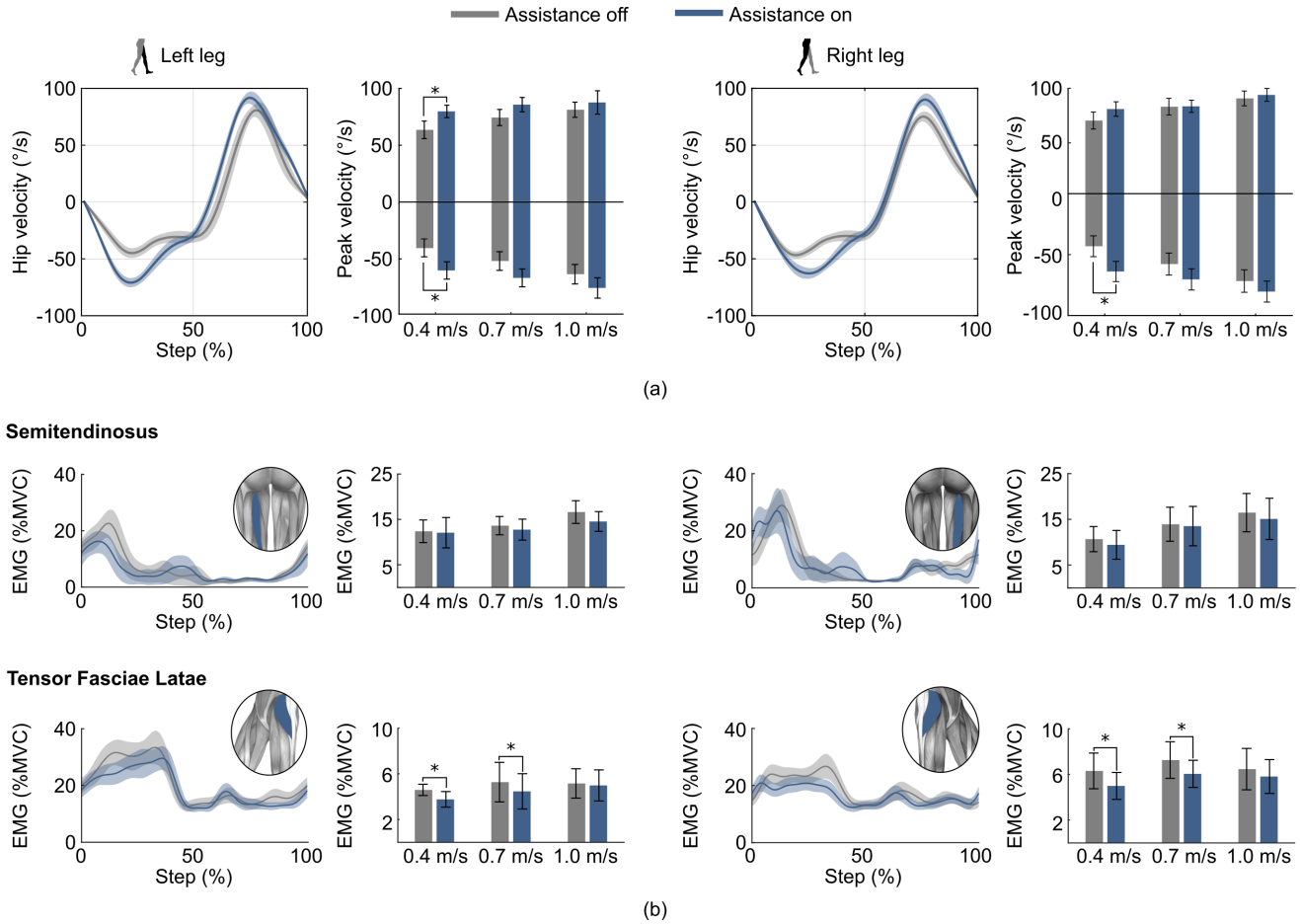


Figure 4.4. Kinematics and muscle activity. (a) Hip velocity profiles as a percentage of step duration for both legs during walking at 0.7 m/s, shown for a representative participant. The bar graph depicts the average positive (swing phase) and negative (stance phase) peak hip velocities across participants for the three constant speed conditions. (b) EMG envelopes of the Semitendinosus (top) and Tensor Fasciae Latae (bottom) muscles for both legs at 0.7 m/s, displayed for a representative participant. The bar graph shows average muscle activation (RMS) across participants for the three constant speed conditions.

(*assistance off*) to $4.41 \pm 1.53\%$ MVC (*assistance on*) ($p = 0.04$). For the right leg, the values changed from $7.88 \pm 1.74\%$ MVC (*assistance off*) to $6.57 \pm 1.29\%$ MVC (*assistance on*) ($p = 0.04$). No significant differences in TFL activation were noted at 1.0 m/s. Furthermore, for the Semitendinosus (ST), Tibialis Anterior (TA), and Gastrocnemius Lateralis (GL), no statistically significant differences in muscle activation were found between the *assistance off* and *assistance on* conditions across all trials.

4.4 Discussion

Human walking is a highly efficient and adaptable process, honed by evolution to respond to both predictable and unpredictable environmental demands. Assistive technologies aimed at enhancing locomotion must align with this inherent adaptability while preserving natural movement patterns.

This study introduces an Adaptive Oscillator (AOs)-based controller to provide bilateral assistance, offering a streamlined approach that reduces the need for extensive calibration or complex hardware. By modeling the leg as a dynamic oscillator, the controller dynamically synchronizes with changes in walking cadence, ensuring seamless integration with the user's natural gait. While prior research demonstrated the feasibility of oscillator-based control in single-joint systems [79], this work extends the concept to bilateral assistance, showcasing how underactuation can be leveraged for balanced and dynamic support.

The system demonstrated robust control performance, achieving low error in gait phase estimation ($0.26 \pm 0.29\,\text{rad/s}$) and rapid adaptation to changes in cadence, typically within a couple of steps (Fig. 4.2). These findings are consistent with previous studies using oscillator-based control in wearable devices [79], reaffirming the efficacy of this approach for adaptive assistance. However, the system's ability to resynchronize during movement initiation from a standing position remains a limitation, requiring up to eight steps for full adaptation. Such delays could present challenges in environments where rapid transitions in gait are frequent or unpredictable.

On the hardware front, the proposed system exemplifies the effective application of AOs in an underactuated configuration. Utilizing a single motor, the system delivers symmetrical assistance to both legs, providing significant advantages in weight and simplicity over traditional multi-actuator solutions. The compact de-

sign (2.2 kg) is particularly notable when compared to similar systems, such as the 6.6 kg suits developed by Panizzolo et al. [67]. Despite its minimalist approach, the system delivers consistent torque and power profiles across different users and walking conditions, as depicted in Fig. 4.3.

The reduction in muscle activation achieved by the suit is a key outcome of this study. Participants exhibited reductions of up to 20% in muscle activity at slower walking speeds (0.4 m/s) and 15% at faster speeds (0.7 m/s), as illustrated in Fig. 4.4. These reductions indicate that the system's assistance closely aligns with the natural dynamics of walking and are comparable to, or exceed, results reported for similar assistive devices [67, 83]. However, muscle activity analysis was limited to the Tensor Fasciae Latae due to the placement of the suit's anchor points, which interfered with electrode positioning for other more relevant muscles, such as the Rectus Femoris.

The system's transparency to users, with minimal impact on their natural movement patterns, is another notable feature (Fig. 4.4). This transparency enhances comfort and ensures that the device does not hinder users when assistance is unnecessary.

While the study highlighted the effectiveness of the AOs-based controller under controlled treadmill conditions, it also revealed limitations. The fixed speed and predictability of treadmill walking do not fully replicate the variability of overground walking, where rapid changes in cadence and complex environmental interactions are common. Furthermore, the study did not investigate the system's metabolic impact, which is a critical metric for evaluating assistive devices. Lightweight hip flexion assistance systems have previously demonstrated significant metabolic savings [83,84], suggesting that the compact design of this suit could yield similar benefits. Future work should include detailed metabolic analyses to evaluate this potential.

The observed limitations in adapting to unpredictable cadence changes and movement initiation naturally lead to the exploration of strategies to improve the system's robustness in dynamic and unstructured environments. While the AOs-based controller proved effective in controlled treadmill tasks, challenges can persist in transitioning between different walking patterns or navigating irregular terrains. In scenarios requiring rapid gait changes, delays in cadence adaptation may hinder performance.

To address these issues, learning techniques can augment the existing system by

providing real-time refinement of desired motor trajectory estimates. Machine Learning (ML) methods have shown great promise in enhancing gait phase classification and improving controller robustness. The next section introduces a ML-augmented AOs controller, designed to address these gaps by integrating the adaptability of AOs with the predictive capabilities of ML. This approach aims to enhance performance in tasks like overground walking, ramps, and u-turns, where rapid resynchronization is crucial.

4.5 Increasing controller robustness via learning

The previous section demonstrated that the AOs-based controller performs effectively during treadmill walking, where cadence remains steady. However, when walking cadence changes, the controller requires few steps (a couple) to resynchronize to the new gait dynamics, with delays of up to approximately eight steps when transitioning from a standing position. Such delays could present significant challenges for unstructured scenarios, where walking patterns are inherently less predictable.

In the current state of the art, Machine Learning (ML) has shown significant potential for improving controller robustness, particularly in real-time gait phase estimation and classification [85–87]. Among these techniques, ensemble learning, which aggregates predictions from multiple weak learners, has proven especially effective in managing noisy or variable data [88, 89].

This section presents a modification of the previously presented control approach to address the need for enhanced robustness in scenarios requiring frequent resynchronization to changing cadences (e.g., overground walking, stepping on a ramp, u-turns etc.). This approach merges the AOs-based method with ensemble learning in a layered controller to improve the performance of dynamical estimators (e.g., AOs) during gait transitions. In this implementation, the high-level controller is divided into two parts: (1) AOs are used to estimate gait phase and extract kinematic features, and (2) these features are processed by an ensemble learning layer to refine the output. This dual-layer strategy combines the adaptability of AOs for rhythmic tasks with the noise rejection capabilities of ML to better handle irregular locomotion patterns.

The proposed framework was evaluated on six healthy subjects by comparing the AOs-only controller with the ML-augmented controller during both treadmill and

short overground walking tasks, comprising ramps and u-turns.

Hypothesis The primary hypothesis posits that, while both controllers perform similarly in fixed cadence scenarios, such as treadmill walking, the ML-augmented controller can exhibit superior performance in overground tasks characterized by more variable and unpredictable walking patterns.

4.5.1 ML-augmented controller

The proposed real-time control framework integrates Machine Learning (ML) into the Adaptive Oscillators (AOs)-based controller introduced earlier in this chapter (Fig. 4.1-(b)). Together, these components constitute the high-level controller: the *AOs layer*, which estimates the gait phase and generates an initial motor reference trajectory, and the *ML layer*, which enhances this trajectory to improve robustness and responsiveness during sudden changes in walking cadence (Fig. 4.5).

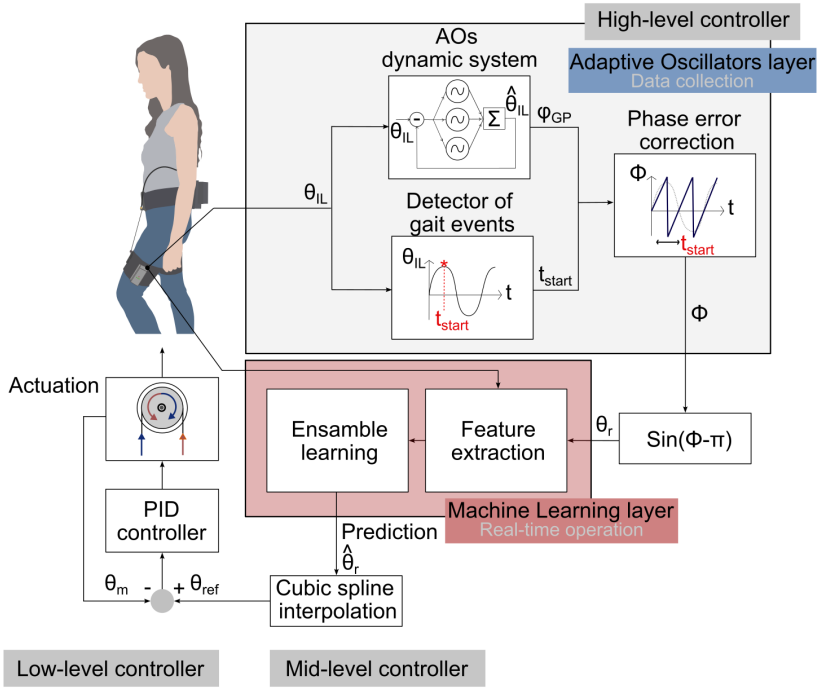


Figure 4.5. ML-augmented controller. The AOs layer in the high-level controller estimates the gait phase from the inter-limb hip flexion angle and generates a preliminary motor reference trajectory. This trajectory, combined with kinematic features, is used to train the ensemble learning model in the ML layer, which refines the reference motion for the actuator during real-time operation.

The mid-level and low-level controllers remain unchanged, as detailed in sections 4.2.2 and 4.2.3. Therefore, the following paragraphs focus on the tuning and implementation of the AOs and ML layers within this hierarchical framework. All stages of the control algorithm were developed and executed in MATLAB/Simulink (MathWorks, Natick, MA, USA). To run the ML layer, the underactuated soft robotic suit (Fig. 4.1-(a)) was complemented an embedded processor (NVIDIA Jetson Nano, Santa Clara CA, USA).

(1) AOs layer: training data collection

In this implementation, the AOs layer retains its mathematical foundation as described in section 4.2.1 but serves a distinct purpose. Here, it is utilized to generate synchronized and noise-free motor reference trajectories based on the estimated gait phase. These trajectories are recorded and subsequently used to train the ML layer for both offline learning and real-time operation.

To train the ML algorithm, a preliminary session was conducted with six healthy participants (Tab. 4.2; four females, two males; age: 26.50 ± 2.35 years; weight: 69.17 ± 20.91 kg; height: 1.72 ± 0.14 m). Participants walked on a treadmill for six minutes at progressively increasing speeds, starting at 0.4 m/s and increasing by 0.15 m/s each minute up to 1.15 m/s. During these trials, the AOs layer estimated clean gait phase trajectories and motor reference positions ($\theta_r(t)$) for each speed in its optimal operational scenario (i.e., treadmill walking). These trajectories formed the training dataset for the ML model.

(2) ML layer: real-time operation

The ML layer is responsible for generating precise motor reference trajectories $\hat{\theta}_r(t)$ during the real-time operation of the robotic suit. This is achieved after training based on data provided by the AOs layer and leveraging Ensemble Learning, a machine learning approach that combines the predictions of multiple weak learners to enhance accuracy and robustness while reducing noise sensitivity [88, 89]. This paradigm operates on the principle of the "wisdom of the crowd", where the aggregation of outputs from several weak models results in superior predictive performance compared to any individual model.

A key subset of ensemble learning is boosting algorithms, which are highly effective for regression and prediction tasks. Boosting builds a strong predictive

model incrementally by training a series of weak learners, each designed to correct the errors of its predecessors. The final prediction is obtained by combining these learners' outputs, with each contribution weighted to optimize accuracy and minimize error.

Among boosting methods, the LSBoost (Least Squares Gradient Boosting) algorithm stands out for its ability to minimize prediction errors using the least squared error as its objective function [90, 91]. LSBoost iteratively improves its model, ensuring progressively refined predictions.

The ML layer was implemented using the LSBoost algorithm via the `fitrensemble` function from the Statistics and Machine Learning Toolbox in MATLAB/Simulink 2021b (MathWorks, Natick, MA, USA).

Parameters optimization The Classification and Regression Trees (CART) algorithm was selected as the weak learner within the LSBoost regression framework. This decision was informed by prior studies demonstrating CART's superior performance compared to neural networks in tasks such as gait phase identification [92]. CART's ability to capture non-linear relationships and its computational efficiency make it well-suited for this application.

To maximize the predictive accuracy of the ML-augmented controller while maintaining real-time performance, three critical hyperparameters were optimized using the pre-recorded dataset. The parameters and their optimization strategies are detailed below:

a) Maximum number of decision tree splits: The maximum allowable splits for each decision tree were selected based on the dataset size, defined as $MaxSplits = 2^s$, where $s \in \{1, \dots, \log_2(m-1)\}$, and m is the total number of samples in the dataset. This ensures the decision tree depth scales appropriately with the available data.

b) Learning rate (η_1): The learning rate, which governs the contribution of each weak learner to the final ensemble, was tested across a range of values: $\eta_1 \in \{0.1, 0.25, 0.5, 1\}$. This parameter balances predictive accuracy with computational cost.

c) Number of regression trees (N): The total number of regression trees in the ensemble was varied from $N \in \{1, \dots, 100\}$. This parameter determines the

complexity of the final model, with more trees providing greater flexibility at the expense of computational efficiency.

The optimal hyperparameters were determined using 10-fold cross-validation [93] to evaluate model performance across different configurations. This approach ensures a robust selection process while mitigating overfitting. Additionally, real-time computational constraints of the embedded processor were considered to balance model complexity with execution speed.

The final hyperparameter values were fixed as follows: $MaxSplits = 1024$, $\eta_1 = 0.25$, $N = 26$.

ML modelling The feature extraction process utilized a sliding time window of 300 ms, sampled at a frequency of 100 Hz. Within each window, 12 features are derived to capture critical aspects of gait dynamics. These features included the first and fifth values, maximum, minimum, mean, and standard deviation of the inter-limb hip angle and hip velocity [94]. The inclusion of the first and fifth values is particularly significant, as they provide insights into motion trends, thereby enhancing the predictive accuracy of the ML model.

During the training phase, the extracted features from each time window were assigned a "label", which corresponded to the final value of the estimated motor reference position trajectory, $\theta_r(t)$, generated by the AOs layer. This labeling strategy aimed to minimize potential delays during real-time computations.

4.5.2 Experimental assessment

To evaluate the effectiveness of the proposed layered control framework compared to the AOs-only controller, a walking experiment was conducted with the six healthy participants recruited to record the training dataset (Tab. 4.2).

Experimental protocol and data collection

To test the initial hypothesis that the ML-augmented controller performs similarly to the AOs-only controller during fixed-cadence walking (e.g., treadmill) but outperforms it in unstructured walking (i.e., overground), the experimental protocol was designed with two distinct tasks:

Participant	Age (year)	Weight (kg)	Height (cm)	Sex (-)
①	24	86	185	M
②	30	48	161	F
③	27	93	193	M
④	24	85	176	F
⑤	26	49	158	F
⑥	28	54	163	F

Table 4.2. Participants demographic.

a) Treadmill task: Participants performed three sessions of treadmill walking at different constant speeds: 0.6 m/s, 0.8 m/s, and 1.1 m/s, with each session lasting 4 minutes.

b) Overground task: Participants walked overground at a self-selected pace for 4 minutes. The path was approximately 20 meters long, with alternating ramps and u-turns every 5 meters.

Both tasks were repeated under three different conditions: (1) assistance using the AOs-only controller (*AOs*); (2) assistance using the ML-augmented controller (*ML*); (3) *assistance off*, where the suit was turned off and the tendons were removed from the thigh harnesses.

To minimize fatigue, participants were given a 10-minute rest between sessions, and the order of trials and conditions was randomized across subjects.

The motor reference position trajectory and gait phase signals from the high-level of both controllers, along with hip angle data from the IMUs, were recorded to evaluate the human motion estimation and tracking capabilities.

Metabolic assessments were employed in this study to evaluate the impact of device-assisted support on users. This method was selected because the previous study revealed limitations in muscular assessments, as EMG sensors could not be placed beneath the suit, restricting the range of muscles analyzed. Additionally, metabolic assessments are widely recognized as the gold standard in the literature for assessing the effects of robotic assistance on users [24].

Metabolic data were collected using indirect calorimetry with a portable gas analyzer (K5, COSMED, Rome, Italy). Prior to the walking trials, participants' baseline metabolic expenditure was recorded during a two-minute period of quiet standing in a resting state. This baseline value was subtracted from the walking

metabolic measurements during offline analysis to calculate the net metabolic cost associated with device-assisted walking.

Data analysis

The performance of the proposed ML-augmented controller were compared to the AOs-only controller, focusing on two key aspects: gait phase estimation accuracy and the impact of assistance on users' metabolic costs.

Performance comparison on human motion estimation To evaluate the ML controller's performance, the error in walking angular frequency estimates was quantified. Specifically, the angular frequencies estimated by the ML controller (ω_{ML}) and by the AOs controller (ω_{AOs}) were compared against the actual walking angular frequency (ω_{stride}) derived from IMU sensor kinematic data. The Root Mean Square Error (RMSE) was used as the performance metric. All angular frequencies were calculated using the formula $\omega_i = 2\pi/T_i$. For ω_{ML} and ω_{AOs}, T_i corresponded to the period of the sinusoidal motor reference trajectory generated during the i^{th} stride. For ω_{stride}, T_i referred to the stride period extracted from IMU data, which was filtered using a fourth-order Butterworth low-pass filter with a 10 Hz cutoff frequency.

The synchronization between the user's motion and the actuator reference motion was further evaluated by computing the magnitude-squared coherence, $C_{U/A}$ [95]:

$$C_{U/A} = \frac{|G_{\theta_{IL}\theta_{ref}}|^2}{G_{\theta_{IL}} G_{\theta_{ref}}} \tag{4.12}$$

where $G_{\theta_{IL}\theta_{ref}}$ is the cross-spectral density between the inter-limb hip flexion angle (θ_{IL}) and the actuator reference trajectory (θ_{ref}). The terms $G_{\theta_{IL}}$ and $G_{\theta_{ref}}$ represent the autospectral densities of the two signals. Since both signals exhibit sinusoidal behavior, the $C_{U/A}$ value at the fundamental frequency indicates the degree of synchronization between the user's motion and the device. Values closer to 1 reflect stronger synchronization.

Metabolic cost The net metabolic cost of walking under the three tested conditions (i.e., *AOs*, *ML*, and *assistance off*) conditions was calculated using the equation by Péronnet and Massicotte [96]:

$$P = 16.89V_{O_2} + 4.84V_{CO_2} \tag{4.13}$$

where P is the metabolic power, and V_{O_2} and V_{CO_2} represent oxygen consumption and carbon dioxide production, respectively. To isolate the walking-related metabolic cost, the baseline metabolic cost recorded during quiet standing was subtracted from the walking data.

Only the final two minutes of metabolic data for each trial were considered for the analysis to ensure steady metabolic state [97]. The metabolic data were normalized to body weight to enable meaningful comparisons among participants.

Statistics The normality of all data was verified using the Shapiro-Wilk test ($\alpha = 0.05$), confirming that all datasets followed a normal distribution.

For the control performance analyses, a two-way ANOVA was conducted to identify significant differences between the AOs-only and ML-augmented controllers under varying speeds and overground walking conditions.

For the metabolic assessments, a two-way ANOVA was performed with repeated measures, incorporating two factors: "condition" (*AOs*, *ML*, *assistance off*) and "trial" (0.6m/s, 0.8 m/s, 1.1 m/s, overground). When significant effects were identified, Fisher's LSD test was used for post-hoc pairwise comparisons.

4.5.3 Results

Performance comparison on human motion estimation Both controllers performed comparably under treadmill conditions, while the ML controller demonstrated superior gait estimation in the unstructured and dynamic overground walking scenario.

Figure 4.6-(a) presents the Root Mean Square Error (RMSE) between the actual walking angular frequency, derived from kinematic data, and the estimated angular frequency produced by the AOs-only (*AOs*) and ML-augmented (*ML*) controllers. The RMSE values, averaged across all strides and participants, were 0.14 ± 0.01 rad/s for *AOs* and 0.12 ± 0.02 rad/s for *ML*, at 0.6 m/s. At 0.8 m/s, the RMSE was 0.15 ± 0.02 rad/s for *AOs* and 0.14 ± 0.02 rad/s for *ML*. At 1.1 m/s, both controllers exhibited similar performance with RMSE values of 0.19 ± 0.03 rad/s and 0.19 ± 0.02 rad/s respectively. During the overground task, the ML-augmented controller outperformed the AOs-only controller, achieving a statistically significant lower RMSE of 0.21 ± 0.02 rad/s compared to 0.31 ± 0.05 rad/s ($p = 0.01$).

Figure 4.6-(b) shows the coherence ($C_{U/A}$) between the user's motion and the

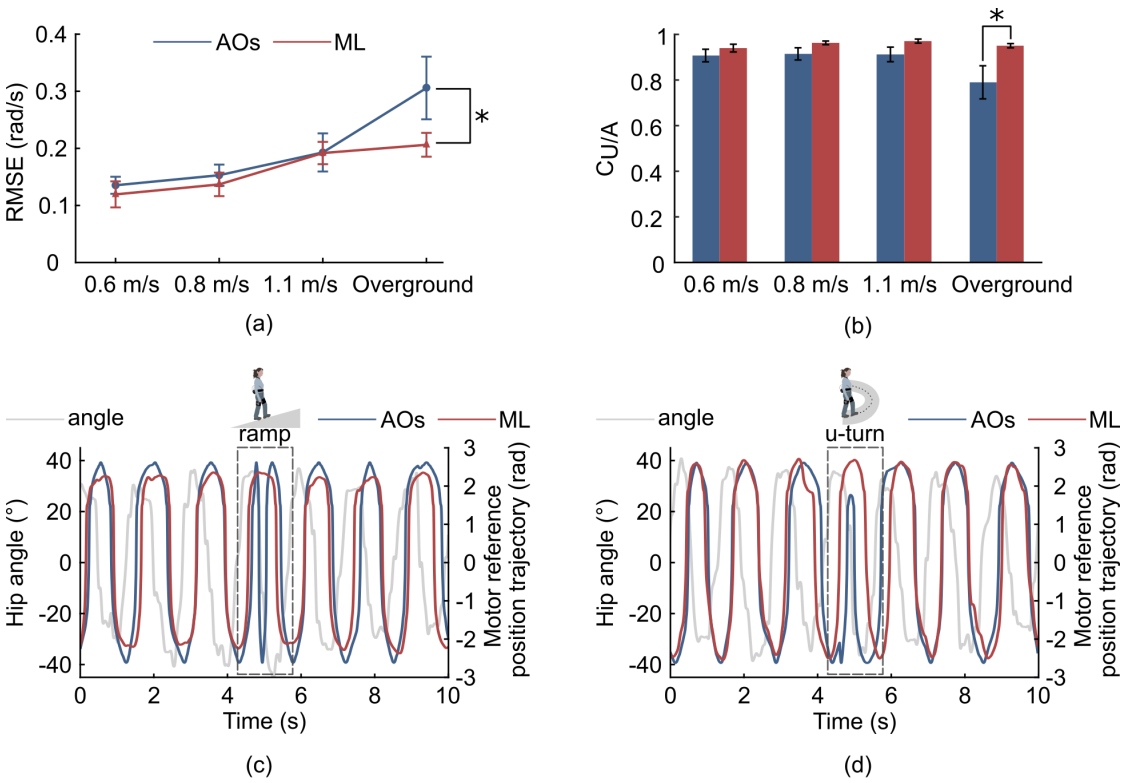


Figure 4.6. Performance comparison on human motion estimation. (a) Average RMSE values between actual and estimated angular walking frequencies for the two controllers: AOs-only (*AOs*, navy) and ML-augmented (*ML*, red), calculated across all strides and participants. (b) Magnitude-squared coherence ($C_{U/A}$) between user motion and actuator motion. (c-d) Inter-limb hip flexion angle (gray) and corresponding estimated motor reference trajectories during an overground trial involving ramp crossing and a u-turn, shown for a representative participant. A step with temporary desynchronization under the AOs-only controller is highlighted.

actuator's motion, averaged across participants. In the overground task, the ML-augmented controller achieved significantly higher coherence values (0.95 ± 0.01) compared to the AOs-only controller (0.79 ± 0.07), with $p < 0.05$. Instead, in treadmill tasks, both controllers exhibited comparable coherence, suggesting similar synchronization performance under fixed cadence conditions.

Figures 4.6-(c) and 4.6-(d) illustrate the motor reference position trajectories estimated in the *AOs* and *ML* conditions during a ramp crossing and a u-turn in the overground task for a representative subject. The plots reveal that the AOs-only controller experienced temporary desynchronization caused by changes in walking cadence, whereas the ML-augmented controller maintained synchronization with the user's movements despite abrupt transitions.

Metabolic cost The results of the metabolic cost analysis are presented in Fig. 4.7. During treadmill evaluations, walking with the assistance from the suit (*AOs* and *ML* conditions) led to a significant average reduction of 7.4% in metabolic cost compared to the *assistance off* condition ($p < 0.05$) across all three treadmill speeds. Notably, no statistically significant differences were observed between the two controllers in any of the treadmill trials, indicating comparable performance in reducing metabolic expenditure under these conditions.

In the overground task, the ML-augmented controller demonstrated a clear advantage, yielding a significantly lower metabolic cost compared to the *assistance off* condition, with an average reduction of 10% ($p < 0.05$). Moreover, the metabolic cost with the ML-augmented controller was also significantly lower than that observed with the AOs-only controller. In contrast, no significant differences were found when comparing the *AOs* to the *assistance off* condition.

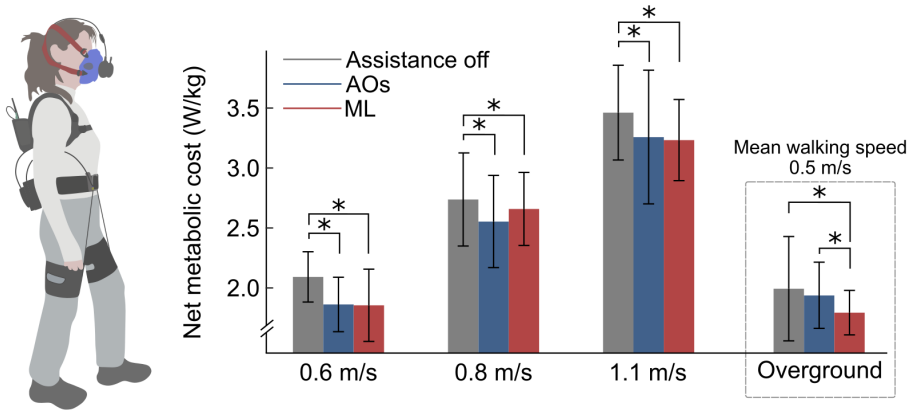


Figure 4.7. Metabolic cost. Comparison of net metabolic cost during walking with the soft robotic suit controlled by the AOs-based (*AOs*, navy) and ML-augmented (*ML*, red) approaches, as well as in the *assistance off* condition (grey).

4.5.4 Discussion

This section presented a control framework for the soft robotic suit, integrating a Machine Learning (ML) layer into the Adaptive Oscillators (AOs) controller detailed in Section 4.2. The ML layer was introduced to overcome key limitations of the AOs controller, particularly its challenges in adapting to cadence changes and terrain transitions, which often require resynchronization. This integration demonstrated significant advancements in stability, robustness, and overall system performance.

The comparison between the two controllers highlights the clear advantages of the ML-augmented framework. The ML layer significantly reduced the error in walking frequency estimation to 0.21 ± 0.02 rad/s compared to 0.31 ± 0.05 rad/s for the AOs-only controller. This enhanced accuracy translated into greater robustness and stability during diverse walking conditions, particularly in overground scenarios involving ramps, and u-turns. These results emphasize the ML layer's superior capability to maintain coherence between the robotic suit and the user's natural movements, ensuring more seamless assistance delivery.

To evaluate the practical implications of these improvements on users, metabolic assessments were conducted. Metabolic measurements were chosen for this study to address the limitations of electromyography evaluations reported in the prior work described in this chapter. Complying with initial hypotheses, the results showed that during treadmill trials, both controllers achieved comparable metabolic savings, averaging a 7.4% reduction, consistent with previous studies [67, 98, 99]. However, during overground trials, the ML-augmented controller demonstrated a distinct advantage, achieving a significant 10% reduction in metabolic cost compared to the AOs-only controller. These findings suggest that the ML layer's enhanced performance in gait phase estimation contributes directly to a more effective reduction in the metabolic demands of walking, particularly in dynamic and less structured environments.

While these results are promising, this study has certain limitations. Importantly, the evaluation was limited to walking speeds and conditions represented in the training dataset, and the performance was based on data from the same participants used for training, restricting generalizability. Additionally, the ML layer introduces increased computational complexity and requires an initial training phase, which demands substantial datasets to ensure reliability and mitigate unpredictable responses when user behavior diverges from the training conditions [71].

A future iteration of the controller that will be presented later in Chapter 6 will introduce an alternative control strategy that does not rely on ML or dynamic gait phase estimation. Instead, this new approach reconstructs gait phase from user angle and velocity data, offering a simpler and computationally lighter solution that can be applied across diverse scenarios. This shift in focus will aim to balance performance and practicality, paving the way for more versatile assistive technologies to be used in the real-world.

4.6 Conclusions

This chapter introduced a control strategy for the soft robotic suit based on an Adaptive Oscillator (AOs)-based controller, focused on dynamic gait phase estimation. This approach effectively adapts to changes in gait cadence, offering simplicity and minimal hardware requirements. The system demonstrated low gait phase estimation errors and reduced muscle activation in controlled environments, but struggles with movement initiation and unpredictable terrains. To address these limitations, a Machine Learning (ML) layer was incorporated, improving robustness, accuracy, and metabolic efficiency in short and structured overground evaluations. However, the ML layer introduced computational complexity and reliance on a training phase.

While the mentioned control strategies address key challenges in gait adaptability, they do not account for the dynamic environmental context that users encounter in real-world settings. Adapting to environmental changes, such as transitioning from level ground to stairs, is critical for enhancing the system's functionality outside the range of straight walking. Chapter 5 builds on the foundation laid in this chapter by integrating computer vision for context-aware assistance modulation. This refinement introduces an additional layer of complexity, enabling the system to dynamically adjust its support based on the context surrounding the user and allowing optimal assistance when transition between locomotion modes.

Chapter 5

Introducing context awareness to wearable assistive robotics

The contents of this chapter are adapted from the journal papers:

E. Tricomi, M. Mossini, F. Missiroli, N. Lotti, X. Zhang, M. Xiloyannis, L. Roveda, and L. Masia, "*Environment-based assistance modulation for a hip exosuit via computer vision*", **IEEE Robotics and Automation Letters**, vol. 8, no. 5, pp. 2550–2557, 2023.

E. Tricomi, G. Piccolo[†], F. Russo[†], X. Zhang, F. Missiroli, S. Ferrari, L. Gionfrida, F. Ficuciello, M. Xiloyannis and L. Masia, "*Leveraging geometric modeling-based computer vision for context aware control in a hip exosuit*", **Accepted at IEEE Transactions on Robotics**, 2024.

This chapter presents a novel control paradigm that incorporates artificial computer vision into the soft robotic suit developed throughout this dissertation. In Chapter 4, an Adaptive Oscillator (AO)-based controller was introduced to track the user's gait and adjust robotic assistance based on walking speed and cadence. However, this approach did not account for the dynamic environmental context, limiting its ability to handle complex real-world activities such as transitioning from walking on the ground level to climbing stairs. By integrating vision-based environmental scanning, this chapter enables the wearable device to dynamically adjust robotic assistance in real-time, responding to the user's surroundings. The chapter introduces two complementary approaches: one is data-driven computer vision and the other is physics-informed. Each method brings unique strengths to adaptive support, offering distinct pathways for improving wearable robotic systems. Both methods were tested experimentally, demonstrating their potential to enhance the real-time adaptability and efficiency of assistive devices in dynamic, real-world conditions.

5.1 Exploring the surroundings through vision

Vision plays a crucial role in human locomotion, enabling individuals to adjust their walking strategy in response to changes in the surrounding environment [100]. The central nervous system relies on sensory feedback, particularly visual input, to continuously adapt gait patterns as we navigate various terrains [101]. This adaptive behavior ensures efficient and coordinated movement, allowing each step to be fine-tuned according to visual cues.

Replicating this feature in wearable robotics has proven to be a significant challenge. Traditional assistive technologies are primarily optimized for level walking, while often neglecting the environmental context in which the user operates [100]. As a result, many robotic systems have been designed for controlled environments, such as treadmills or flat paths, that do not capture the complexities of real-world conditions [85, 102, 103].

The integration of environmental context into wearable robotics is therefore a crucial next step in improving the functionality of these systems. The challenge lies not only in tracking the user's gait but also in adjusting robotic assistance in real-time to account for external factors such as terrain type and obstacles [104].

The concept of "context-aware control" has gained significant attention in recent research, where robots use environmental perception to adjust their behavior based on contextual changes. These systems, by scanning and interpreting their surroundings, enable robots to dynamically modify their assistance in response to environmental cues [103, 105].

A recent perspective paper in Science Robotics by Gionfrida et al., stated "*Wearable robots for the real-world need vision*" [106]. Drawing a parallel to human sensory vision, it highlighted how integrating computer vision can significantly enhance wearable assistive robotics. In areas such as wheeled and legged robots, vision-based algorithms have already shown great promise in improving path planning and navigation [107, 108]. However, incorporating computer vision into wearable assistive devices remains an emerging field, with only a few studies exploring its potential for real-time dynamic assistance modulation [109, 110].

Chapter 4 introduced an Adaptive Oscillator (AO)-based controller to track the user's gait phase, adjusting in real-time to variations in walking speed and cadence. Although effective in adapting to changes in cadence, this controller did not take into account the external environment of the user. As such, it lacked the ability

to adjust assistance levels in response to changes in terrain, key considerations for real-world locomotion.

Building upon this foundation, the current chapter presents a further level of complication of the AO-based controller, integrating a vision-based module to improve its adaptability. This upgraded system combines the strengths of the previous AOs framework with real-time environmental scanning, enabling the robotic suit to respond not only to the user's gait but also to contextual cues, such as terrain type. By incorporating an onboard camera, the system classifies the environment (e.g., distinguishing between flat ground and stairs) and dynamically adjusts the level of assistance provided.

Two complementary computer vision strategies are outlined to integrate contextual awareness: a data-driven approach using Convolutional Neural Networks (CNNs) and a physics-informed approach based on geometric modeling (GM). The data-driven model employs CNNs to classify environmental states for tasks such as climbing stairs and walking on flat ground. While CNNs exhibit strong generalizability when properly trained, they are computationally intensive, limiting their real-time application in wearable robotics, where computational efficiency is critical [102,110]. In contrast, the physics-informed approach uses geometric modeling (GM), which interprets the environment based on physical properties of the scene. By leveraging stereo camera-based depth sensing, GM provides a more computationally efficient means of inferring terrain characteristics and classifying the environment in real-time in 3D images [111, 112]. This approach reduces the reliance on large datasets and deep learning models while maintaining high accuracy in environmental interpretation. While GM has been successfully applied in autonomous vehicles and mobile robots [113,114], its application in wearable assistive devices remains underexplored.

The performance of both approaches is evaluated experimentally in the context of two separate studies using an identical experimental protocol, allowing for a meaningful comparison to evaluate their respective strengths and performance.

Hypotheses The primary hypothesis is that a context-aware controller improves metabolic efficiency for the user compared to a static assistance profile, which remains unchanged across different tasks. Specifically, it is hypothesized that context awareness can be achieved through artificial computer vision, through both commonly used data-driven methods and geometric-modeling approaches.

5.2 Context-aware controller

The context-aware controller was integrated into the fully-actuated version of the soft robotic suit described in Chapter 3 for enhanced controllability in tasks like stair climbing. The suit was equipped with a camera mounted on the waist belt, as shown in Fig. 5.1. To support the vision-based control, this version of the suit incorporates two control boards: an NVIDIA Jetson Nano (NVIDIA, Santa Clara, CA, USA) for running vision algorithms, and an Arduino MKR 1010 WiFi (Arduino, Ivrea, Italy) for managing gait phase estimation and actuator control at 100 Hz. The computer vision module processes data from either an RGB or RGB-D camera, depending on the specific methodology used (further details provided below).

The overall control architecture consists of three layers: a high-level, mid-level, and low-level controller (Fig. 5.2). In the high-level controller, the *computer vision module* and *gait phase module* operate concurrently. The computer vision module monitors the user's environment to identify specific contexts such as ascending stairs (AS), level ground (LG), and descending stairs (DS), while the gait phase module estimates the user's gait phase in parallel based on motion data. The outputs from the high-level controller inform the mid-level controller, which adjusts the shape and amplitude of the actuator's reference profile accordingly. Lastly, the low-level controller translates these adjustments into precise actuator control through a PID loop.

Although this control structure is designed for the current hardware, it can be adapted for other assistive devices with appropriate modifications to the assistance profile, provided it is tailored to the specific lower-limb joint being targeted.

5.2.1 High-level controller

The high-level controller runs in parallel the *computer vision module* and the *gait phase module*, detailed henceforth.

Computer vision module

The *computer vision module* processes images from a camera mounted on the waist belt of the soft robotic suit to classify the user's environment in real time into one of three categories (AS, LG, and DS).



Figure 5.1. Hardware design. The soft robotic suit incorporates the camera (either RGB or RGB-D depending on the perception approach) on the waist belt for scanning the surrounding environment. The computer vision algorithm runs on a vision processing module (NVIDIA Jetson Nano) on the back of the belt.

The following sections describe two distinct implementations of the *computer vision module*, each independently integrated into the control framework. The first utilizes a data driven approach based on Convolutional Neural Networks (CNNs), while the second employs a geometric modeling (GM) method.

Data-driven based computer vision The data-driven based computer vision framework, written in Python, operates at 30 Hz and relies on an RGB camera (Logitech C920s PRO HD Webcam, Newark, CA, USA) positioned on the front of the user's belt for image acquisition. The camera captures real-time environmental

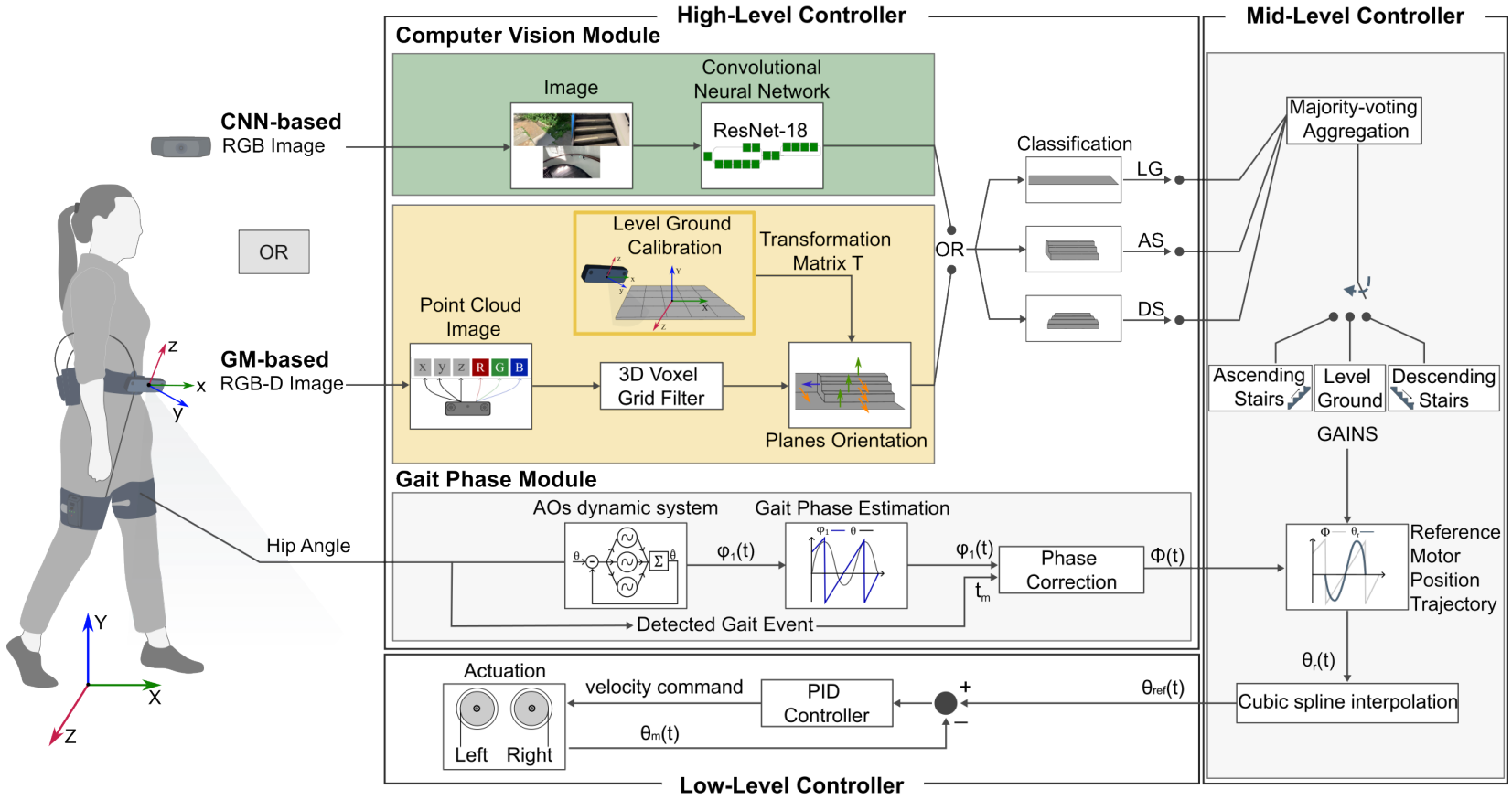


Figure 5.2. Context aware control framework. The high-level manages both the *computer vision module* and the *gait phase module* concurrently. The *computer vision module* employs either a Convolutional Neural Network based model (CNN, green block) or a geometric modeling approach (GM, yellow block) to process images from a camera (RGB or RGB-D respectively), classifying environments into level ground (LG), ascending stairs (AS), or descending stairs (DS). The *gait phase module* processes kinematic data from the user to determine the phase of the gait using Adaptive Oscillators (AOs). Outputs from these modules are integrated at the mid-level to generate a precise motor reference trajectory, then transmitted to the actuators at the low-level through a PID.

images, which are processed at a resolution of 400x400 pixels.

This framework incorporates a Convolutional Neural Network (CNN) model, which analyzes images captured by an RGB camera to interpret the user's nearby environment (Fig. 5.2, Fig. 5.3-(a)). For this application, a ResNet-18 model, consisting of 18 layers was selected. The net was trained on a dataset comprising 5000 images from the open-source ExoNet dataset [115], supplemented by 5500 additional images manually captured. In total, the 10500 images were divided into the three targeted categories (AS, LG, DS). For training, the dataset was split as follows: 80% for training, 10% for validation, and 10% for testing. The model was trained over 60 epochs using the Adam optimizer, with a batch size of 16 and an initial learning rate of 0.1, which was reduced tenfold every 20 epochs to ensure convergence.

Geometric modeling based computer vision The geometric modeling based computer vision framework uses prior knowledge of the orientation and structure of 3D scene elements instead of learned features (Fig. 5.2, Fig. 5.3-(a)). The algorithm is adapted from Pérez et al. [116,117] and has been modified specifically for real-time integration within a lower-limb assistive device controller.

The vision framework runs at 20 Hz and was developed using the Robot Operating System (ROS) and the Point Cloud Library (PCL). It receives and processes data from an RGB-D camera (OAK-D Lite, Luxonis, Castel Bolognese, Italy) that integrates a monocular RGB camera (13MP resolution, 4208x3120, and maximum frame rate of 35 FPS), and a pair of stereo cameras (480P resolution, 640x480, a maximum frame rate of 120 FPS, and 300,000-point stereo depth).

The *computer vision module* based on geometric modeling executes several steps, detailed henceforth, related to the identification of geometric features and the orientation of elements in the RGB-D point cloud images recorded from the waist-mounted camera. These point cloud images provide both the 3D coordinates of each pixel relative to the camera and the corresponding color information. To handle the large volumes of data produced, the number of points in each point cloud image is reduced post-acquisition. This downsampling utilizes a 3D Voxel Grid filter [118], which groups the point cloud data into a structured grid of cubic cells, known as voxels. Each voxel is represented by a single point, or centroid, which replaces the original collection of points. The voxel side length is set to 5 cm. Following downsampling, the point cloud (P_C) image is defined as $P_C = \{p_1, p_2, ..., p_i, p_n\}$, where each point in the scene p_i is described in the camera

reference with the coordinates x_i, y_i, and z_i of the centroid of the voxel $p_i = (x_i, y_i, z_i)$.

Level ground calibration

The very first step of the algorithm calibrates the absolute position of each object in the image relative to the camera's coordinate system by projecting the camera's axes onto an absolute reference frame, which aligns with the orientation of a level ground plane. This calibration is performed immediately and only once when activating the *computer vision module* and involves positioning the user in front of a flat surface within the camera's field of view. The calibration typically takes 5-10 seconds, depending on lighting conditions.

During this process, the algorithm identifies a plane that likely represents level ground and calculates a rotation matrix to transform the camera's relative reference frame into the absolute one. This process is carried out using the RANSAC algorithm [119], which segments the point cloud image data based on the Sample Consensus (SAC) random sampling model, following these key steps:

i. Random Sample Selection: a subset of points is selected at random to define an initial plane, considering at least 150 points set as a minimum set size.

ii. Estimation of the Plane Model: the plane equation

$$Ax + By + Cz + D = 0 \tag{5.1}$$

is calculated using the selected points, where A, B, and C are the directional coefficients that form the normal vector $\vec{n} = (A, B, C)$, orthogonal to any vector lying within the plane. The term D represents the perpendicular distance from the camera origin to the floor along the y-axis. To improve computational efficiency, the algorithm restricts its focus to data points located beyond 70 cm along the y-axis, given the camera's position at waist level.

iii. Determination of Consensus Set: the algorithm computes the distance from each point to the estimated plane, and only those points that are within a designated threshold (set at 2 cm, which approximates half the size of a voxel) are identified as belonging to the consensus set.

iv. Iterative Process: the outlined procedure is repeated for a specified number

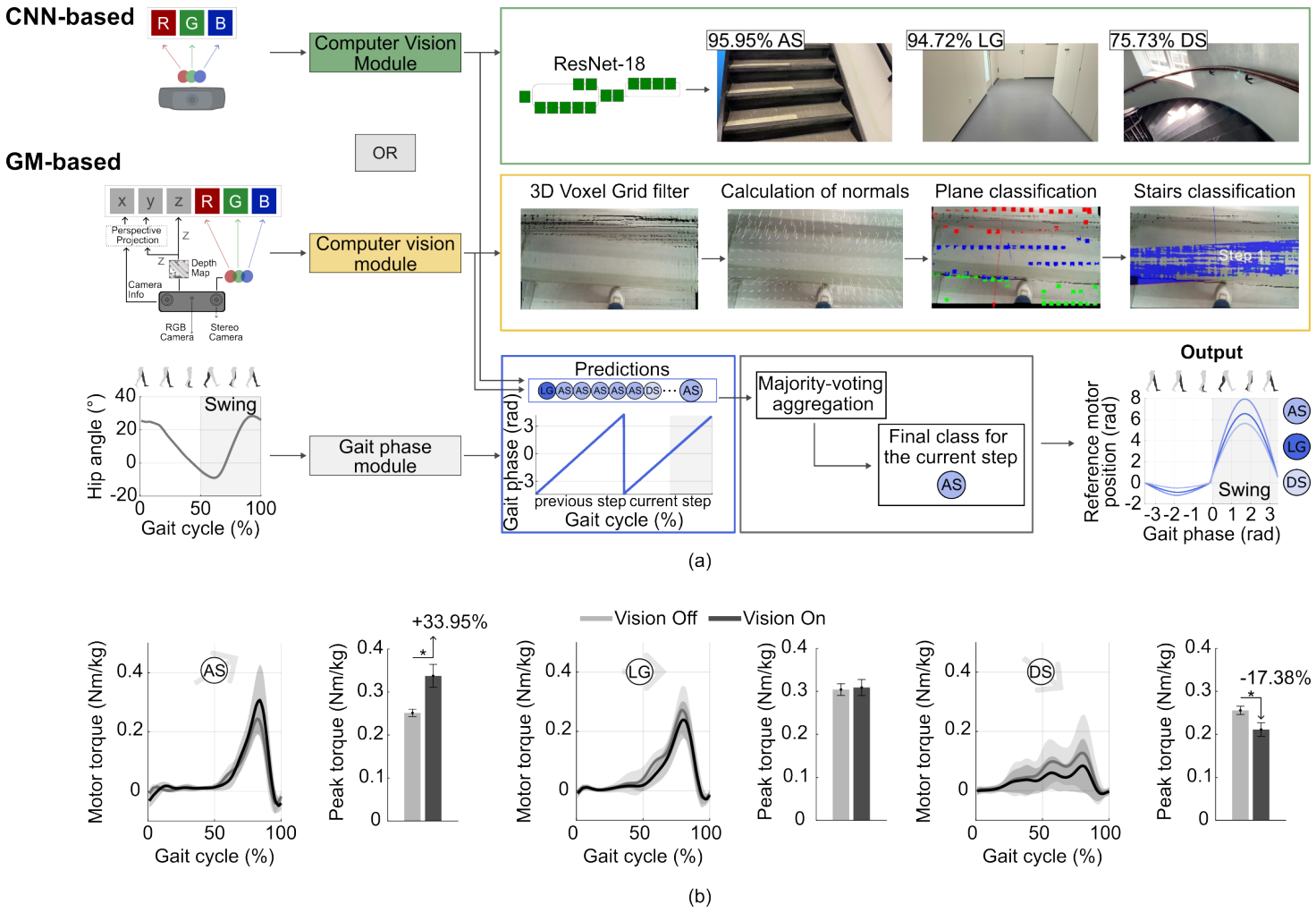


Figure 5.3. (a) Graphical overview of the key steps in the vision algorithms: the top and middle layer shows environment classification, the bottom layer demonstrates class aggregation within each step to determine the final one. (b) Assistive torque modulation using the context-aware controller (*Vision On*) versus no modulation (*Vision Off*). Exemplary motor torque data were recorded on six users (2 males and 4 females; age 26.0 ± 2.1 years, weight 59.5 ± 9.6 kg, and height 168.8 ± 6.3 cm.

of iterations, fixed at 100.

v. Selection of the Best Model: the final result is the plane model that has the largest consensus set.

Once a suitable plane candidate has been identified, the transformation matrix between the absolute reference frame and the camera's relative frame is computed as follows. Here, α represents the angle of rotation around the z-axis (R_z), while θ indicates the angle of rotation around the x-axis (R_x). The values of these angles are derived by ensuring that the vector $\vec{n}$, which is normal to the plane, aligns parallel to the y-axis of the camera $\vec{y} = (0, 1, 0)$.

$$R_z R_x \vec{n}^T = \begin{pmatrix} \cos\alpha & -\sin\alpha & 0 \\ \sin\alpha & \cos\alpha & 0 \\ 0 & 0 & 1 \end{pmatrix} \begin{pmatrix} 1 & 0 & 0 \\ 0 & \cos\theta & -\sin\theta \\ 0 & \sin\theta & \cos\theta \end{pmatrix} \begin{pmatrix} A \\ B \\ C \end{pmatrix} = \vec{y} \tag{5.2}$$

$$T = \begin{pmatrix} \cos\alpha & -\sin\alpha\cos\theta & \sin\alpha\sin\theta & 0 \\ \sin\alpha & \cos\alpha\cos\theta & -\cos\alpha\sin\theta & -D \\ 0 & \sin\theta & \cos\theta & 0 \\ 0 & 0 & 0 & 1 \end{pmatrix} \tag{5.3}$$

Real-time geometric modeling based Classification

Once the level ground has been calibrated, the system is ready for user operation. The following steps are executed:

1. *Calculation of normal vectors*: a framework utilizing Principal Component Analysis (PCA) is employed to estimate the normal vectors $\vec{n}_i$ for each point p_i based on a specified number of neighbors k, which is set to 20. The task of determining the normal at a given surface point is approached as an approximation of the normal to a tangent plane at that surface location. This solution is derived by examining the eigenvectors and eigenvalues from a covariance matrix generated using the nearest neighbors of the query point p_i. Specifically, for each point p_i, the covariance matrix Cov is constructed using the following equations:

$$Cov = \frac{1}{k} \sum_{n=1}^{k} (p_i - \overline{p}) \cdot (p_i - \overline{p})^T \tag{5.4}$$

$$Cov \cdot \vec{v}_j = \lambda_j \cdot \vec{v}_j, \quad j \in 0, 1, 2 \tag{5.5}$$

$\overline{p}$ signifies the 3D centroid of the nearest neighbors, while λ_j indicates the j^{th} eigenvalue of the covariance matrix, and $\vec{v}_j$ refers to the j^{th} eigenvector. To ensure that all the normal vectors $\vec{n}_i$ are oriented in relation to the viewpoint v_p (i.e., the camera's origin), the following condition must be satisfied:

$$\vec{n}_i \cdot (v_p - p_i) > 0 \tag{5.6}$$

The output surface curvature σ is calculated based on the relationship between the eigenvalues of the covariance matrix as follows:

$$\sigma = \frac{\lambda_0}{\lambda_0 + \lambda_1 + \lambda_2} \tag{5.7}$$

2. *Region growing method*: the next stage utilizes the region-growing segmentation method [120] to divide a point cloud image into coherent clusters based on local surface features. This technique produces clusters, each representing points that are regarded as belonging to the same smooth surface. The algorithm operates by assessing the angles between the normals of the points. It begins by selecting a "seed" point, identified as the one with the lowest curvature σ, and then expands the region to adjacent points that exhibit minimal normal variation (with a threshold of $\theta_{th} = 6^\circ$) and comparable curvature values (with a threshold of $c_{th} = 0.5$). Points that are in close proximity and satisfy the established normal and curvature criteria are designated as new seeds, and this iterative process continues until the region can no longer expand. Additional parameters include a minimum cluster size of 30 points and a minimum of 16 neighbors. The initial set of point clouds, along with their corresponding normals, is then established, applying a smoothness constraint that considers the angle between the normal of the current seed (n_s) and those of its neighbors (n_p), defined as:

$$\|n_p \cdot n_s\| > \cos(\theta_{th}) \tag{5.8}$$

with θ_{th} the threshold value for the angular deviation.

3. *Planar assessment*: once the regions have been identified, the next goal is to analyze their geometric characteristics and verify their planar nature. This phase utilizes the RANSAC algorithm, treating each region separately to derive the equation for the dominant plane (as outlined in the *level ground*

calibration step). Following this, the algorithm calculates the distance from every point in the point cloud within the selected region to the corresponding plane. This calculation aims to determine if the distance is less than a predetermined threshold, set at $d_{th} = 4$ cm. If a point's distance is below this threshold, it is classified as an inlier. After all points have been labeled, the proportion of inliers is assessed against the total number of points in the region. If the inliers constitute more than 80% of the points, the region is then categorized as planar.

4. *Plane classification*: once the planes have been detected, the next step is to categorize their orientation as horizontal, vertical, or frontal, depending on their alignment relative to the level ground. This classification is important for identifying steps, which can be defined as a combination of a horizontal and a frontal plane, following specific height-to-step ratio guidelines. To determine the orientation of each plane, the angle γ between the normal vector of the identified plane ($\vec{n_{pl}} = (A, B, C)$ from Eq. 5.1) and the normal vector of the level ground is calculated. This calculation is critical for evaluating whether a plane is approximately normal, using an angular threshold of $T_\gamma = 15°$. The angle γ is computed as follows:

$$\gamma = \arccos(\vec{n}_{pl} \cdot \vec{y}) \tag{5.9}$$

Here, $\vec{y}$ signifies the unit vector aligned with the y-axis, while $\vec{n}_{pl}$ indicates the normal vector of the plane. When the angle γ nears 0°, the planes are classified as horizontal; on the other hand, if the angle is close to 90°, the planes are considered vertical.

5. *Level ground and stairs classification*: after classifying the orientation of the planes in the environment, it becomes feasible to differentiate between level ground and stairs, whether they are ascending or descending. For horizontal planes, a distance threshold of $H_{ref} = 8$ cm is established to evaluate whether a plane is sufficiently close to the level ground based on Euclidean distance measurements from calibration, allowing it to be classified LG. If this condition is not met, the plane is considered a potential step. When at least one candidate step is identified, a series of checks are conducted in order:

   (a) Step candidate identification: the next stage involves assessing the heights (H_k) of horizontal planes in relation to the reference heights

(H_{ref}). Broadly speaking, a step can be conceptualized as comprising two components: the tread, which is the horizontal surface where a foot rests, and the riser, which represents the vertical height of the step, associated with the horizontal and frontal planes, respectively. In this research, the criteria for defining step dimensions are based on international standards [121], which establish a maximum step height of approximately 20 cm. To account for measurement noise, a tolerance margin is included, leading to a total height limit of $H_{\text{max}} = 24$ cm. The following condition is then evaluated:

$$S_i = \{R_k \mid \|\vec{n}_k \times \vec{y}\| = 0,\ |H_k| \geq H_{\text{ref}})\} \tag{5.10}$$

S_i represents the i^{th} step candidate, while R_k refers to the analyzed region, $\vec{n}_k$ denotes the normal vector of that region, and $\vec{y}$ is the unit normal vector of the level ground established during calibration. The expression $\|\vec{n}_k \times \vec{y}\| = 0$ signifies that the plane of the step candidate is parallel to the level ground, which is crucial for confirming that the step's orientation aligns with the ground reference. Within the algorithm, the step height H_k is derived from the y-coordinate of the centroid, which is transformed into the floor reference frame using the transformation matrix T in Eq. (5.3). Specifically, if the value of H_k exceeds H_{ref}, it indicates that the step is sufficiently elevated to qualify as an ascent, thus categorizing it as a candidate for AS. Conversely, if the step height falls below the negative of the minimum height $-H_{\text{ref}}$, it is considered low enough to be classified as a descent, making it a candidate for DS.

(b) Step connectivity test: steps can be effectively differentiated from various objects due to their consistent manifestation of connectivity between planes, suggesting the presence of common points within a defined proximity. To perform this connectivity assessment, the kD-tree algorithm is utilized [122]. Once the level ground (LG) is established, the algorithm advances to identify valid step candidates that fulfill the height criteria and are connected to the LG. Specifically, if a plane meets the height criteria within the bounds of H_{ref} and H_{max}, the algorithm evaluates its connectivity to the LG through a neighbor search defined by a search radius of $r_n = 50$ cm and a minimum neighbor threshold of $n_n = 5$. Should the plane be connected to the LG, it is

classified as a potential first step. The subsequent analysis involves examining planes within a minimum distance from the identified step plane (H_{step}) to evaluate their connectivity. Connected planes are merged, while two planes of similar heights that do not exhibit connectivity are interpreted as potentially representing two distinct steps. The detection process adopts a conservative approach, selecting only one candidate between the two. Specifically, once the connection with the floor is confirmed for both planes, the one with the greater point cloud density is chosen.

(c) Step validation: before a final classification decision is made, candidate steps are validated based on their dimensions. Specifically, steps are defined by a horizontal rectangular surface with dimensions $l_{\text{width}} \times l_{\text{length}}$ and a vertical rectangular surface with dimensions $\text{l}_{\text{width}} \times l_{\text{height}}$, creating a connection between the horizontal plane and the level beneath. The intersection of these two surfaces is referred to as the step's edge. To compute these parameters, the directions for width, length, and height at each step are identified. These dimensions are considered principal and are derived again using PCA. The first principal component corresponds to the highest eigenvalue (width, z_{Φ}), the second to the second highest eigenvalue (length, x_{Φ}), and the third to the lowest eigenvalue (height, c_{Φ}). For a more straightforward estimation of step dimensions, emphasis is placed on the primary directions of width and length, given that height has a negligible effect. A two-dimensional plane identified by the RANSAC algorithm is selected, where all points from a specific level are projected. This projection allows for a compact representation of the points enclosed within a bounding box that reflects the width and depth of the step accurately. Specifically, this bounding box can be defined as a rectangular entity, with its edges extending through the minimum and maximum coordinates along the principal directions, remaining parallel to these axes. Consequently, the required dimensions can be computed as follows:

$$l_{\text{width}} = z_{\Phi_{\text{max}}} - z_{\Phi_{\text{min}}} \tag{5.11}$$

$$l_{\text{length}} = x_{\Phi_{\text{max}}} - x_{\Phi_{\text{min}}} \tag{5.12}$$

The vertical dimension is obtained by measuring the distance along the

y-axis between the centroids of the plane designated as LG and that of the candidate step:

$$l_{\text{height}} = c_{y_{\text{step}}} - c_{y_{\text{LG}}} \tag{5.13}$$

Candidate steps are subsequently assessed against baseline dimensions concerning length, height, and their combined measurement. If the candidates pass this validation, they are ultimately categorized as either ascending (AS) or descending (DS) based on their initial classification.

Once all elements in the scene have been classified, a criterion is applied that considers the user's distance from the candidate plane, specifically evaluating its centroid along the z-axis. This approach is founded on the premise that the user's next intended step is more likely to be near the classified elements rather than those positioned farther away.

Gait phase module

The *gait phase module* operates simultaneously with the *computer vision module*, estimating the user's gait phase in real-time based on hip joint kinematics recorded by two IMUs. This method is based on the Adaptive Oscillators approach outlined in Chapter 4. For a comprehensive explanation of the AOs-based gait phase estimation approach, the reader can refer to section 4.2.1, only the key steps are summarized below. For this implementation, the algorithm is adapted to the fully actuated system, therefore kinematic signals are processed separately for the two legs.

The hip flexion angle for each leg, denoted as $\theta(t)$, is modeled as the sum of three sinusoids:

$$\hat{\theta}(t) = \alpha_0(t) + \sum_{n=1}^{3} \alpha_n(t) \sin(\varphi_n(t)) \tag{5.14}$$

The parameters, amplitude $\alpha_n(t)$, phase $\varphi_n(t)$, frequency $\omega(t)$, and offset $\alpha_0(t)$, are updated using an error-driven method defined by:

$$\dot{\alpha}_0(t) = \eta F(t) \tag{5.15}$$

$$\dot{\alpha}_n(t) = \eta F(t) \sin(\varphi_n(t)) \tag{5.16}$$

$$\dot{\varphi}_n(t) = \omega(t) \cdot n + \nu_\varphi \frac{F(t)}{\sum \alpha_n} \cos(\varphi_n(t)) \tag{5.17}$$

$$\dot{\omega}(t) = \nu_\omega \frac{F(t)}{\sum \alpha_n} \cos(\varphi_1(t)) \tag{5.18}$$

where $F(t) = \theta(t) - \hat{\theta}(t)$. The gains η, ν_φ, and ν_ω are set to 5, 20, and 20, respectively, for optimal convergence.

The fundamental phase $\varphi_1(t)$ is normalized and adjusted to ensure that the start of each step aligns with 0 radians:

$$\varphi_1'(t) = \mathrm{mod}(\varphi_1(t), 2\pi) \tag{5.19}$$

The overall gait phase is computed as:

$$\phi(t) = \mathrm{mod}\left(\varphi_1'(t) + \int E_\psi \omega(t) e^{-\omega(t)(t-t_m)}, 2\pi\right) \tag{5.20}$$

where t_m indicates the times of maximum hip flexion, and E_ψ is defined as:

$$E_\psi = \begin{cases} -\varphi_1'(t_m) - \psi(t_m), & \text{if } 0 \leq \varphi_1'(t_m) < \pi \\ 2\pi - \varphi_1'(t_m) - \psi(t_m), & \text{if } \pi \leq \varphi_1'(t_m) < 2\pi \end{cases} \tag{5.21}$$

5.2.2 Mid-level controller

The mid-level controller is responsible for dynamically adjusting the assistance levels for each leg based on input from both the *computer vision module* and the *gait phase module*. To ensure robustness in decision-making, a majority-voting procedure aggregates the classification results from the previous steps, ultimately determining the final class for each step taken by the user (Fig. 5.3-(a)).

The *gait phase module* identifies specific temporal points t_i that correspond to the stance and swing phases of the previous step, as well as the stance phase of the current step. These temporal points are used for compiling classification outcomes and establishing the definitive class for the upcoming swing phase.

For the data-driven approach, which utilizes a CNN, the majority-voting procedure considers the confidence levels associated with the class provided by the CNN. The confidence counters for the various classes are computed as follows:

$$C_{CNN} = \begin{cases} C_{AS} = \sum_{n=1}^{N_{AS}} conf_{AS} & \forall\ t_i \text{ with class AS} \\ C_{LG} = \sum_{n=1}^{N_{LG}} conf_{LG} & \forall\ t_i \text{ with class LG} \\ C_{DS} = \sum_{n=1}^{N_{DS}} conf_{DS} & \forall\ t_i \text{ with class DS} \end{cases} \tag{5.22}$$

where C_{AS}, C_{LG}, and C_{DS} are counters that reflect the total confidence values for

each class across all relevant timestamps t_i.

Conversely, for the geometric modeling based algorithm, where confidence information is not available, the majority-voting procedure relies solely on the count of instances in which a class has been detected:

$$C_{GM} = \begin{cases} C_{AS} = \sum_{n=1}^{N_{AS}} n_{AS} & \forall\ t_i \text{ with class AS} \\ C_{LG} = \sum_{n=1}^{N_{LG}} n_{LG} & \forall\ t_i \text{ with class LG} \\ C_{DS} = \sum_{n=1}^{N_{DS}} n_{DS} & \forall\ t_i \text{ with class DS} \end{cases} \tag{5.23}$$

Finally, the class with the highest counter value is then selected as the final predicted class for the subsequent swing phase, and all counters are reset to zero for the next evaluation.

Once the final class is determined, the controller formulates a reference motor position trajectory $\theta_r(t)$ to create a corresponding assistance profile during the swing phase of each leg. The trajectory is defined as follows:

$$\theta_r(t) = \begin{cases} G_{AS} \sin(\phi(t) - \pi) & \text{if AS} \\ G_{LG} \sin(\phi(t) - \pi) & \text{if LG} \\ G_{DS} \sin(\phi(t) - \pi) & \text{if DS} \end{cases} \tag{5.24}$$

In this equation, G_{AS}, G_{LG}, and G_{DS} are gains that modulate the amplitude of $\theta_r(t)$ based on the classified environment (AS, LG, or DS). These gains were tuned through preliminary trials, taking into account kinematic factors such as the variations in hip flexion profiles during the swing phase, as established in prior studies [123]. Ultimately, the final actuator reference motion $\theta_{\text{ref}}(t)$ is obtained from $\theta_r(t)$ after applying cubic spline interpolation, and this signal is forwarded to the low-level controller.

5.2.3 Low-level controller

The low-level controller operates as a PID system, comparing the reference angle $\theta_{\text{ref}}(t)$ with the actual motor position $\theta_m(t)$, as measured by the motor encoder. This closed-loop position control generates an output that is converted into a command for the motor's angular velocity. Consequently, the assistive torque adjusts dynamically across different environments to meet the user's needs.

To examine the influence of the computer vision module on assistance, compared to a static assistance scenario, Fig. 5.3-(b) illustrates the peak torque and motor profiles along the three path segments.

5.3 Performance evaluation and human experiments

The two computer vision approaches described in previous the section, data-driven (CNN-based) and geometric modeling (GM-based), were each evaluated in separate human studies using an identical experimental protocol. This consistent setup enabled a meaningful comparison of their respective strengths and performance.

The following sections provide a detailed assessment of the real-time performance of each computer vision module as integrated within the controller, along with the results of the human trials and a comparative discussion of findings.

5.3.1 Experimental protocol

Healthy participants were recruited across two separate studies following a consistent experimental protocol for comparison (Table 5.1). Seven participants evaluated the system using the CNN-based context-aware controller (3 males and 4 females, mean age 25.0 ± 2.2 years, weight 60.9 ± 13.7 kg, height 169.0 ± 9.9 cm), while six participants tested the GM-based approach (2 males and 4 females, mean age 26.0 ± 2.1 years, weight 59.5 ± 9.6 kg, height 168.8 ± 6.3 cm).

Before participating in the experiments, all individuals provided written informed consent. The study protocols were conducted in accordance with the Declaration of Helsinki and received ethical approval from the Heidelberg University Ethics Committee (resolution S-313/2020).

Participants were instructed to walk along a path comprising ten consecutive stair ramps (totaling 111 stairs, each measuring 120 cm $\times$ 18 cm $\times$ 26 cm) and level ground, covering a total distance of 220 meters. The route involved ascending the stairs, walking across a level surface, and then descending to the starting point, in that order (Fig. 5.4). This sequence was repeated three times under different conditions: (a) suit powered off (*assistance off*); (b) suit turned on with the computer vision module disabled (*vision off*); and (c) suit turned on with the

Study	Participant	Age (year)	Weight (kg)	Height (cm)	Sex (-)
CNN	①	24	85	180	M
	②	24	49	160	F
	③	28	48	158	F
	④	24	60	171	M
	⑤	24	74	184	M
	⑥	23	56	167	F
	⑦	29	54	163	F
GM	①	25	60	167	F
	②	24	48	163	F
	③	28	70	180	M
	④	24	70	170	M
	⑤	26	60	170	F
	⑥	29	49	163	F

Table 5.1. Participants demographic.

computer vision module enabled (*vision on*). The *vision on* condition dynamically adjusted the assistance gains as defined by Eq. (5.24), whereas the *vision off* condition applied a fixed gain across all scenarios. In the latter case, a baseline intermediate value, G_{LG}, was used, corresponding to the controller implementation described in Chapter 4.

To minimize fatigue effects, participants rested for 20 minutes between trials, with condition order randomized across subjects. A portable speaker delivered audio cues at regular intervals (60 bpm) to help participants maintain a consistent walking pace.

Classification data for the *vision on* condition was logged along the path for all participants, with each segment marked by an external switch to establish true class labels for accuracy assessments. Hip angle data was also recorded for kinematic evaluation. To measure metabolic energy expenditure, oxygen and carbon dioxide consumption were recorded with a portable gas analyzer (K5, COSMED, Rome, Italy). A four-minute resting period was recorded at the beginning of each trial to establish baseline metabolic cost during quiet standing.

5.3.2 Data analysis

Classification accuracy and computational load The primary metric for evaluating the *computer vision module*'s performance was its real-time classifica-

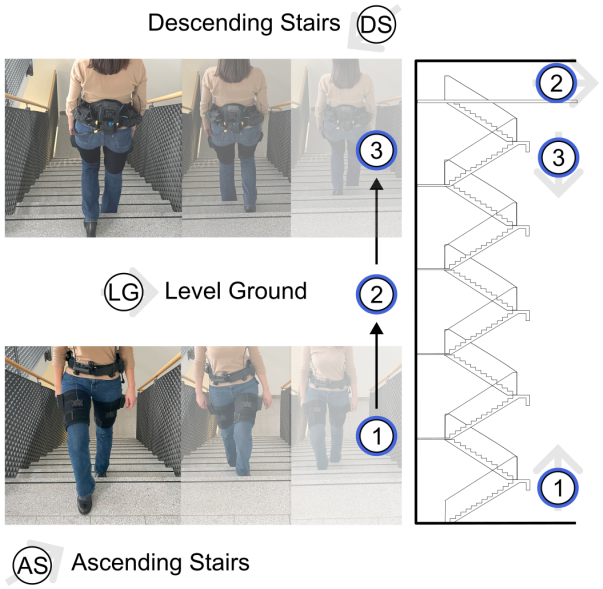


Figure 5.4. Experimental protocol. The experiment consisted of ascending a stairway (1), walking on level ground (2), and then descending back to the starting point (3).

tion accuracy. Accuracy per class was calculated from the percentage of correct predictions derived from the majority-voting procedure (Eq. 5.23) within each gait cycle, relative to the total classifications. A prediction was considered correct if it matched the true class determined by the external switch used to segment the path.

Since scene transitions are critical to performance, classification accuracy at transitions between different path segments were further analyzed. Specifically, the analysis focused on the steps at the edge of environment change between stairs and level ground based on the experimental path composition (i.e., AS to LG, LG to DS, DS to LG, and LG to AS). This analysis aimed to determine how accurately the system predicted the new environment at the very first step of each transition, assessing its ability to detect scene changes effectively.

Computational load was evaluated by measuring the real-time demands of both computer vision algorithms during a continuous 10-minute period of environment scanning and classification. Metrics included (i) RAM usage, (ii) GPU utilization, (iii) CPU utilization, and (iv) processing time per classification instance.

Kinematics Kinematic assessments focused on hip velocity profiles to verify that context-aware modulation driven by computer vision does not restrict users' natural kinematic patterns, consistent with previous studies related to this dissertation [124, 125].

Raw IMU data were segmented into steps and filtered with a fourth-order Butterworth low-pass filter (cut-off frequency of 10 Hz) before being time-normalized as a percentage of the gait cycle. The impact of the *vision off* and *vision on* conditions, relative to the *assistance off* baseline, was analyzed in terms of peak velocities and movement smoothness. Movement smoothness was evaluated using the Spectral ARC length (SPARC) index on the hip angular velocity norm [126].

Metabolic cost Oxygen and carbon dioxide data were analyzed to estimate the energy efficiency of walking across the *assistance off*, *vision Off*, and *vision On* conditions for each path segment. To establish a baseline, data from the last two minutes of quiet standing were averaged, providing the mean metabolic cost at rest, $\overline{QS}$. Metabolic data collected during each trial were then segmented by path segment (AS, LG, and DS).

To account for variations in walking speed from the set audio cue, data were analyzed in terms of cost of transport (CoT). The net metabolic power P was estimated using Péronnet and Massicotte's equation [96], subtracted by $\overline{QS}$, and then normalized by the product of the subject's weight w, gravitational acceleration g, and average walking speed $\overline{v}$ for each path segment:

$$CoT = \frac{P - \overline{QS}}{wg\overline{v}} \tag{5.25}$$

Average walking speed $\overline{v}$ was calculated as the distance covered divided by the time taken for each respective segment. Since many segments did not allow for a steady-state estimate within two minutes [127], a decaying exponential fit was applied to approximate the steady-state metabolic cost, as recommended in the literature [128, 129]. This fit used a one-term exponential model with parameters a, τ, and c:

$$CoT_{\mathrm{FIT}}(t) = a \exp\left(-\frac{t}{\tau}\right) + c_{ss} \tag{5.26}$$

Here, c_{ss} represents the approximate steady-state CoT. The quality of this fit was evaluated using the coefficient of determination R^2 and residuals analysis to ensure robustness.

Statistics Data distribution was first assessed using a Shapiro-Wilk test, which confirmed normality for all datasets. A significance level of $p < 0.05$ was set for all statistical tests. Further statistical analysis was performed using a linear mixed-effects model with least squares regression (MATLAB, MathWorks Inc., Natick,

MA, USA). The model included "condition" (*assistance off*, *vision off*, *vision on*) as a dummy-encoded categorical fixed-effect variable, with "participant" specified as a random-effect variable. Results are presented as mean values ± s.e.m. (standard error of the mean).

5.3.3 Results

Classification accuracy and computational load Figure 5.5 illustrates the classification accuracy of the *computer vision module*, presenting mean accuracy across subjects and conditions by class (Fig. 5.5-(a, b)) and during transition phases (Fig. 5.5-(c)). The CNN-based and GM-based computer vision controllers are represented in green and yellow, respectively. Confusion matrices show the distribution of misclassifications, with rows corresponding to true classes and columns representing predicted classes. Diagonal cells indicate correct classifications, while off-diagonal cells display errors, with percentages provided for both correct and incorrect classifications within each true class.

For the CNN-based approach, class-specific prediction accuracies were as follows: $85.6 \pm 3.6\%$ for AS, $97.6 \pm 0.7\%$ for LG, and $91.1 \pm 2.3\%$ for DS. Lower accuracy rates were observed for transition phases: $57.1 \pm 7.1\%$ from AS to LG, $67.9 \pm 9.0\%$ from LG to DS, $57.1 \pm 9.0\%$ from DS to LG, and $46.4 \pm 3.6\%$ from LG to AS.

For the GM-based approach, classification accuracy by class was $82.4 \pm 2.9\%$ for AS, $85.0 \pm 4.8\%$ for DS, and $97.9 \pm 0.4\%$ for LG. Transition phases accuracies were $59.3 \pm 7.8\%$ from AS to LG, $60.0 \pm 4.5\%$ from LG to DS, $75.0 \pm 6.2\%$ from DS to LG, and $59.4 \pm 6.2\%$ from LG to AS.

Figure 5.6 further exemplary shows the motor reference trajectory, modulated by environmental classification, across all steps (right leg) for a representative subject in the *vision on* condition.

Table 5.2 provides a comparative analysis of computational demands for real-time execution between the two approaches, both evaluated on the same experimental path. The GM-based method demonstrated significantly higher efficiency in memory use, requiring only 11.4% of RAM compared to the CNN-based 26.2%. Additionally, the GM-based approach does not require GPU resources, operating entirely on the CPU. This resulted in a CPU utilization of 76.7% with zero GPU demand, in contrast to the CNN-based approach, which heavily utilized the GPU at 98.8% with 26.8% CPU usage. In terms of inference time, however, the

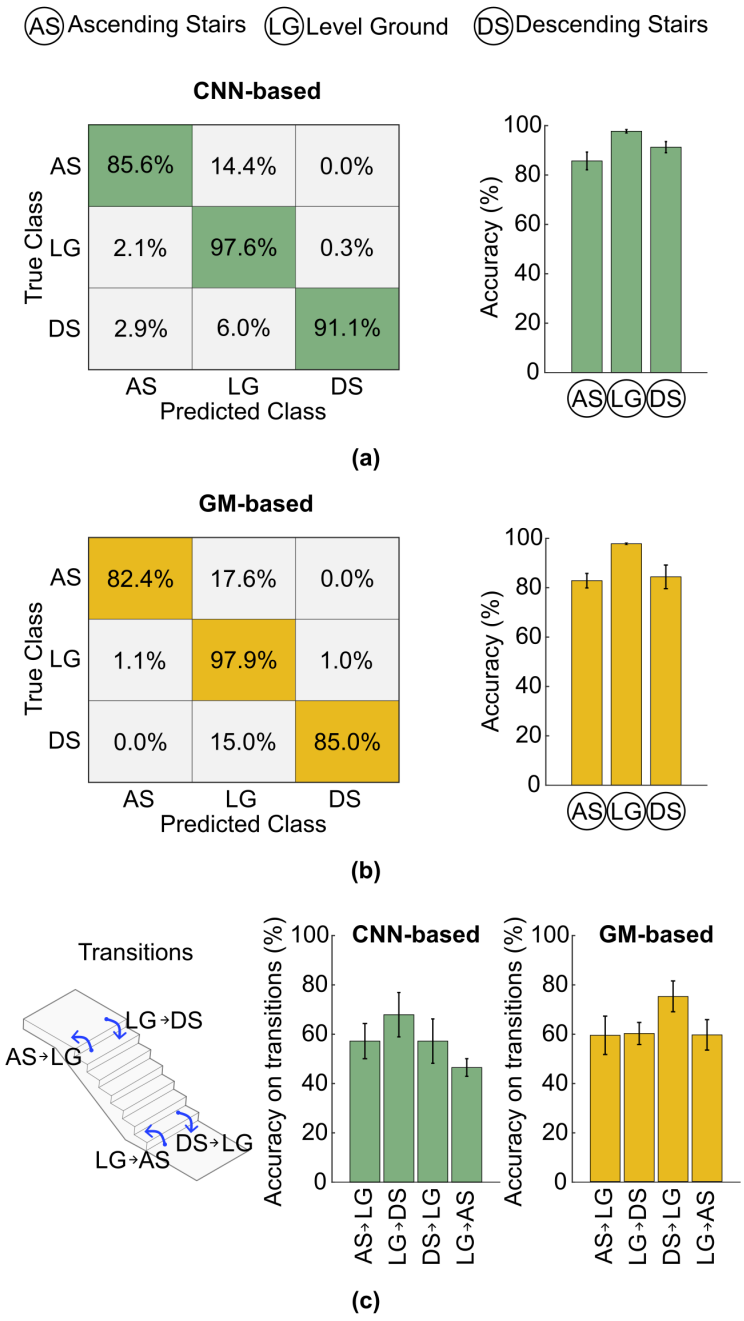


Figure 5.5. Classification accuracy. (a) Classification accuracy for each environment class for the CNN-based method. (b) Classification accuracy for each environment class for the GM-based method. AS represents ascending stairs, LG represents level ground, and DS represents descending stairs. (c) Classification accuracy during transitions between different environments for both methods.

CNN-based approach was faster, with an average classification time of 45.6 ms per instance, compared to 103.5 ms for the GM-based algorithm.

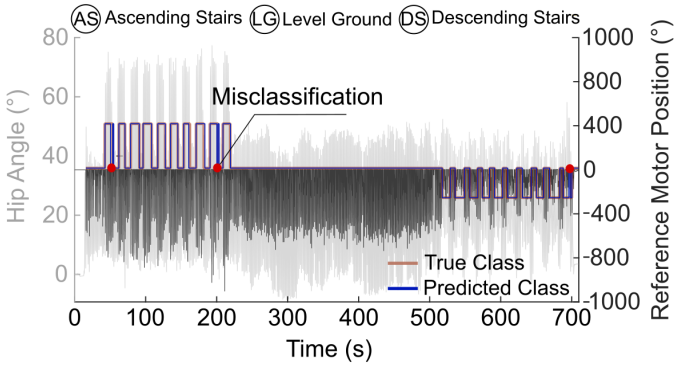


Figure 5.6. Motor reference modulation. An example showing how the motor reference position trajectory adapts along the pathway in response to detected scenes for each step of a participant using the context-aware controller, with misclassifications marked by red dots.

CV method	RAM [%]	GPU [%]	CPU [%]	Processing time [ms]
CNN-based	26.2	98.8	26.8	45.6
GM-based	11.4	0	76.7	103.5

Table 5.2. Computational load of the two computer vision methods.

Kinematics The results of the kinematic assessments for the two computer vision methods (CNN and GM) across the three path segments, ascending stairs (AS), level ground (LG), and descending stairs (DS), are presented in Figure 5.7. To simplify the analysis, data were averaged between legs, as no significant side-related differences were found. The figure illustrates the time series of hip angular velocity for a representative subject, averaged across steps for the three conditions and path segments, along with peak velocities observed during the swing and stance phases, and a measure of movement smoothness.

For the CNN-based method (Fig. 5.7-(a)), the statistical analysis revealed that positive peak velocities (swing phase) during the *vision on* condition were significantly higher than those in the *vision off* condition during AS and the *assistance off* condition during DS ($p < 0.05$). Negative peak velocities (stance phase) showed significant differences between *vision off* and *assistance off* during AS, as well as between *vision off* and *assistance off*, and between *vision on* and *assistance off* during DS ($p < 0.05$).

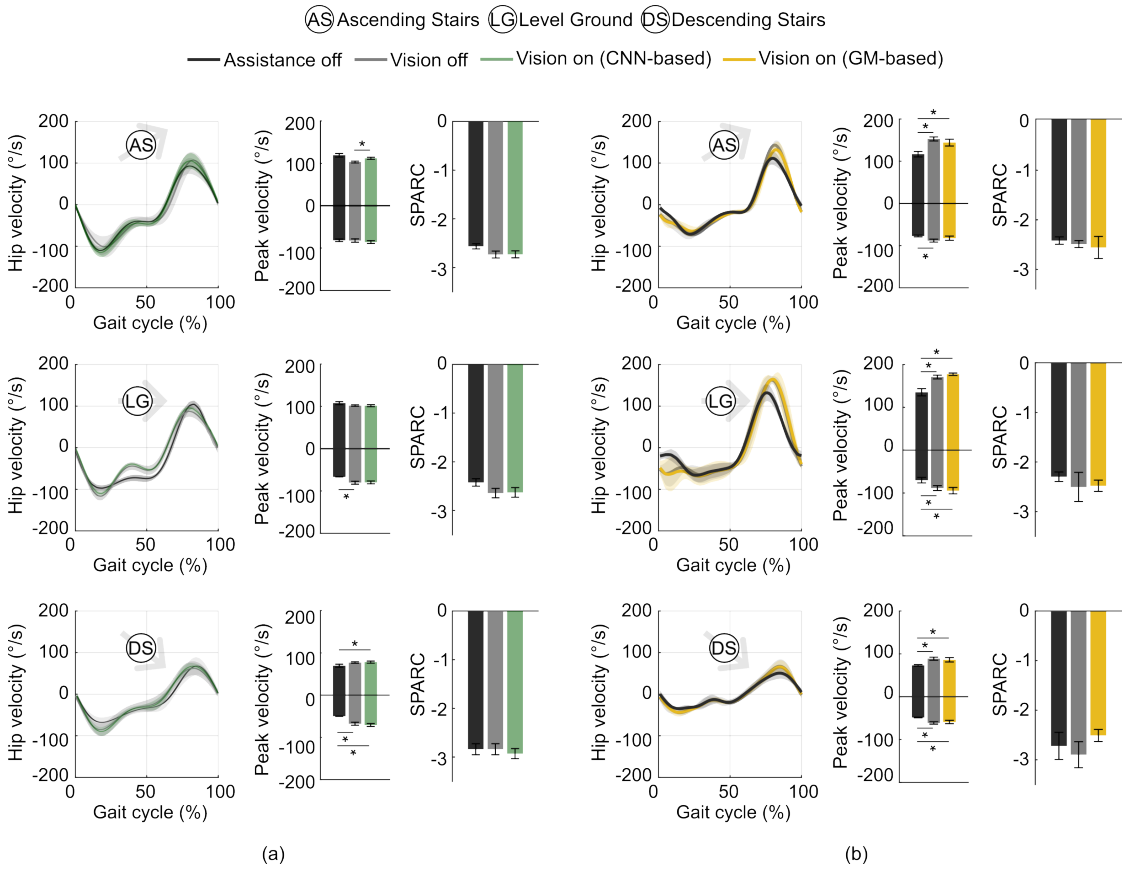


Figure 5.7. Kinematics. Timeseries of hip velocity for a representative subject, averaged across steps, along with peak velocities during the swing and stance phases, and a measure of movement smoothness (SPARC) for the (a) CNN-based approach and the (b) GM-based method.

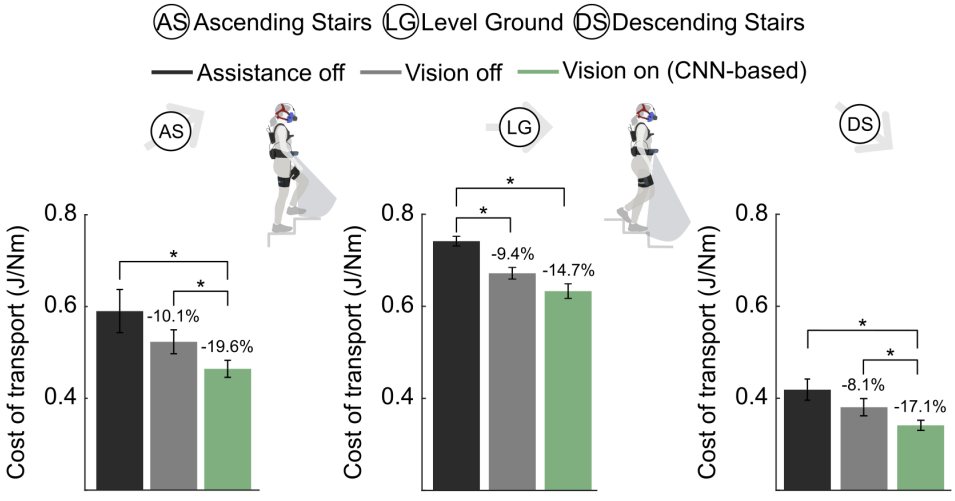


Figure 5.8. Metabolic cost with CNN-based computer vision. Comparison of the metabolic cost of transport across the *vision on* condition (green), *assistance off* (black), and *vision off* (grey).

For the GM-based method (Fig. 5.7-(b)), positive peak velocities were significantly higher in both the *vision off* and *vision on* conditions compared to *assistance off* during AS ($p < 0.01$). Negative peak velocities during AS decreased significantly in the *vision off* condition compared to *assistance off* ($p < 0.01$). During LG, positive peak velocities increased significantly in both *vision off* and *vision on* compared to *assistance off* ($p < 0.01$), while negative peak velocities decreased significantly in *vision off* ($p = 0.012$) and *vision on* ($p = 0.002$) compared to *assistance off*. In DS, positive peak velocities were significantly higher in both *vision off* and *vision on* compared to *assistance off* ($p < 0.01$), while negative peak velocities showed significant reductions in both *vision off* and *vision on* compared to *assistance off* ($p < 0.01$).

Finally, the assessment of movement smoothness using the SPARC Index showed no significant differences across the experimental conditions in any of the path segments.

Metabolic cost In the analysis using the CNN-based method (Fig. 5.8), one of the seven subjects was excluded due to fatigue onset during subsequent tests. Across the three walking segments, *vision off* and *vision on* conditions resulted in average savings of $10.1 \pm 3.8\%$ and $19.6 \pm 5.0\%$ during ascending stairs (AS), $9.4 \pm 1.8\%$ and $14.7 \pm 1.5\%$ during level ground (LG), and $8.1 \pm 5.7\%$ and $17.1 \pm 5.5\%$ during descending stairs (DS). Significant differences were observed between *vision off* and *assistance off* only during LG walking ($p = 0.004$), whereas *vision on* consistently showed significant savings compared to *assistance off* across all segments ($p < 0.05$). Additionally, comparisons between *vision off* and *vision on* revealed significant differences in all cases except during LG walking, where *vision on* exhibited slightly higher savings but failed to reach significance ($p = 0.09$).

For the GM-based method (Fig. 5.9), significant CoT reductions were observed in the *vision on* condition compared to *assistance off* during AS, with average savings of $18.9 \pm 4.1\%$ ($p < 0.01$). While *vision off* exhibited a mean saving of $5.2 \pm 4.1\%$ during AS, this did not reach statistical significance ($p > 0.05$). Savings under *vision on* during AS were significantly greater than those under *vision off* ($p < 0.01$). During LG walking, both *vision off* and *vision on* conditions showed significant reductions compared to *assistance off*, with savings of $14.2 \pm 3.2\%$ ($p < 0.01$) and $13.4 \pm 5.6\%$ ($p < 0.01$), respectively, but no significant difference was observed between *vision off* and *vision on* ($p = 0.89$). For the DS segment, *vision on* resulted in a significant CoT reduction compared to *assistance off*, with average

savings of $10.1 \pm 3.6\%$ ($p < 0.01$). No significant differences were found between *vision off* and *assistance off*, nor between *vision on* and *vision off* during DS.

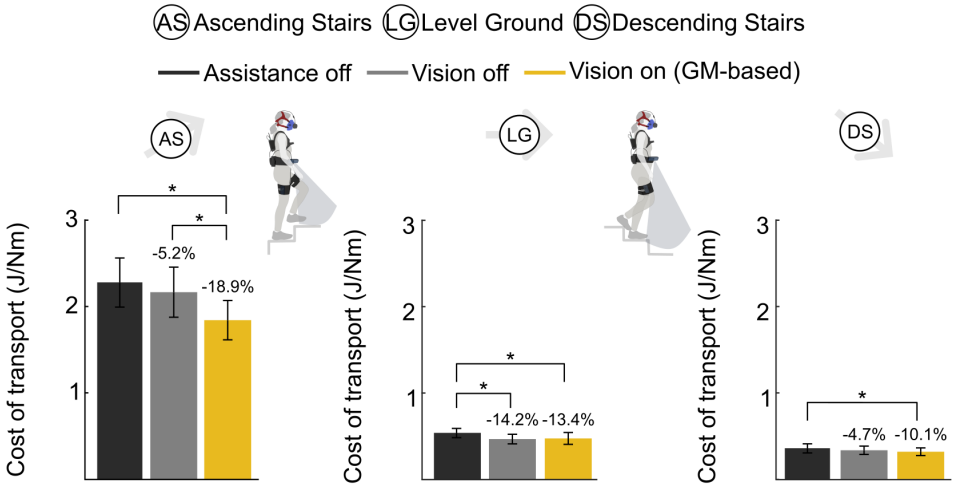


Figure 5.9. Metabolic cost with GM-based computer vision. Comparison of the metabolic cost of transport across the *vision on* condition (green), *assistance off* (black), and *vision off* (grey).

5.4 Discussion

The transition toward context-aware control in wearable assistive robotics represents a significant paradigm shift aimed at overcoming the inherent limitations of existing assistive devices. These limitations primarily relate to the difficulty of effectively adapting assistance across diverse tasks, such as transitioning between level walking and stair climbing, where device efficacy often becomes compromised [103, 105].

This chapter illustrates how computer vision (CV) can serve as an integral component of the control framework in the soft robotic suit, enabling improved adaptability. Two approaches were explored to achieve this goal: a data-driven method using a Convolutional Neural Network (CNN) and a physics-informed method based on geometric modeling (GM). The CNN-based method classified images captured by an RGB camera, leveraging a large dataset of 10,500 images for training. This integration, for the first time, demonstrated the advantages of using visual cues to modulate assistance, enhancing the device's performance across different environments. Conversely, the GM-based method employed geometric modeling of elements captured by an RGB-D camera to infer scene properties such as plane

orientations, dimensions, and interconnections. After a brief calibration step requiring less than 10 seconds to align camera and environmental reference frames, the GM-based system is ready for real-time use.

To the best of the author's knowledge, these studies represents the first instance of successfully deploying such context-aware approaches in real-time embedded mode within a wearable robotic suit. This addresses a critical research question: can assistance modulation be effectively achieved using visual inputs? The initial hypotheses proposed that integrating context-awareness into a robotic suit enhances assistance adaptation across various locomotion tasks and that this could be achieved using both data-driven and physics-informed approaches with comparable results. These hypotheses were evaluated by assessing user benefits, such as metabolic energy savings, and through a comparative analysis of the two methods.

Comparative performance of CNN-based and GM-based context-aware controllers Experimental conditions in two separate studies allowed for the evaluation of the CNN-based and GM-based approaches under controlled conditions. Although conducted in a single laboratory trial, the standardized protocol and independence of the vision module from individual subjects lend credibility and generalizability to the findings.

As summarized in Table 5.2, the GM-based method offers a more resource-efficient alternative to the CNN-based approach, making it particularly suitable for real-time embedded applications where hardware complexity and power consumption are critical constraints. Unlike the CNN-based system, which relies on GPU acceleration, the GM-based method processes point cloud data directly on the CPU, significantly reducing memory requirements and eliminating the need for a GPU. This makes it an attractive option for cost-effective, power-efficient systems. However, the CNN-based approach excels in scenarios demanding high processing speed, leveraging GPU acceleration for faster inference times. Despite its slower processing speed, the GM-based method meets the sampling frequency requirements of the application, as classifications are needed only once per step (approximately every 500 ms at typical walking speeds).

Both methods achieved comparable classification accuracies (Fig. 5.5-(a,b)), consistently exceeding 80% across all path segments. While the accuracy for ascending stairs and level ground segments was similar, the GM-based method showed slightly lower accuracy for descending stairs. Importantly, sporadic misclassifications did not pose safety risks due to the soft nature of the robotic suit, which allows for

easy backdriving. Misclassifications resulted only in minor variations in assistance levels, ensuring the system remained user-safe.

During transitions between environmental conditions, the GM-based method outperformed the CNN-based approach in three of four transitions, attributed to its use of depth information and attention to the user's immediate surroundings. However, its assumption of interconnected, geometrically consistent staircases may limit performance in environments with irregular or unmodeled geometries, where a CNN-based system trained on diverse datasets might generalize more effectively.

Comparison with existing literature is constrained by the limited number of studies that have implemented and tested assistance modulation in wearable assistive devices, especially those moving beyond conceptual frameworks or isolated testing of vision algorithms. Most prior research focuses on evaluating vision algorithms independently, with minimal integration into real-time embedded robotic systems. For instance, Zhang et al. [130, 131] developed a CNN-based system for environmental feature recognition in lower-limb prosthetic control, achieving an estimation error of less than 5% in indoor settings. However, their approach relies on an IMU sensor for calibration and involves an extensive training phase, which can complicate deployment. In contrast, the approaches presented in this study streamline implementation by eliminating the need for additional sensors and bypassing the training phase, enabling faster and simpler deployment.

Similarly, Kurbis et al. [132] introduced a large-scale automated stair recognition system using CNNs for indoor and outdoor environments, reporting classification accuracies between 86% and 94% for transitions such as LG to AS, depending on dataset size ($25,000$ to $400,000$ images per class). While the classification accuracy in our implementation appears lower, our system operates without labeled transition classes. Instead, it classifies scene elements based on their proximity to the user, prioritizing those closest. The accuracy figures reported in this study reflect the final aggregated classifications derived through a majority voting procedure across the previous and current steps at the mid-level controller. This approach effectively reduces the system's "effective" sampling frequency to that of a single step, contrasting with raw frame-by-frame accuracy typically reported in vision module outputs.

It is important to recognize that while the current method demonstrates promising results, its generalizability in unmodeled scenarios requires further evaluation. Data-driven approaches trained on more diverse datasets may potentially achieve

higher accuracy in such contexts, warranting further investigation.

Assistance modulation allows higher metabolic savings The metabolic results highlight the robustness of the methods presented. While metabolic savings are inherently subject-specific, the demographic similarities among participants allow for comparison of the findings.

The modulation of assistive torque achieved by the context-aware controller, as shown in Fig. 3.3-(b), highlights its ability to dynamically adjust hip flexion assistance in response to the environment, outperforming the fixed assistance condition. In the *vision off* condition, assistive torque was preset to an intermediate level optimized for level ground walking, as detailed in Chapter 4. Adjusting the motor position trajectory based on environmental detection allows the robotic suit to deliver forces that align with the physiological demands of the hip flexor muscles, which are particularly active during stair climbing to lift the legs and propel the body upward [133]. Conversely, during stair descent, the hamstrings play a more significant role in controlling forward motion and decelerating the body [134], reducing the need for hip flexion assistance.

The benefits of this modulation are further supported by the observed metabolic results (Figs. 5.8 and 5.9). Metabolic cost, a widely accepted metric for assessing wearable robotic devices [24], demonstrated notable improvements under the *vision on* condition during stair climbing. Specifically, significant reductions of approximately 19% during ascent were observed compared to the unassisted condition (*assistance off*). In contrast, the *vision off* condition yielded metabolic savings only on level ground (approximately 10–14%), with no significant differences from *vision on* on this terrain, reflecting the consistent controller behavior for level walking.

During stair descent, the data-driven method exhibited a significant reduction in metabolic cost with *vision on* compared to *vision off*. However, no significant differences were observed between the GM-based approach and the data-driven method in this segment, which may be attributed to lower classification accuracy in the GM-based method for this specific task. This reduced accuracy occasionally resulted in misclassifications as level ground (15% of cases), leading to higher-than-required assistance and necessitating increased effort from participants to counteract the torque. Conversely, misclassifications during stair ascent resulted in reduced assistance, which, while not optimal, was less detrimental than excessive assistance during descent. Future work should focus on improving classification

accuracy for descending stairs.

Unrestricted natural motion The hip kinematic analysis confirmed that the robotic suit did not restrict natural motion. On the contrary, peak hip velocities increased in some conditions, suggesting enhanced movement without hindrance (Fig. 5.7). This highlights the system's ability to provide effective assistance without compromising user mobility.

Practical remarks and future directions The proposed control strategy opens up opportunities for diverse applications. By refining the computer vision algorithm, the system's capabilities can be extended to a wider range of scenarios. For instance, the algorithm could be adapted to detect obstacles in the environment, going beyond stair recognition. This adaptation has considerable potential in wearable assistive technologies aimed at improving human mobility in unstructured environments. Such advancements could help individuals navigate crowded or cluttered spaces, ensuring smoother and safer movement in challenging conditions. Integrating these additional features in future iterations of the system could significantly enhance its utility in real-world applications.

While this study demonstrates the effectiveness of integrating computer vision to modulate walking assistance, certain limitations should be acknowledged. The experiments involved a relatively small sample size (n=6) and were conducted in a controlled laboratory setting. These factors may limit the generalizability of the findings to broader populations or more varied environments.

To build on this work, future efforts should address these limitations. Expanding the participant pool will increase the statistical robustness of the findings and provide a deeper understanding of the algorithm's performance across diverse user profiles. Additionally, transitioning from controlled laboratory settings to real-world environments with varying conditions will better evaluate the algorithm's practical applicability. Introducing advanced features, such as obstacle detection, could further broaden the system's scope, making it a more versatile solution for assisting users in complex, real-world scenarios.

Up to this point in the dissertation, evaluations have been carried out in controlled laboratory environments, where the AOs-based control strategy, enhanced by context-awareness including computer vision, showed promising results in modulating assistance. However, the practicality of these methods in the real-world, characterized by unpredictability and complexity, presents several challenges. While visual data effectively supports environmental recognition in controlled settings, it

is limited by high computational demands, can struggle with diverse, unmodeled conditions and being influences by lightening factors.

Chapter 6 shifts the focus to a real-world evaluation of the soft robotic suit, where the translation of these control strategies has underscored the need for a more straightforward and efficient approach. The next chapter will introduce a refined controller that bridges the framework discussed in Chapter 3 with the requirements for responsiveness and computational efficiency, making it better suited for outdoor, dynamic settings. This transition represents a critical step toward advancing wearable assistive technologies for real-world applications, with implications for upcoming trials involving older adults in Chapter 7.

Chapter 6

From the laboratory to the real-world: a hiking study

The contents of this chapter are adapted from the journal paper and patent application:

E. Tricomi, F. Missiroli†, M. Xiloyannis†, N. Lotti, X. Zhang, M. Stefanakis, M. Theisen, J. Bauer, C. Becker, and L. Masia. "*Soft robotic shorts improve outdoor walking efficiency in older adults*". **Nature Machine Intelligence** pp. 1-11, 2024.

E. Tricomi, L. Masia, F. Missiroli, L. Lotti, "*Assistance system for walking assistance, computer-implemented method for controlling an assistance system, and corresponding non-transitory computer readable storage medium*", WO 2024/160839 A1, 2024.

This chapter presents a real-world evaluation of the soft robotic suit during uphill outdoor walking, representing a crucial step in advancing the developed assistive technology from controlled laboratory settings to practical, real-world environments. The study introduces a novel control strategy for gait phase estimation, relying on a deterministic set of equations with more predictable outcome than dynamic estimators (e.g., AOs) or stochastic learning processes, which improves the system's responsiveness and computational efficiency. Tested on healthy young adults navigating a hiking trail, the suit was assessed for metabolic efficiency, gait patterns, and the psychophysical sense of agency (i.e., the perception of control over one's movements). The results revealed a significant 17.79% reduction in the metabolic cost of transport during uphill walking, with no disruption to natural movement patterns and a preserved sense of agency. These findings underscore the potential of wearable assistive devices to augment motion in challenging outdoor environments, laying the groundwork for upcoming trials with older adults in Chapter 7 and further development for wider applications.

6.1 Out of the lab, into the field

In 2009, Daniel P. Ferris envisioned a future where wearable robotic technologies would play a central role in daily life, predicting that by 2024, individuals would navigate streets, malls, and homes equipped with robotic exoskeletons [135]. This vision highlighted the transformative potential of wearable assistive devices to enhance mobility and independence for diverse populations. Yet, despite significant advancements, wearable technologies remain predominantly confined to controlled laboratory settings, with limited deployment in unstructured, real-world environments [136, 137].

The transition from laboratory prototypes to real-world systems poses numerous challenges, particularly in designing assistive devices capable of responding reliably to the variability of natural human locomotion. These systems must function autonomously across diverse walking speeds, uneven terrains, and changing gait patterns, all while preserving the user's sense of agency, the perception of control over their own movements [52, 138]. These demands exceed the capabilities of many existing systems and highlight the need for robust, reliable control strategies capable of supporting diverse activities without compromising computational efficiency or responsiveness.

In Chapters 4 and 5, an Adaptive Oscillators (AOs)-based control framework was introduced, combining machine learning and artificial computer vision for adaptive gait phase estimation and context-based assistance tuning. These approaches showed promising results in structured environments; however, several limitations persisted. The AOs-based controllers experienced delays during transitions between different cadences and gait initiation. Furthermore, despite being governed by a deterministic set of equations, the system's performance results heavily influenced by noise recorded by the sensors and tuning characteristics. While machine learning and vision-based methods enhanced adaptability and modulation, they also added computational complexity and the need for extensive training phases, raising concerns about reliability and generalizability in dynamic, real-world conditions.

Before delving into a field validation, this chapter introduces a novel approach to gait phase estimation to address the challenges of the previously explored control strategies. The new controller eliminates the need for oscillatory dynamical models, learning algorithms, or vision-based techniques.

The high-level controller in this implementation directly estimates the gait phase

from raw measurements by analyzing the angular separation of position and velocity vectors within the hip phase portrait [74]. This deterministic method enhances responsiveness, robustness, and computational efficiency, making it particularly well-suited for varied and unstructured environments.

To achieve objective 2 ("Real-world assessment") and validate general hypothesis 3 outlined in Chapter 1, an outdoor hiking study was carried out. Healthy young adults navigated an uphill path while wearing the soft robotic suit, providing an opportunity to assess the system's performance under realistic and challenging conditions. The study focused on the suit's ability to deliver biomechanical and physiological assistance, with key metrics including energy efficiency, gait patterns, and user perception of control. This evaluation represents a significant step in transitioning wearable assistive technologies from controlled laboratory settings to practical, real-world applications.

Hypotheses The specific hypotheses tested in this study are as follows:

1. The soft robotic suit reduces the metabolic cost of walking compared to unassisted walking;
2. The system does not restrict natural kinematic patterns of locomotion;
3. Users retain full control over their voluntary movements, fostering a strong sense of agency.

6.2 Phase portrait-based control framework

To achieve robust assistance in real-world scenarios, the focus here is shifted on a refined control framework that prioritizes responsiveness and adaptability while maintaining computational efficiency. While the general structure of the framework remains consistent with the design outlined in Chapter 3, Figure 3.5, this implementation introduces several advancements.

Specifically, the suit employs a high-level controller that calculates a monotonically increasing gait phase variable using raw data from the inertial sensors on each leg. This is supported by a mid-level controller that generates actuator reference motions based on the user's gait phase and a Kalman filter. Finally, a low-level controller ensures precise assistance delivery by executing the commands from the preceding layer (Fig. 6.1).

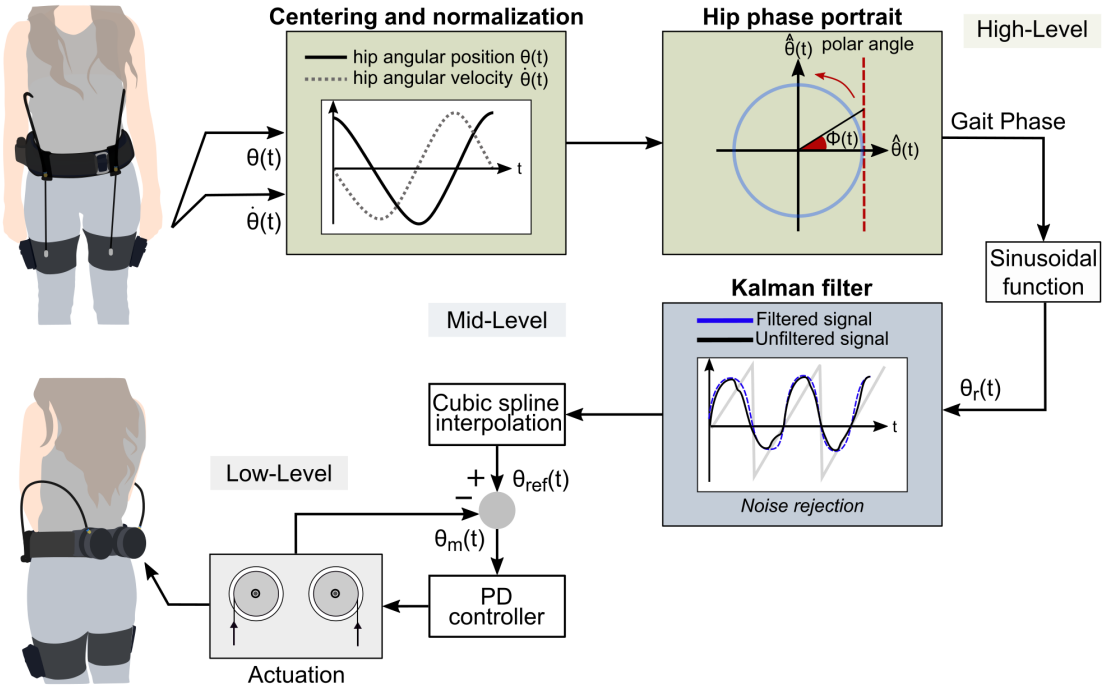


Figure 6.1. Phase portrait-based controller. At the high-level, the controller calculates the gait phase in real-time by determining the polar angle between the hip's position and velocity, and generates an initial motor position trajectory using sinusoidal interpolation. The mid-level then processes this trajectory by applying a Kalman filter to minimize noise and further refines it through cubic spline interpolation. At the low-level, the system actuates tendon displacement by executing motor commands based on the refined trajectory and the feedback from the current motor position.

The phase portrait-based control framework was implemented in both actuation configurations of the suit, underactuated and fully actuated (Chapter 3) to determine which design offered greater benefits during real-world use. A preliminary trial demonstrated superior results for the fully actuated configuration, which was subsequently adopted as the optimal design for the main study detailed in this Chapter. Results from the preliminary trial are included in the Appendix.

6.2.1 High-level controller

The gait phase estimation strategy on the high-level controller builds on principles from the general theory of oscillating dynamical systems. During natural locomotion, the angular position of the hip joint, $\theta(t)$, follows a periodic trajectory that closely resembles a sinusoidal waveform, similarly to the motion of an undamped oscillator [139, 140]. Consequently, the hip angular velocity, $\dot{\theta}(t)$, exhibits a phase

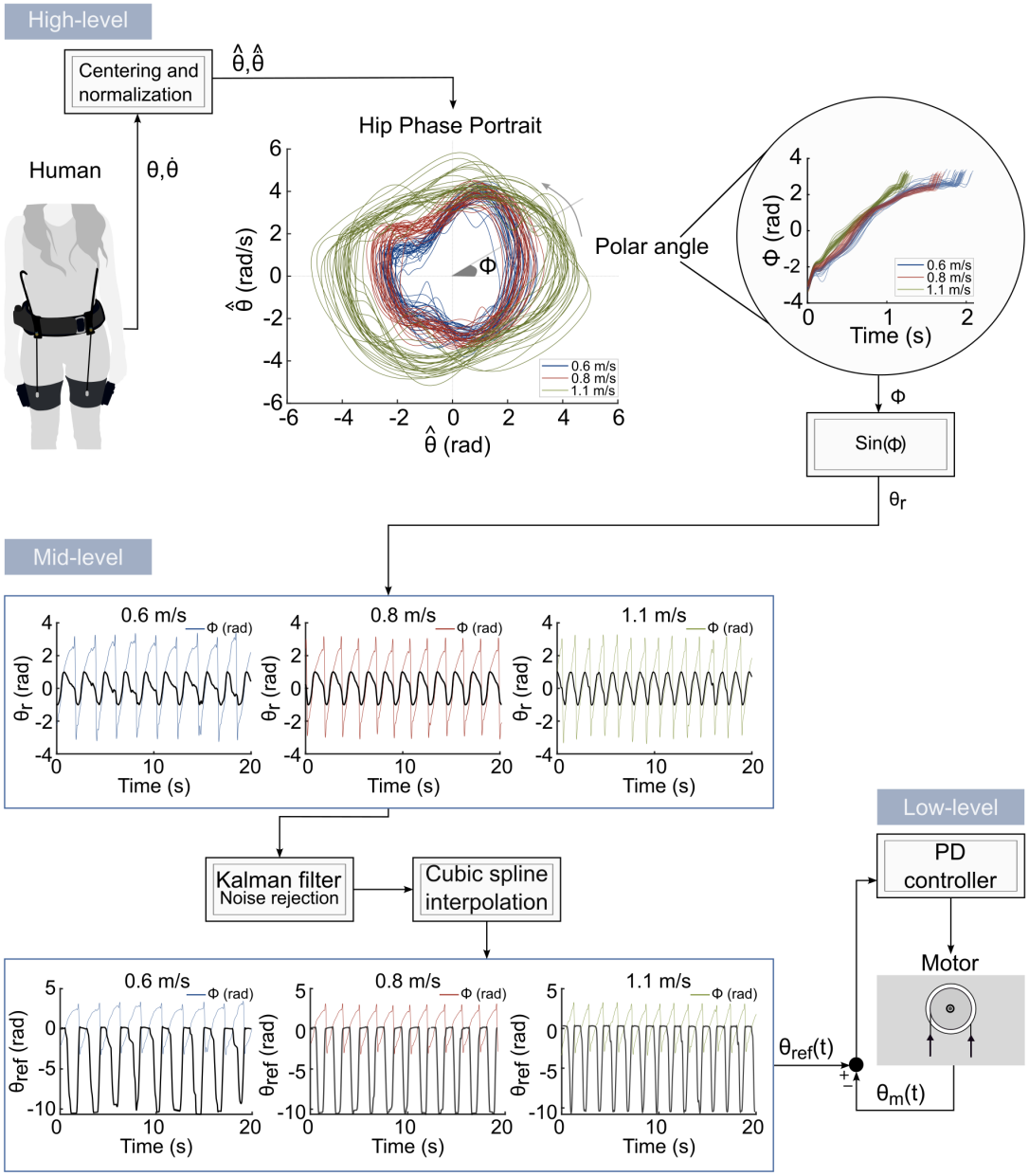


Figure 6.2. Schematic representation of the phase portrait-based control framework. The high-level controller tracks the circular movement of the hip joint's position and velocity, visualized in the hip phase portrait. From this, it computes a gait phase variable that increases linearly, based on the angle between the hip's position and velocity during each step. At the mid-level, a Kalman filter is used to enhance the signal's sensitivity to sensor noise. The filtered signal is then used by the controller to generate a reference position trajectory, which is transmitted to the motor at the low-level.

shift of $\pi/2$ relative to $\theta(t)$, resulting in a counterclockwise circular orbit in the position-velocity phase plane, referred to as the *hip phase portrait* (Fig. 6.2).

The gait phase, denoted as $\phi(t) = f([\theta(t), \dot{\theta}(t)])$, is computed in real time by determining the polar angle between these two quantities in the phase portrait. This polar angle reflects the progression of the gait phase through the gait cycle and is calculated using the following equation, presented in Iverson bracket notation:

$$\phi(t) = \arctan\left(\frac{\hat{\dot{\theta}}(t)}{\hat{\theta}(t)}\right)[\hat{\theta}(t) \neq 0] + \eta(t) \tag{6.1}$$

where $\hat{\theta}(t)$ and $\hat{\dot{\theta}}(t)$ are the normalized and centered angular position and velocity of the hip, respectively. The term $\eta(t)$ is a corrective factor that resolves the ambiguity arising from the back-and-forth motion of the hip, which creates at least two potential solutions for each $\theta(t)$. This factor is defined as:

$$\eta(t) = \text{sgn}(\hat{\dot{\theta}}(t))\left(\pi[\hat{\theta}(t) < 0] + \frac{\pi}{2}[\hat{\theta}(t) = 0]\right) \tag{6.2}$$

To ensure accurate computation of $\phi(t)$, both variables are preprocessed for each step. The variables are shifted to center the origin of the hip phase portrait, and $\theta(t)$ is rescaled to match the amplitude of $\dot{\theta}(t)$. This step ensures that the phase portrait forms a near-perfect circular orbit, increasing the linearity of $\phi(t)$ over each stride, as outlined by Quintero et al. [141]:

$$\hat{\theta}(t) = \frac{|\dot{\theta}_{max_i}(t) - \dot{\theta}_{min_i}(t)|}{|\theta_{max_i}(t) - \theta_{min_i}(t)|}\left(\theta(t) - \frac{\theta_{max_i}(t) + \theta_{min_i}(t)}{2}\right) \tag{6.3}$$

$$\hat{\dot{\theta}}(t) = \dot{\theta}(t) - \frac{\dot{\theta}_{max_i}(t) + \dot{\theta}_{min_i}(t)}{2} \tag{6.4}$$

Here, the maximum and minimum values of $\theta(t)$ and $\dot{\theta}(t)$ correspond to the extrema of the i^{th} stride, determined by identifying the zero-crossings of $\dot{\theta}(t)$ and $\ddot{\theta}(t)$, respectively. These steps are critical to refining the walking limit cycle into a circular shape, which enhances the precision and consistency of $\phi(t)$ across strides.

Importantly, this gait phase estimation inherently captures information about walking speed, allowing the system to instantly adapt to changes in the user's gait pattern. To generate a motor reference trajectory consistent with the sinusoidal characteristics of hip flexion in the sagittal plane, a sinusoidal interpolation

is applied to the estimated gait phase. The resulting signal, $\theta_{\mathrm{r}}(t) = \sin(\phi(t))$, serves as the foundation for the actuator's reference motion.

6.2.2 Mid-level controller

The method for extracting gait phases can be vulnerable to noise detected by the inertial sensors, especially on uneven terrains. This noise may originate from impacts during heel strikes at consistent speeds or from movement in the textile frame on the user's thigh, potentially affecting the motor reference motion signal, $\theta_{\mathrm{r}}(t)$.

To improve the control strategy's resilience to disturbances caused by noise, a Kalman filter [142] is cascaded with the gait phase estimator in the mid-level controller (Fig. 6.2):

$$\begin{bmatrix} \hat{\theta}_{r_t} \\ \hat{\dot{\theta}}_{r_t} \end{bmatrix} = A \begin{bmatrix} \hat{\theta}_{r_{t-1}} \\ \hat{\dot{\theta}}_{r_{t-1}} \end{bmatrix} + K_t \Big(\theta_{r_t} - C \begin{bmatrix} \hat{\theta}_{r_{t-1}} \\ \hat{\dot{\theta}}_{r_{t-1}} \end{bmatrix} \Big) \tag{6.5}$$

being $\begin{bmatrix} \hat{\theta}_{r_t} \\ \hat{\dot{\theta}}_{r_t} \end{bmatrix}$ the current state estimate (i.e., motor reference trajectory and its derivative), $\begin{bmatrix} \hat{\theta}_{r_{t-1}} \\ \hat{\dot{\theta}}_{r_{t-1}} \end{bmatrix}$ the predicted state estimate given past measurements of $\theta_{\mathrm{r}}(t)$ up to time $t-1$, and being $\theta_{\mathrm{r}}(t)$ the current approximated motor reference.

The system matrix A and the output matrix C are set as follows:

$$A = \begin{bmatrix} 1 & \Delta t \\ 0 & 1 \end{bmatrix}; C = \begin{bmatrix} 1 & 0 \end{bmatrix} \tag{6.6}$$

The update cycle time frame, denoted as Δt, is set to 0.01. The Kalman gain, K_t, is used to characterize the noise, with its parameters defined by the process noise covariance matrix Q and the measurement noise covariance matrix R, such that:

$$K_t = (APC^T)(CPC^T + R)^{-1} \tag{6.7}$$

where P is the state covariance matrix chosen to minimize the error in the estimate and it is defined as:

$$P = AP_{t-1}A^T + Q \tag{6.8}$$

$$Q = \begin{bmatrix} 0.02 & 0 \\ 0 & 0.02 \end{bmatrix}; R = 0.75 \tag{6.9}$$

The actuator's final position reference trajectory, $\theta_{\text{ref}}(t)$, is created using a motion mapping method that applies cubic spline interpolation to the sinusoidal profile $\theta_{\text{r}}(t)$. The amplitude of $\theta_{\text{r}}(t)$ is modified according to the physiological range of motion of the hip.

Stop condition A stop detection condition is established based on the gait speed. The gait speed (s_{gait}) is estimated by calculating the vector norm between $\hat{\theta}(t)$ and $\hat{\dot{\theta}}(t)$ (i.e., the polar radius) in the hip phase portrait [141].

$$s_{gait} = \sqrt{\hat{\theta}(t)^2 + \hat{\dot{\theta}}(t)^2} \tag{6.10}$$

This value is then compared to a pre-defined stop threshold, which is determined experimentally based on the noise from the kinematic sensors when at rest. If the stop condition is satisfied, $\hat{\theta}_r(t)$ is set to zero before applying the Kalman filter and subsequent interpolation. This ensures that the actuator reference signal smoothly approaches zero, leveraging the dynamic properties of the filter to avoid abrupt changes or discontinuities.

6.2.3 Low-level controller

A feedback position control loop continuously compares the motor's actual position, $\theta_{\text{m}}(t)$, with the reference position, $\theta_{\text{ref}}(t)$, provided by the preceding layer. The position error, $(\theta_{\text{ref}}(t) - \theta_{\text{m}}(t))$, is then translated into motor angular velocity using a Proportional-Differential (PD) controller.

6.3 Technology assessment on hiking trail

6.3.1 Experimental Protocol

The primary goal of this study was to assess the effectiveness of the soft robotic suit in improving walking performance under real-world conditions. To this end, a technology assessment was conducted on an uphill outdoor hiking trail with young adults serving as their own controls across multiple walking conditions.

Twelve young and physically fit individuals, seven men and five women, were recruited for the technology assessment (mean age 25.42 ± 2.27 years, mean height 173.50 ± 11.63 cm, and weight 66.25 ± 11.73 kg, Table 6.1).

Participant	Age (year)	Weight (kg)	Height (cm)	Sex (-)
(01)	24	74	184	M
(02)	28	60	156	F
(03)	23	60	171	M
(04)	27	93	193	M
(05)	28	54	163	F
(06)	23	70	171	M
(07)	25	62	170	F
(08)	29	48	158	F
(09)	27	60	168	F
(10)	23	73	185	M
(11)	25	67	178	M
(12)	23	74	185	M

Table 6.1. Participants demographic.

Participants were recruited based on specific inclusion criteria: they were aged between 18 and 35 years, with no visual or auditory impairments and no neurological, cardiovascular, metabolic, or mental disorders that could interfere with task performance. Before the study began, all participants provided informed written consent, and the research was conducted in compliance with the principles of the Declaration of Helsinki. The study was approved by the Ethics Committee of Heidelberg University under resolution No. S-313/2020.

The experimental path selected for the study was a section of the Philosophenweg trail in Heidelberg, Germany (49°24'55.1"N 8°42'00.9"E), known for its steep and winding terrain (Fig. 6.3). A 500 m segment of the trail was used, featuring an altitude change from 127 m to 184 m. This section began with 108 uneven sandstone steps followed by a steep uphill pathway. Participants were asked to walk the trail at their preferred speed in two primary conditions: without assistance (*assistance off*) and with assistance provided by the fully actuated configuration of the soft robotic suit (*assistance on*). In the *assistance off* condition, the system was worn in an unpowered mode to allow for the collection of baseline kinematic data. To mitigate fatigue-related effects, each condition was performed on separate days, given the physically demanding nature of the trial.

The decision to use the fully actuated configuration of the soft robotic suit was

informed by preliminary trials involving a subgroup of participants (n = 7). These trials compared the system's performance under the two actuation setups presented in Chapter 3 during the hiking task. As reported in the Appendix, the fully actuated configuration demonstrated superior metabolic benefits, making it the preferred setup for the main study. The same subgroup of participants walked the trail downhill after completing the uphill segment, covering a total distance of 1 km. This data, also presented in the Appendix, focused on assessing the system's impact during downhill walking, where hip flexion assistance is less critical due to reduced demands for ground clearance [143].

Another subgroup (n = 5) performed an additional uphill trial without donning the suit (*no suit*) to evaluate the metabolic impact of the device's weight, with these results also included in the Appendix.

Familiarization In order to mitigate any disparities coming from prior device use, all participants were first-time users. A familiarization process was conducted prior to data collection. During this phase, participants were allowed enough time to become accustomed to the device by walking with the suit along a straight 100m outdoor path located near the starting point of the hiking trail. They were encouraged to repeat the procedure as many times as needed until they felt comfortable and confident operating the device. After completing the familiarization, participants were given adequate rest to minimize any fatigue effects before beginning the experimental tasks.

Data collection To validate the initial hypotheses, the study evaluated metabolic walking efficiency, kinematics, and the sense of agency. Metabolic efficiency was the primary outcome, assessed by measuring oxygen and carbon dioxide consumption using a portable respirometer (K5, COSMED, Italy). Kinematic performance was analyzed using data from the suit's integrated IMU sensors. The sense of agency was evaluated through a ten-item questionnaire, with participants rating their responses on a Likert scale from 1 (strongly disagree) to 7 (strongly agree).

6.3.2 Data analysis

Metabolic cost The net metabolic cost was calculated using Péronnet and Massicotte's formula based on oxygen and carbon dioxide data [96]. To establish a baseline, participants stood at rest and breathed normally for three minutes be-



Figure 6.3. Uphill outdoor walking task. Participants walked a challenging 500 m uphill trail, with an elevation gain from 127 m at the start to 184 m at the end. Young adults completed the task at their preferred pace under two conditions: unassisted (*assistance off*) and assisted with the soft robotic suit (*assistance on*).

fore each experiment began. The mean metabolic cost from the final minute of this baseline period was subtracted from the overall metabolic data to isolate the cost of walking for each condition. To adjust for variations in walking speed across conditions, the metabolic data were expressed as the cost of transport [144], calculated by dividing the net metabolic cost by the product of the participant's weight, gravitational acceleration, and average walking speed. Walking speed was determined by dividing the total distance covered by the duration of the experiment. Since it takes approximately two minutes for metabolic data to stabilize following significant physical activity, data from the initial two minutes of recording were excluded, and the remainder were analyzed.

Kinematics Kinematic assessments focused on the hip angle and velocity profiles for both the left and right legs, utilizing data captured by the inertial sensors integrated into the system. The raw motion data were processed by applying a low-pass filter (fourth-order Butterworth, cutoff frequency of 10 Hz) and segmented into individual steps. For each participant, the range of motion (ROM) and the average peak velocity during the stance and swing phases were analyzed across all steps, comparing the unassisted and assisted conditions.

Sense of agency To assess the sense of agency, participants completed a 10-items questionnaire comprising six positively worded items (number 1, 4, 5, 7, 9, and 10) and four negatively worded items (number 2, 3, 6, and 8), which evaluated their perceived control while using the soft robotic suit. The items were adapted from theoretical frameworks on the sense of agency and tailored to the context of wearable mobility devices [145]. Negatively worded items were recoded so that

higher scores consistently reflected a stronger sense of agency. A mean score across all items was computed for further analysis.

Statistics Results are reported as mean ± standard error of the mean (s.e.m.) or depicted using boxplots to illustrate linear walking velocity. Data normality was confirmed through the Shapiro-Wilk test, indicating that the dataset followed a normal distribution. Statistical significance was determined with $p < 0.05$.

Statistical analysis of metabolic and kinematic data was conducted using a linear mixed-effects model, implemented via least squares regression in MATLAB (MathWorks Inc., Natick, MA, USA). The model included "condition" (*assistance off* vs. *assistance on*) as a categorical fixed-effect explanatory variable, encoded as dummy variables. Additionally, "participant" was incorporated as a random-effect variable to account for inter-individual variability.

For the sense of agency analysis, participants' responses were evaluated to determine whether they perceived greater self-control over their movements or influence from the device. A two-tailed, one-sample t-test was conducted to compare the mean questionnaire score against the midpoint of the scale (4, indicating "neither agree nor disagree"). A mean score significantly above this midpoint was interpreted as participants perceiving themselves as primarily in control of their movements rather than the device.

6.4 Results

Metabolic cost The use of the soft robotic suit led to a significant reduction in the metabolic demand required to traverse the outdoor uphill trail, decreasing by $17.79 \pm 2.03\%$ (mean ± s.e.m., $n = 12$, $p < 0.001$) (Fig. 6.4-(a, b)). Linear walking velocity (Fig. 6.4-(c)) showed no statistically significant difference between conditions ($p = 0.07$), although there was a noticeable trend toward an average increase of 6.34% with *assistance on* compared to *assistance off*. Notably, eight of the twelve participants exhibited increased walking speeds while using the suit.

Kinematics Fig. 6.5-(b) displays the raw mean hip phase portrait for the twelve young adults walking along the uphill trail. Notably, wearing the suit did not interfere with the natural progression of hip angle and velocity throughout the gait cycle. The range of motion in the hip joint significantly increased when using the assistive robotic shorts (Fig. 6.5-(c)): in the *assistance off* condition, the

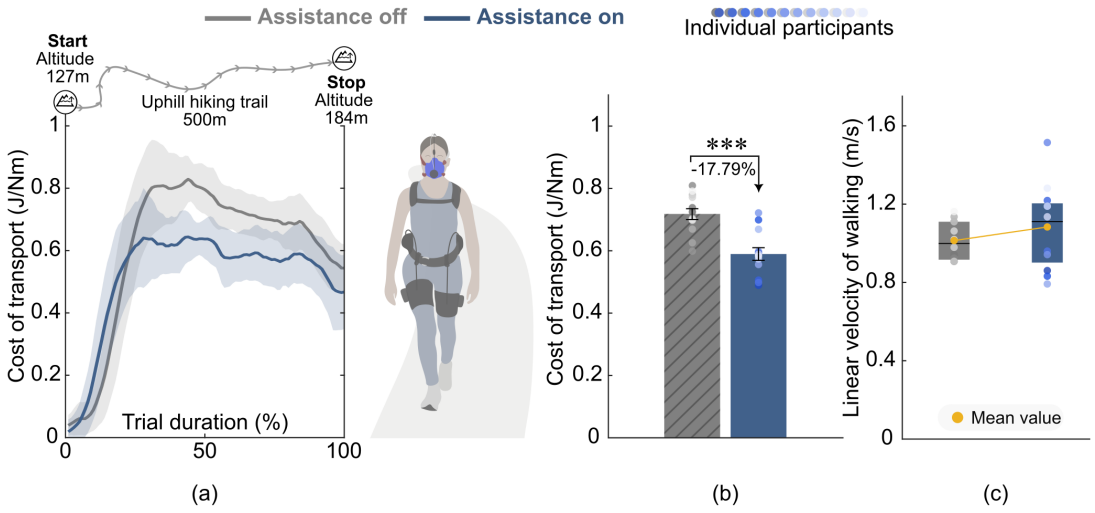


Figure 6.4. Metabolic cost. The metabolic results revealed a significant reduction in the cost of transport when performing the walking task with the soft robotic suit (*assistance on*, navy). (a) Cost of transport time series, with the thick line representing the average across participants and the shaded area indicating the standard deviation. (b) Mean cost of transport values (± s.e.m.). (d) Preferred walking speed along the trail, shown as boxplots where the horizontal line represents the median, and the orange circle indicates the mean. *** denotes statistical significance with $p < 0.001$.

average range of motion was $51.42 \pm 1.16°$ across both legs and subjects, which increased to $56.76 \pm 1.54°$ with *assistance on* ($+10.38 \pm 1.77\%$, $n = 12$, $p < 0.001$). However, the use of the device did not result in any significant change in hip peak velocities throughout the gait cycle (Fig. 6.5-(d)).

Sense of agency The questionnaire demonstrated good internal consistency after recoding ($\alpha = 0.84$, 95% CI [0.71; 0.92]). On average, the mean self-reported score on the questionnaire was 6.20 ± 0.20 (mean ± s.e.m.) out of 7 (Fig. 6.6). This score was significantly higher than the midpoint of 4 on the Likert scale ($n = 12$, $t = 11.26$, $p < 0.001$). These results indicate that the users' sense of control over their movements remained unchanged while using the device.

6.5 Discussion

Most research on wearable assistive devices has been confined to controlled laboratory conditions, typically involving flat terrain or treadmill walking, which restricts the applicability of findings to real-world scenarios. By contrast, this study is among the few to rigorously assess the effectiveness of such technologies in outdoor environments, addressing a critical gap in the literature and providing a

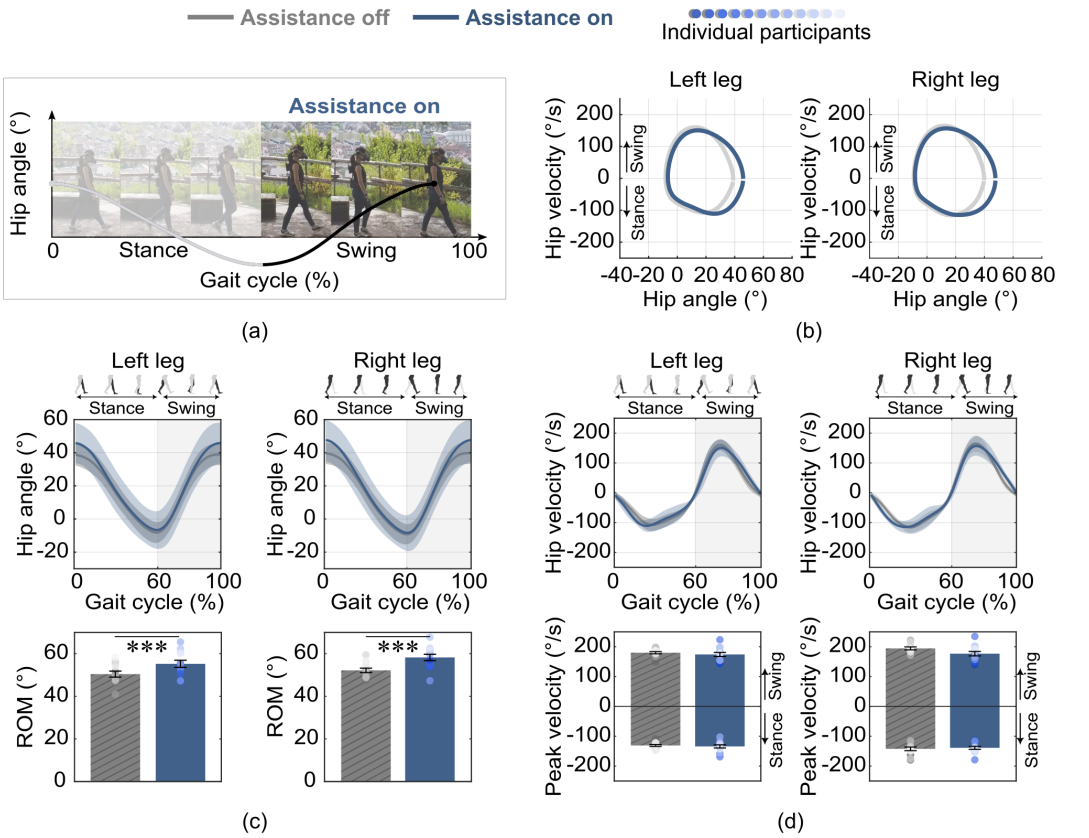


Figure 6.5. Kinematics. (a) The soft robotic suit provides active assistance to the hip joint during the swing phase. (b) Average hip phase portrait, combining hip angle and velocity in the sagittal plane, aggregated across steps and participants. (c) Hip range of motion (ROM) significantly increased with assistance (*assistance on*, navy) compared to the unassisted condition (*assistance off*, grey). (d) Peak hip velocities showed no significant differences between conditions. The upper row of (c) and (d) displays the mean time series across participants and steps (shaded areas represent standard deviation), while the lower row presents bar plots showing mean $\pm$ s.e.m. for hip ROM and peak velocity. *** indicates statistical significance with $p < 0.001$.

foundation for future exploration.

Direct comparisons with existing literature are limited due to the scarcity of studies evaluating wearable assistive technologies in outdoor environments. For example, Haufe et al. [146] tested the Myosuit, a commercial wearable robot designed to assist hip and knee extension, on a 400 m uphill gravel path with young participants. Their study showed an average metabolic saving of 10.6% compared to an unpowered condition. In contrast, Slade et al. [52] developed an ankle exoskeleton that reduced the cost of transport by 17% in young, healthy individuals on a 566 m flat path. While the ankle exoskeleton demonstrated notable efficiency gains, the system required significant personalization and adjustments, complicating its

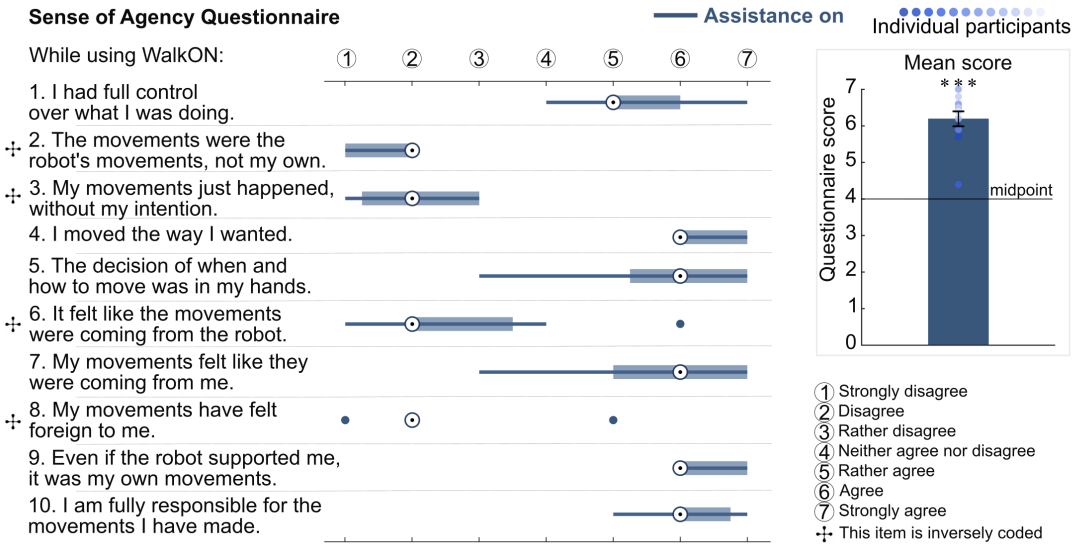


Figure 6.6. Sense of Agency. The sense of agency was assessed using a ten-item questionnaire on motor control, rated on a 7-point Likert scale (1 = strongly disagree, 7 = strongly agree). Items 2, 3, 6, and 8, which were inversely coded, were re-coded prior to analysis. The response distribution is illustrated with box-plots (white circles denote medians). The mean score (± s.e.m.) for young adults indicates that participants perceived significantly greater control over their movements compared to the device. Statistical significance was evaluated against the scale's midpoint value of 4 ("Neither agree nor disagree"). ***$p < 0.001$.

use.

The soft robotic suit controlled by the algorithm herewith described, on the other hand, continuously analyzes the user's movement in real-time and adjusts assistance accordingly, without requiring complex pre-programmed data or learning algorithms, as used in previous studies [52, 53]. This allows for a more responsive, efficient, and scalable solution, making the suit a true plug-and-play system that can easily integrate into daily routines.

Moreover, unlike the rigid systems tested in previous studies, the suit features a soft structure that conforms to the body like regular clothing, offering enhanced comfort and wearability. While this design enhances user comfort, it does make the force transmission less predictable, requiring more careful modeling and control of the system. Despite these challenges, the soft robotic suit demonstrated significant metabolic benefits in a physically demanding task, highlighting its effectiveness even without restricting natural movement.

The soft robotic suit significantly reduced the energy required for uphill outdoor walking The metabolic cost of transport, which measures the amount

of metabolic energy required to cover a unit of distance during walking [144], serves as a key indicator of the effectiveness of wearable robotic assistive devices. In this study, the suit demonstrated a significant improvement in walking efficiency, resulting in a 17.79% reduction in the metabolic cost of transport on average, compared to the *assistance off* condition (Fig. 6.4-(b)). In practical terms, these energy savings are equivalent to removing 10.3 kg from the waist [66].

These metabolic reductions were achieved without requiring high power outputs from the system, with a mean peak motor power of only 1.52 W/kg during walking, highlighting the efficiency of the assistance provided. These results are consistent with previous studies [147], which have shown that assistance with hip flexion, compared to other lower-limb movements such as hip extension [148] or ankle plantarflexion [35], is particularly effective in reducing metabolic costs. Even modest mechanical assistance from the device is sufficient to achieve substantial metabolic savings [147].

Natural hip joint movement was not restricted with assistance A critical aspect of wearable assistive devices is that they should not interfere with natural movement, especially for individuals without significant impairments [24]. This principle is central to the design of the soft robotic suit, which seeks to optimize energy efficiency without restricting natural movement patterns.

When evaluating hip joint movement during uphill walking, the use of the suit significantly increased the range of motion at the hip joint (Fig. 6.5-(c)). From a physiological perspective, uphill walking requires increased hip joint range of motion and reduced knee extension as the swing phase concludes [133]. The assistance from the system likely accentuated this adaptation, contributing to improved metabolic efficiency without interfering with natural movement.

The sense of agency was preserved The sense of agency, or the perception of control over one's actions, plays a critical role in the acceptance of wearable robotic devices [138]. It is defined as the feeling of being in control of an action [149]. In the context of assistive technologies, preserving the user's sense of agency is vital for the device's acceptance and usability. While there is a lack of studies on the real-world application of assistive devices that simultaneously quantify metabolic improvements and assess the psychophysical impact, this aspect is essential for ensuring a positive user experience [150].

In this study, participants reported a strong sense of agency, with mean Likert-scale ratings of 6.20 for young adults and 6.09 for older adults out of a possible score

of 7. This suggests that users felt a strong sense of control over their movements while using the device (Fig. 6.6). This outcome can primarily be attributed to the system's control strategy, which synchronizes the device's actions with the user's natural movement. By ensuring that no extraneous actions are imposed on the user, the assistance harmonizes with the walking pattern, adapting to changes in walking speed. This approach not only simplifies the user experience but also reduces barriers to use, making the suit a technology that users can integrate seamlessly into their daily lives.

Limitations and future work One of the primary limitations of this study is the absence of a control measurement of metabolic activity without wearing the device. The analysis relied on comparisons based on gross metabolic changes, using a condition where the device was worn but turned off as a reference. While this method is commonly used in the literature [24, 146, 151], it may not fully capture the real-world impact of the device. This approach allowed to isolate the active biomechanical effects of assistance from the passive effects of wearing the suit.

However, due to the physically demanding nature of the protocol, it was chosen not to include an additional experiment where participants walked without the suit. Only a subset of individuals participated in a trial without the suit's weight. Results for this subgroup, which are included in the Appendix, show that the system's weight had minimal impact on metabolic costs. Given the soft structure and positioning of the suit, its weight (2.93 kg) is unlikely to significantly affect the results, as demonstrated by previous biomechanical studies on added mass [66].

By demonstrating the effectiveness of the soft robotic suit in real-world applications, this chapter bridges the gap between laboratory research and practical deployment. The findings presented here establish a foundation for further development and validation of the soft robotic suit in diverse and unstructured settings, setting the stage for its testing in older adults, which will be introduced in the following chapter.

Chapter 7

Enhancing walking efficiency in older adults

The contents of this chapter are adapted from the journal paper:

E. Tricomi, F. Missiroli†, M. Xiloyannis†, N. Lotti, X. Zhang, M. Stefanakis, M. Theisen, J. Bauer, C. Becker, and L. Masia. "*Soft robotic shorts improve outdoor walking efficiency in older adults*". **Nature Machine Intelligence** pp. 1-11, 2024.

As the global population ages, preserving mobility and independence becomes a urgent matter, particularly as muscle strength declines and walking demands become more energy-intensive. This chapter presents the first outdoor evaluation of a soft robotic suit with older adults, extending the prior work with young adults presented in Chapter 6. Here, the focus shifts to frail individuals to assess the suit's impact on energy expenditure and mobility during outdoor walking. Findings demonstrate a significant 10.48% reduction in the metabolic cost of transport, an outcome that has important implications for reducing fatigue and improving daily activity engagement. Crucially, the suit enhanced walking efficiency without disrupting natural gait patterns, ensuring that users maintained their normal kinematics. While the results presented here are focused on the specific use case of older adults, the suit's potential extends beyond this demographic. The ability to improve mobility and reduce fatigue makes the soft robotic suit a promising solution for individuals suffering by minor motor impairments. Future research will be key to exploring its broader applicability in various settings, understanding the long-term effects, and addressing the device's integration into diverse real-world environments.

7.1 The age of aging

In one of the closing scenes of Paolo Sorrentino's acclaimed movie "Youth" [152], 2016, the lead character confronts his own aging process and remarks, "*I've become old and I don't know how I got here*". This Sorrentinian sentiment profoundly echoes within our society, where aging is representing a significant demographic shift. According to the World Health Organization, by 2030, one in six people worldwide will be aged 60 or older [12]. Aging, however, is not just a statistical phenomenon; it represents an escalating biological process that reshapes daily life [9]. Simple actions such as walking, climbing stairs, or rising from a chair gradually demand more energy, restricting mobility and compromising independence [60, 153].

In response to these challenges, significant progress has been made in developing wearable assistive technologies that enhance mobility [16]. Many of these devices, including traditional exoskeletons, rely on rigid actuated mechanisms that generate substantial joint torque to support movement [36, 154, 155]. However, their weight and bulkiness have constrained their use primarily to laboratory settings, while low user acceptance further limits their integration into daily life [156]. On the other end, soft robotic suits, like the one herewith featured, have demonstrated superior benefits, as well as to improve comfort and usability compared to rigid exoskeletons [14, 146, 157–159].

The previous chapter presented the real-world evaluation of the designed soft robotic suit with healthy young adults, highlighting its ability to reduce the energy cost of uphill walking without disrupting natural gait patterns or diminishing the users' sense of agency. This chapter advances the investigation by focusing on a specific use case: the application of the suit to enhance walking in older adults, a demographic for whom mobility challenges are often pronounced.

The rationale for targeting hip flexion as a key area of assistance for this population has already been discussed in Chapter 3: aging exacerbates the biomechanical demands placed on the hip flexors, which are among the first muscle groups to show significant strength declines [60]. This decline necessitates compensatory mechanisms that increase energy expenditure and diminish walking efficiency [8]. Interventions aimed at supporting hip function, therefore, hold significant promise for preserving mobility in aging populations.

The soft robotic suit presented in this work is specifically designed to meet these demands. By assisting hip flexion during the swing phase, the suit reduces the physical burden on the user, enabling more efficient walking, as demonstrated in

the real-world evaluations in Chapter 6.

This chapter builds on previous trials with younger adults, shifting the focus to older adults to investigate how the soft robotic suit addresses age-related mobility challenges. An efficacy study was conducted with participants aged 67 years and older on an outdoor walking track to evaluate the suit's impact. The study examines the fully-actuated system (Fig. 7.1), driven by hip phase portrait-based control presented in Chapter 6, which adaptively synchronizes assistance with the user's natural gait. By targeting age-related declines in hip strength, the suit aims to make walking more efficient and less physically demanding.

Hypotheses Consistent with the real-world evaluation in Chapter 6, it is hypothesized that the soft robotic suit can reduce the metabolic cost of walking compared to unassisted conditions. Furthermore, the system is expected to preserve natural kinematic patterns, ensuring physiological movement. Lastly, it is posited that users maintain a strong sense of agency, retaining full control over their voluntary movements while using the device.

7.2 Efficacy study with older adults

7.2.1 Experimental protocol

The efficacy study included ten older adults (n = 10) who met the selection criteria of being over 65 years old and classified as either "robust" or "pre-frail" according to the LUCAS Functional Ability Index [160]. Participants with severe uncorrected visual or auditory impairments or significant neurological, cardiovascular, metabolic, or mental conditions were excluded.

Recruited participants' age ranged from 67 to 82 years (mean age 74.10 ± 6.30 years), with a mean height of 176.10 ± 9.53 cm and a mean weight of 73.10 ± 12.84 kg (Table 7.1). The group had a balanced gender distribution, with an equal number of male and female participants. Based on the LUCAS Functional Ability Index [160], nine participants were classified as "robust", indicating they were active individuals for whom health promotion and physical exercise are recommended. The remaining participant was categorized as "pre-frail", reflecting a higher risk of mobility challenges.

To accommodate the physical capabilities of the participants, particularly those



Figure 7.1. An older adult wearing the soft robotic suit.

in the pre-frail category, the study was conducted on a less demanding and more accessible path than the hiking trail described in Chapter 6. This approach minimized the risk of physical strain while ensuring an effective evaluation of the device. The chosen route was an outdoor 400 m flat athletic track (located at 49°25'16.0"N 8°39'37.0"E, Heidelberg, Germany, Fig. 7.2-(a)), which provided a controlled yet realistic environment.

Participants walked at their preferred speed under two conditions: wearing the device in unpowered mode (*assistance off*) and with assistance (*assistance on*). Both conditions were completed on the same day, with a minimum 20-minute rest period between trials to prevent fatigue. The order of conditions was randomized to eliminate potential order effects.

Additionally, a subset of four participants (n = 4) took part in a third testing condition without wearing the suit (*no suit*). These results are provided in the Appendix.

Familiarization All recruited older adults were first-time users of the device. To mitigate any potential biases associated with the familiarization process, participants were provided enough time to get accustomed to the device. They walked along a straight 100-meter outdoor path, corresponding to the first straight section of the athletic track. Participants were encouraged to repeat the familiarization path as many times as needed until they felt comfortable and confident using the device. After the familiarization phase, sufficient rest was provided to prevent any fatigue before beginning the experimental tasks.

Data collection The study aimed to validate the initial hypotheses by assessing metabolic walking efficiency, kinematic performance, and the sense of agency. Metabolic efficiency, the primary outcome, was measured using a portable respirometer (K5, COSMED, Italy) to capture oxygen and carbon dioxide consumption. Kinematic performance was evaluated through data collected from the integrated IMU sensors embedded in the suit. Finally, the sense of agency was assessed using the ten-item questionnaire presented in Chapter 6, with participants providing ratings on a Likert scale ranging from 1 (strongly disagree) to 7 (strongly agree).

Participant	Age (year)	Weight (kg)	Height (cm)	Sex (-)	LUCAS
01	69	63	173	F	Robust
02	82	90	186	M	Robust
03	78	58	168	F	Robust
04	67	70	165	F	Robust
05	69	66	166	F	Robust
06	82	65	179	M	Pre-frail
07	68	90	187	M	Robust
08	69	90	191	M	Robust
09	81	61	168	F	Robust
10	76	78	178	M	Robust

Table 7.1. Participants demographic.

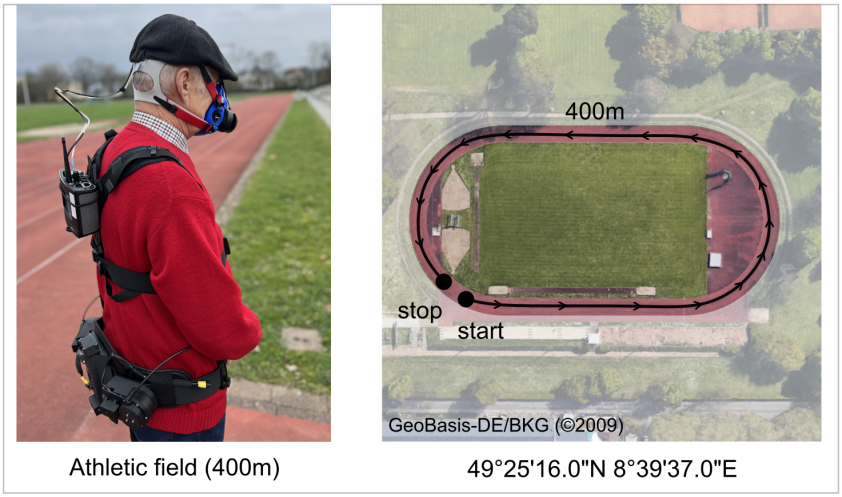


Figure 7.2. Outdoor walking task. Older participants completed a 400m walk on a flat athletic track at their preferred speed in two conditions: *assistance off* and with *assistance on*.

7.2.2 Data analysis and statistics

Metabolic cost Net metabolic cost was calculated using Péronnet and Massicotte's formula based on oxygen and carbon dioxide data [96]. A three-minute standing rest period established a baseline, with the mean metabolic cost from the final minute subtracted from walking data to isolate walking-related energy expenditure. To account for speed differences, the cost of transport was calculated by dividing the net metabolic cost by the product of body weight, gravitational acceleration, and average walking speed. Data from the last two minutes, during which metabolic measurements stabilize, were analysed.

Kinematics Hip angle and velocity profiles were analyzed using data from the suit's integrated inertial sensors. After low-pass filtering (10 Hz cutoff, fourth-order Butterworth) and segmenting steps, key metrics such as range of motion (ROM) and average peak velocity during the stance and swing phases were compared between unassisted and assisted conditions.

Sense of agency Participants completed a 10-item questionnaire assessing perceived control while using the suit. Responses on a 7-point Likert scale were averaged, with negatively worded items recoded to ensure higher scores indicated stronger agency. The mean score was used to evaluate participants' perception of control during assisted walking.

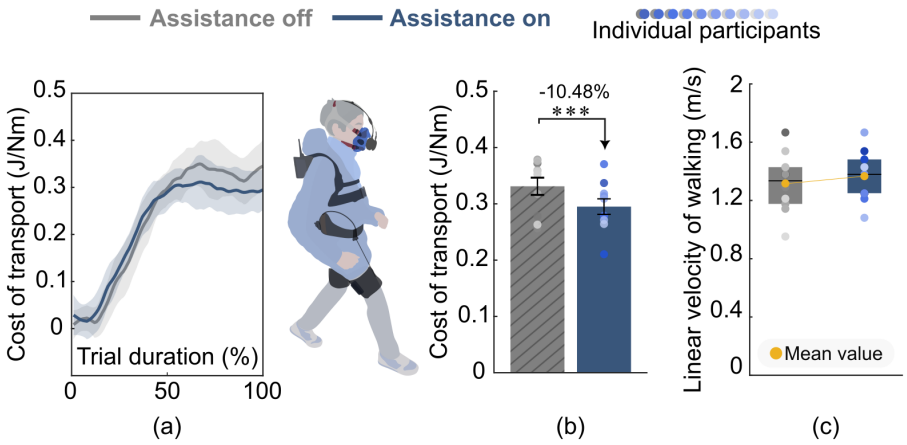


Figure 7.3. Metabolic cost. Using the soft robotic suit significantly reduced the metabolic cost of transport. (a) Metabolic cost of transport timeseries displayed as mean and standard deviation (shaded area). (b) Mean values presented as mean ± s.e.m. (c) Linear walking speed. Results are presented as boxplots where the horizontal line is the median and the orange circle is the mean. Grey is *assistance off*, while navy is *assistance on*, ***p < 0.001.

Statistics Data are reported as mean ± standard error of the mean (s.e.m.) or visualized with boxplots. Normality was confirmed via the Shapiro-Wilk test, and significance was set at $p < 0.05$. Linear mixed-effects models assessed metabolic and kinematic data, accounting for *condition* (*assistance off* vs. *assistance on*) as a fixed effect and *participant* as a random effect. For the sense of agency, a one-sample t-test compared mean questionnaire scores to the neutral midpoint (i.e., 4), with scores above this indicating a stronger sense of self-control.

7.3 Results

Metabolic cost Using the soft robotic suit reduced the metabolic cost of transport during the outdoor walking task by an average of $10.48 \pm 2.96\%$ (mean ± s.e.m, $n = 10$, $p < 0.001$) compared to the *assistance off* condition (Fig. 7.3-(a, b)). Additionally, five participants demonstrated increased walking velocity, leading to a slight overall average increase of 5.31%, though this trend was not statistically significant ($p > 0.05$) (Fig. 7.3-(c)).

Kinematics The soft robotic suit did not disrupt the natural progression of hip joint movements as indicated by the raw hip angle and velocity in the phase portrait (Fig. 7.4-(a)). Both the physiological range of motion (Fig. 7.4-(b)) and the peak velocities at the hip joint (Fig. 7.4-(c)) were preserved, with no significant

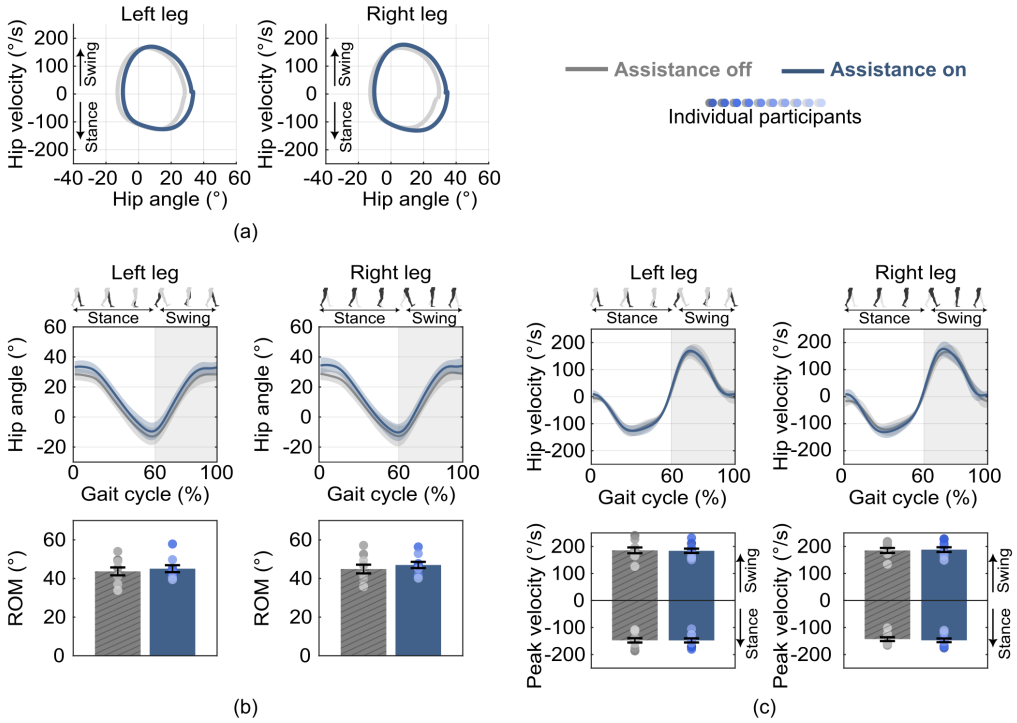


Figure 7.4. Kinematics. (a) Mean hip phase portrait across participants. (b) Hip flexion angle timeseries and Range of motion (ROM). (c) Hip velocity timeseries and peak velocity in swing (positive) and stance (negative). Results in bar plots are presented as mean ± s.e.m; timeseries are displayed as mean and standard deviation (shaded area). Grey is *assistance off*, while navy is *assistance on*, ***p < 0.001.

differences observed compared to the *assistance off* condition ($p > 0.05$).

Sense of agency Participants reported a strong sense of agency while using the soft robotic suit, with a mean self-assessment score of 6.09 ± 0.26 on a 7-point Likert scale. This score was significantly above the neutral midpoint of 4 ($n = 10$, $t = 8.34$, $p < 0.001$), reflecting a high perception of control over their movements (Fig. 7.5).

7.4 Discussion

As the global population grows older, the challenges associated with age-related mobility decline demand innovative solutions to preserve independence, quality of life, and overall well-being in older adults. Among these challenges is the progressive decline in muscle strength during walking, which can limit daily activity and increase energy demand.

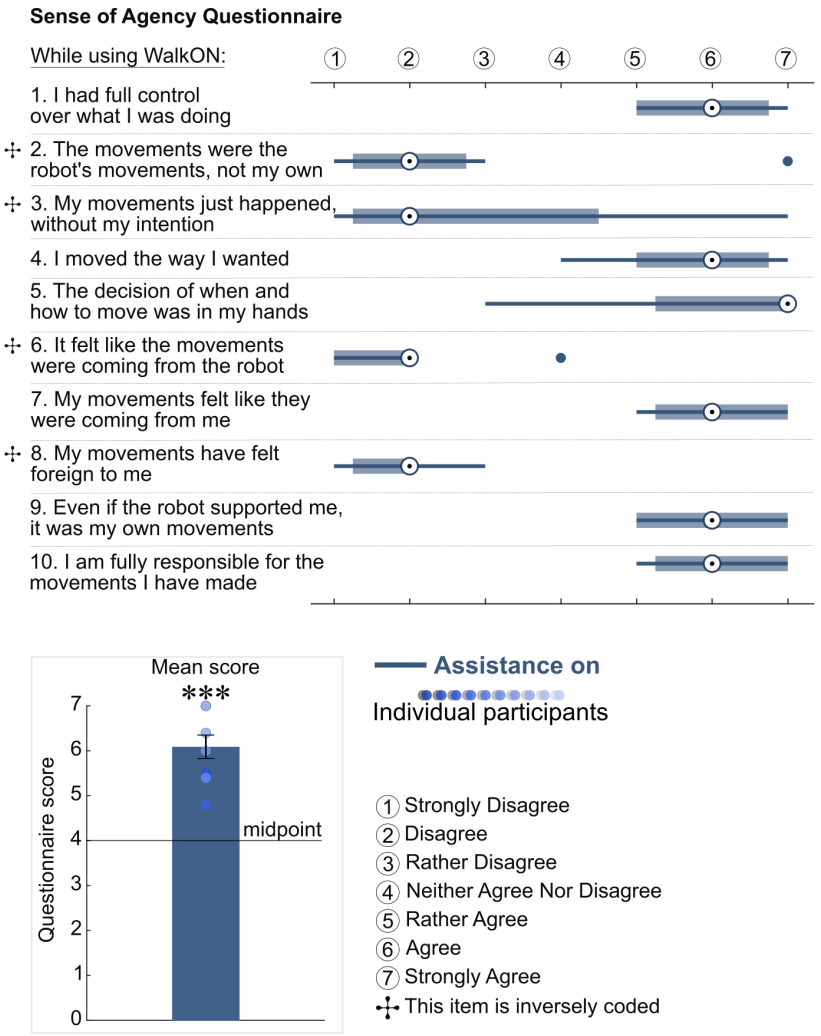


Figure 7.5. Sense of agency. Older adults reported strong perceived sense of control over voluntary movements while using the soft robotic suit. ***$p < 0.001$.

Soft robotic suits have emerged as a promising intervention, offering adaptive assistance to reduce the energy demands of walking while aligning seamlessly with natural gait [24]. The present study focused on evaluating the metabolic, kinematic, and subjective outcomes of using the device developed herein in older adults to assess its efficacy and explore its potential for improving everyday mobility.

The study revealed that the suit significantly reduced the metabolic cost of transport during outdoor walking, achieving an average reduction of 10.48% (Fig. 7.3). This improvement is comparable to the physiological effects of offloading approximately 6.3 kg of weight during walking [66], highlighting its potential to ease the physical burden of everyday movement.

Enhanced metabolic efficiency could have implications that extend beyond immediate energy savings; by reducing fatigue, older adults can potentially engage

in longer or more frequent walking sessions, thereby enhancing endurance and supporting cardiovascular and musculoskeletal health. Walking has indeed been strongly associated with numerous health benefits, including lower cardiovascular risk, improved respiratory function, and reduced all-cause mortality, as well as psychological advantages such as decreased depression and improved emotional well-being [6, 7]. By facilitating more efficient walking, the suit could not only addresses the physical constraints of aging but may also foster better health outcomes over the long term. While the benefits were observed in a level-ground setting, the metabolic advantages may be even more pronounced in more demanding conditions, such as walking uphill as shown for young adults in Chapter 6, where energy requirements are substantially higher due to increased engagement of the hip flexors during limb advancement [59,60]. This suggests the suit's broader applicability in diverse real-world environments.

In terms of kinematic outcomes, the study demonstrated that the soft robotic suit preserved natural hip joint movements, as evidenced by unaltered range of motion and peak velocities during walking (Fig. 7.4). This is a crucial finding, as maintaining physiological movement patterns is essential for user comfort and long-term adaptability. The device's ability to synchronize assistance with the user's gait cycle ensures that no extraneous constraints are imposed, allowing for seamless integration into natural walking behavior. This feature is particularly important for older users, as deviations from natural kinematics could risk discomfort or long-term maladaptation. The preservation of hip kinematics supports the notion that such devices can be safely and effectively used without affecting the biomechanical integrity of gait.

Subjectively, participants reported a strong sense of agency while using the suit, as reflected by high scores on the administered questionnaire (Fig. 7.5). This underscores their perception of control over their movements and alignment between their intentions and the device's actions. Such a strong sense of agency is vital for ensuring user acceptance, as it fosters confidence in the technology and minimizes the psychological barriers to adoption. The adaptive control system of the suit (i.e., phase portrait-based), which synchronizes assistance with the user's natural gait patterns, likely played a pivotal role in these outcomes by avoiding any imposition of unintended actions. Beyond enhancing usability, this alignment may also contribute to long-term adherence, as users are more likely to engage with a device that feels like an extension of their own movement rather than an external aid.

While the study demonstrates promising outcomes, several limitations warrant consideration. The short-term nature of the experiments and the controlled outdoor environment may not fully capture the device's impact under more varied and prolonged usage scenarios in this target population. Future research should explore the long-term effects of repeated use, as well as its influence on secondary factors such as muscle strength and reliance. To address these gaps, randomized controlled trials with longitudinal designs are essential, as they can shed light on the broader implications of using such assistive technology over time. Furthermore, studies incorporating usability and acceptance metrics will help refine the design and implementation of these devices, ensuring they meet the needs of diverse users.

By reducing the metabolic demands of walking, the soft robotic suit holds promise as an effective tool for enhancing mobility, autonomy, and quality of life in older adults. While the current study focuses on this specific demographic, the potential applications of the suit extend far beyond aging populations. The benefits observed in improving walking efficiency and maintaining natural movement patterns suggest that the suit could also be valuable for individuals with neurological disorders, such as stroke, Parkinson's or Multiple Sclerosis, as well as those recovering from injuries. These conditions often lead to compromised mobility and increased physical exertion. Future research expanding the scope of testing will be crucial in understanding how the suit can be adapted and integrated into diverse daily or clinical settings, ultimately contributing to strategies aimed at enhancing mobility and quality of life for a wider range of users.

Chapter 8

Conclusion

8.1 General overview

Guided by the objectives and hypotheses set forth in Chapter 1, and building upon the challenges identified in Chapter 2, this thesis focused on the development of a fully portable, lightweight solution designed to assist hip flexion during walking.

The suit was developed with dual applicability: walking augmentation for healthy fit individuals and offering a pathway to enhanced mobility for frail populations, demonstrated here with older adults.

A key emphasis of this work has been the translation into real-world applicability by addressing critical barriers such as portability, user comfort, and adaptability to natural human locomotion. The approach prioritized a minimal sensory network and a plug-and-play design to ensure ease of use and seamless integration into everyday environments.

8.1.1 Major contributions of the thesis

This thesis makes significant contributions to the field of wearable assistive robotics by tackling critical challenges across three core pillars: (1) **design**, (2) **control**, and (3) **real-world evaluation**. These efforts encompass both technological innovation and empirical validation, aligning with the objectives outlined in Chapter 1. Specifically, Pillars (1) and (2) address **objective 1**, while Pillar (3) fulfills **objective 2**.

1. **Design.** In alignment with **hypothesis 1**, the soft robotic suit was devel-

oped with a tendon-driven, textile-based design that prioritizes portability, low weight, and user comfort. Two actuation configurations, underactuated and fully actuated, were implemented to provide tailored assistance for users with diverse needs, allowing task-specific performance optimization.

2. **Control.** Robust and efficient control strategies were developed to ensure the system's functionality in both controlled laboratory settings and dynamic real-world conditions. To enhance usability and eliminate the need for complex calibration procedures, the suit employs a minimal sensory network based on inertial sensors in its standard configuration (without context-aware modulation). This approach validates **hypothesis 2** by demonstrating the feasibility of delivering effective assistance with simplified sensing requirements. This design allows the exploitation of control algorithms that can scale effectively to a wide variety of user profiles without the need for calibration. Consequently, it provides a plug-and-play solution ideal for extended use across diverse environments.

   AOs-based controller Initially, the research explored a dynamic model based on Adaptive Oscillators (AOs) for gait phase estimation, utilizing only motion data from inertial sensors. However, the AOs approach faced limitations, particularly delays during abrupt gait transitions. To address this, machine learning models were integrated to dynamically adjust assistance in real-time, improving the system's responsiveness to cadence changes. While this approach showed promise in controlled settings, it introduced additional computational complexity and the need for model training.

   Phase portrait-based controller To overcome these challenges and improve performance in real-world, the research transitioned to a phase portrait-based control system. This method analyzes angular separation vectors in the hip phase portrait to estimate gait phases, eliminating the need for dynamical estimation models or machine learning algorithms. This approach demonstrated instead low-latency and enhanced responsiveness in dynamic, real-world conditions.

   Context-aware controller based on computer vision A key innovation of this thesis is the integration of computer vision into the control framework of the suit, enabling context-aware modulation of assistance. To the best of the author's knowledge, this is the first instance of fully inte-

grated and validated vision-based contextual modulation in wearable assistive robotics. The system's ability to interpret environmental features, such as distinguishing between ascending, descending, or level walking terrain, significantly improves its adaptability to diverse conditions demonstrating higher benefits for users. This innovation bridges a critical gap in wearable robotics by incorporating environmental awareness into assistive technology.

3. **Real-world evaluation and use case demonstration.** A central goal of this thesis was to transition from laboratory testing to real-world deployment, demonstrating the suit's efficacy both for augmenting the performance of fit users and assisting frail individuals. This addresses the persistent challenge of real-world applicability in wearable robotics.

   To validate general **hypothesis 3**, the system underwent extensive outdoor evaluations, including trials on uphill hiking paths. These tests demonstrated the suit's robustness and effectiveness in real-world conditions, revealing that the suit successfully reduced metabolic costs and preserved natural gait mechanics while ensuring user control on own movements in challenging environments.

   The research extended its testing to frail populations, specifically older adults, a group that remains underexplored in current literature despite the significant potential benefits of walking assistance for them. This evaluation marks a critical step forward in the thesis, as it addresses a significant gap in wearable robotics research focused on mobility limitations due to aging. Although the study was conducted over a short term, the results were highly encouraging, showing that the suit effectively reduced energy expenditure and improved walking efficiency in the participants. This underscores the suit's potential to make a substantial impact on improving the quality of life for frail populations, representing a major advancement in wearable assistive technology for those with reduced mobility.

8.2 Current limitations and future work

Several limitations and opportunities for future work remain.

One of the key limitations of the presented studies is the relatively small participant sample size, which may limit the generalizability of the findings. To address this,

future research should involve a larger and more diverse participant pool to better understand the broader applicability of the results across different user groups.

Another limitation is the lack of a control measurement for metabolic activity in the absence of the device. In all presented studies, comparisons were made using a condition where the device was worn but turned off, rather than comparing to a baseline without the device altogether. While this approach is commonly used in the literature for practical reasons [24, 146, 151], it may not fully reflect real-world conditions. Nonetheless, this method allowed for a meaningful comparison isolating the active biomechanical effects of the suit, separate from the passive impact of wearing it. For a more comprehensive analysis, future evaluations should include metabolic measurements in a condition where the device is not worn to better assess its true impact. During the real-world evaluations presented in Chapters 6 and 7, only a subset of both young and older adults repeated the trials without the suit's weight, demonstrating minimal impact on results. Such results are included in the Appendix and suggest that the soft and lightweight design of the suit, positioned closer to the user's center of mass, do not significantly affect the outcomes, as supported by previous biomechanical studies on added mass effects on body segments [66].

Additionally, the present research primarily focused on short-term experimental results, which provide valuable insights but leave questions regarding the long-term implications of using the soft robotic suit. Potential risks associated with prolonged use of the soft robotic suit, such as reduced reliance on natural muscle function, remain unknown and require further evaluation. Future research should aim to investigate these aspects by conducting pilot randomized controlled trials in more ecologically valid settings and evaluating the system's impact in everyday use. This should include a comprehensive assessment of usability, user satisfaction, and acceptance to gain a deeper understanding of the technology's benefits and limitations.

Future research should also focus on enhancing user comfort and addressing aesthetic concerns to ensure broad acceptance of the technology across different user populations. As wearable robotics become more widely used, these factors will play a key role in ensuring the technology's widespread adoption.

Appendix

A comparative study on two hardware configurations for the soft robotic suit

According to design requirements, the soft robotic suit was conceived primarily with the objective of capitalizing on lightweight design, efficient weight distribution, and a comfortable textile interface.

In reference to the first two aspects, two hardware configurations were explored. As presented in Chapter 3, the soft robotic suit had been designed either using an underactuated configuration (namely UA), having one motor to assist both legs, or in a fully-actuated version (namely FA), where each leg is assisted via an independent actuator.

Each configuration presents strengths: the UA has a simpler and lighter design enforcing symmetricity of assisted movements, the FA instead allows greater controllability of independent legs in case walking happens in less structured environments.

To investigate the best actuation approach to assist hip flexion in the real-world, a comparative study was conducted with young adults on a hiking trail. The controller presented in Chapter 6 was adapted to the hardware configuration following the generalization rules explained in section 3.4.

Hiking study

The main objective of this comparative study is to assess the impact of two distinct hardware configurations to identify the most effective actuation strategy for supporting walking in real-world conditions. To this end, a subgroup of seven young adults (mean age 25.43 ± 2.23 years, height 172.57 ± 12.42 cm, weight

67.57 ± 13.06 kg) who participated in the hiking-like trail evaluations (Chapter 6) were instructed to walk at their preferred speed while using both the underactuated and fully actuated systems.

The three experimental conditions were defined as follows: (1) *assistance off*: the system was turned off; (2) UA: assistance was provided by the underactuated system; and (3) FA: assistance was delivered by the fully actuated system.

Participants walked a 500-meter uphill route (Fig. A.1, Philosophenweg, Heidelberg, 49°24'55.1"N 8°42'00.9"E), after which they retraced the same path downhill, resulting in a total walking distance of 1 kilometer per condition.

Results are presented separately for the uphill and downhill segments. While downhill walking is included for comprehensive evaluation, the assistance provided by the soft robotic suit for hip flexion plays a less prominent role on descents, as ground clearance requires less leg lifting [143]. The downhill segment primarily serves to demonstrate that the system's weight does not hinder motion or impose additional metabolic effort.

To minimize fatigue effects, the different conditions were tested on separate days. Data on metabolic cost of transport, hip joint kinematics, and sense of agency were analyzed following the methods outlined in Chapter 6.

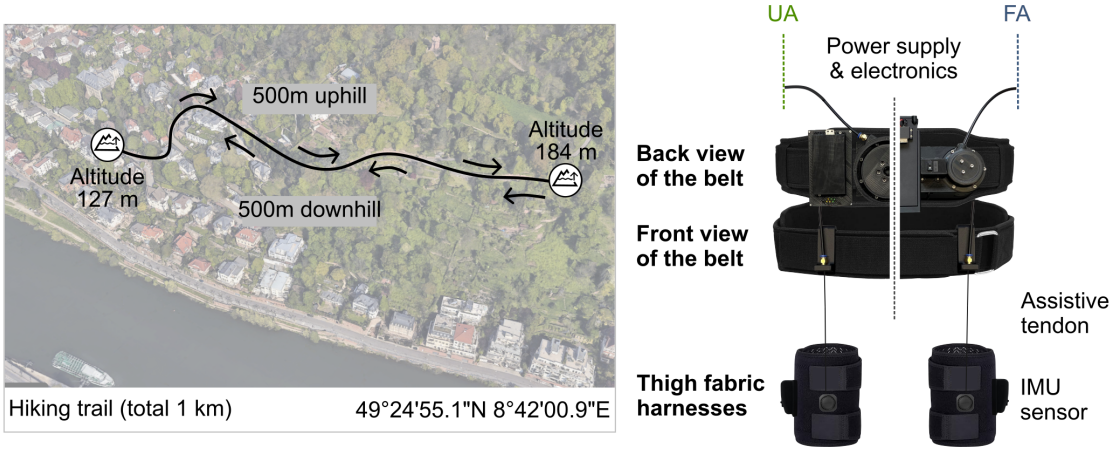


Figure A.1. Hiking study. The task required participants to walk along a steep, winding hiking trail covering a total distance of 1 km (500 m uphill and 500 m downhill). Young adults completed the walk at their preferred pace under three conditions: without assistance (*assistance off*), using the underactuated system (UA), and using the fully-actuated system (FA).

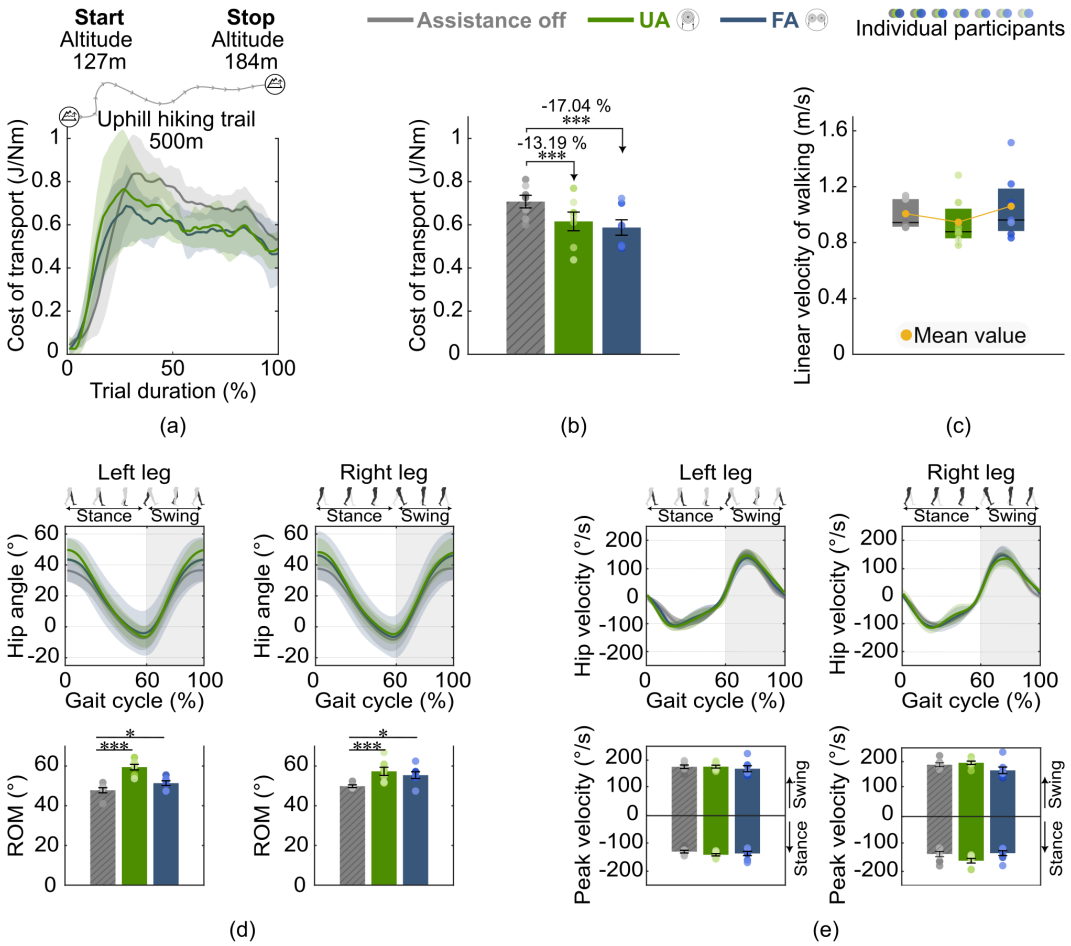


Figure A.2. Uphill hiking results. (a) Cost of transport timeseries (solid line is the mean, shaded area is the standard deviation). (b) Mean cost of transport was significantly reduced with assistance. (c) Linear walking speed was unaltered with assistance. (d) The hip range of motion significantly increased with assistance. (e) No significant variations in hip velocity.

Results

Uphill hiking When using the UA soft robotic suit, the metabolic demand for traversing the uphill outdoor trail decreased significantly by an average of $13.19 \pm 4.38\%$ (mean $\pm$ s.e.m., $n = 7$, $p < 0.001$), while the FA system achieved a reduction of $17.04 \pm 3.21\%$ ($p < 0.001$) (Fig. A.2-(a, b)).

The linear walking velocity (Fig. A.2-(c)) showed no statistically significant differences across conditions, although a trend was observed: a 6% decrease with *UA* and a 5% increase with *FA* compared to the *assistance off* condition.

The use of the soft robotic suit did not restrict hip joint motion (Fig. A.2-(d, e)). In the *assistance off* condition, the average range of motion across both legs and participants was $48.82 \pm 0.68°$ (mean $\pm$ s.e.m.). This increased significantly to

$58.40 \pm 1.50°$ with *UA* and $53.40 \pm 1.28°$ with *FA*.

These results correspond to an average increase of $19.69 \pm 3.04\%$ ($p < 0.001$) with *UA* and $9.45 \pm 2.85\%$ ($p < 0.05$) with *FA*, relative to the *assistance off* condition (Fig. A.2-(d)). Additionally, the assistance provided by the device did not result in significant changes to hip peak velocities throughout the gait cycle (Fig. A.2-(e)).

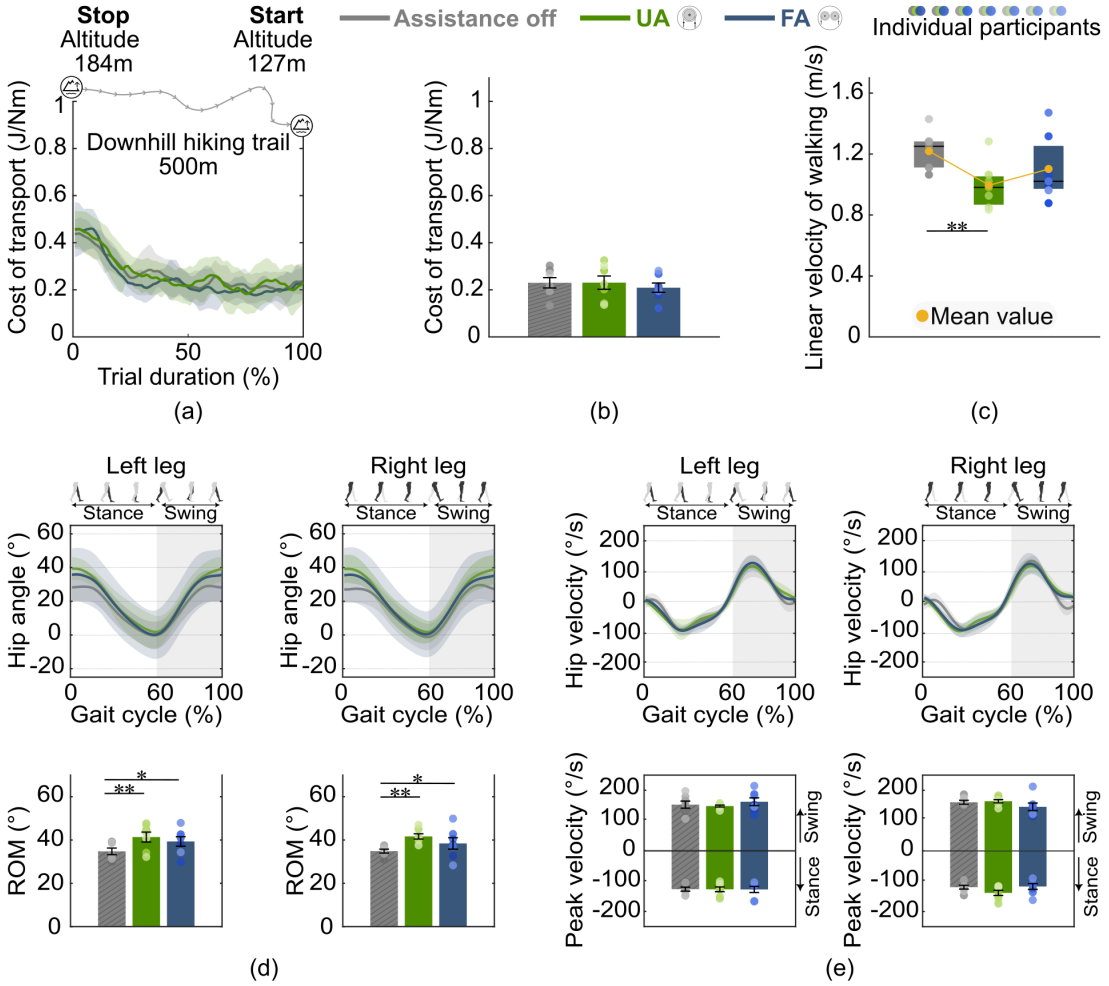


Figure A.3. Downhill hiking results. (a, b) Downhill walking with both configurations of the device did not result in any significant metabolic burden. (c) Linear walking velocity significantly decreased with the underactuated configuration, but remained unchanged with the fully-actuated configuration. (d, e) The hip joint's range of motion (ROM) showed a significant increase with both configurations. However, hip peak velocities were not significantly impacted by either device.

Downhill hiking The use of the soft robotic suit during downhill walking did not significantly impact the metabolic cost of transport (Fig. A.3-(a, b)). However, linear walking velocity showed a significant decrease with *UA* ($p = 0.005$) but remained unchanged with *FA* (Fig. A.3-(c)).

The suit supported unrestricted and natural hip movement, as evidenced by a significant increase in range of motion (ROM) with both configurations. In the *assistance off* condition, the average ROM across legs and participants was $34.85 \pm 1.02°$. This increased to $41.55 \pm 1.20°$ with *UA* ($+19.69 \pm 4.19\%$, $p < 0.05$) and to $38.92 \pm 2.24°$ with *FA* ($+12.16 \pm 6.89\%$, $p < 0.05$). Additionally, hip peak velocities were not significantly affected by the use of either configuration.

Sense of agency For both hardware configurations, young adults consistently reported that their sense of agency was largely preserved while using the system (Fig. A.4). The mean score was 5.67 ± 0.30 (mean $\pm$ s.e.m.) with *UA* and 5.93 ± 0.31 with *FA*, with both conditions showing significantly higher scores ($p < 0.001$) compared to the midpoint value of 4 on the Likert scale.

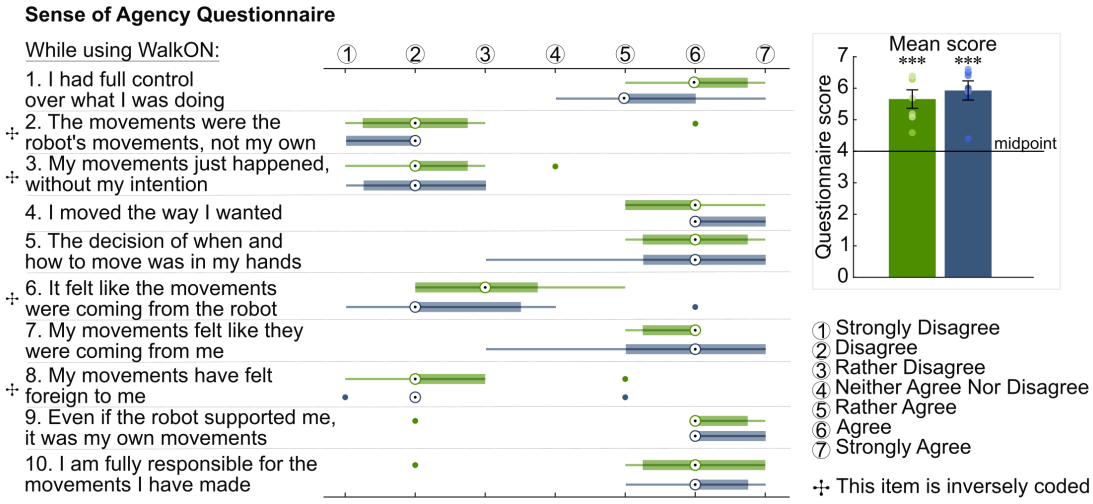


Figure A.4. Sense of agency. The sense of agency assessment showed strong perceived sense of control when using the device in both configurations.

Selection of the most efficient hardware configuration in the real-world

In this comparative study involving young adults, the fully-actuated version of the system demonstrated greater metabolic efficiency uphill, with a 17.04% reduction in energy expenditure, ranging from 7.44% to 33.64% across individuals. In

contrast, the underactuated configuration yielded a more modest average saving of 13.19%. Kinematically, the underactuated system produced a more significant increase in the physiological range of motion, both uphill and downhill, while the fully-actuated system resulted in smaller changes in natural movement. In terms of psychophysical evaluation, both configurations showed no differences in the sense of agency, though higher scores were reported with the fully-actuated system.

The improved performance of the fully-actuated system can likely be attributed to its ability to independently and precisely control each leg, allowing for better synchronization with the user's natural gait. This feature is especially beneficial on uneven or sloped terrains, where the legs often need to move asymmetrically. This capability was particularly advantageous on the challenging hiking path, where the system's ability to accommodate the distinct movements of each leg was essential for adjusting to variations in slope and terrain.

Given the superior performance of the fully-actuated system across all evaluated metrics, it was selected as the preferred configuration for further real-world testing and for the final design of the assistive system, which will be assessed with older adults in the efficacy study outlined in Chapter 6.

Supplementary metabolic evaluations

Technology assessment with young adults

Chapter 6 presents a technology assessment of the soft robotic suit in the real-world during a hiking task. Within the main study, a subset of five young adults (average age 25.40±2.61 years, height 174.80±11.69 cm, and weight 64.40±10.74 kg) undertook an additional trial.

In this trial, they climbed the hiking trail (refer to Fig. 6.3 in Chapter 6) solely equipped with the metabolic analyzer and without wearing the soft robotic shorts. The purpose was to demonstrate the minimal metabolic impact resulting from the additional weight of the device. The comparison results of this third condition, termed as the *no suit* condition, in relation to both the *assistance off* and *assistance on* conditions, are illustrated in Fig. A.5. Given the small sample size, no statistical analysis was conducted on this comparison. However, it is evident that the *assistance on* condition exhibits the lowest metabolic cost of transport. In detail, the cost of transport in the *assistance on* condition with respect to the *no suit* condition is reduced by 11.86±2.03%, and by 18.85±2.24% compared to the *assistance off*.

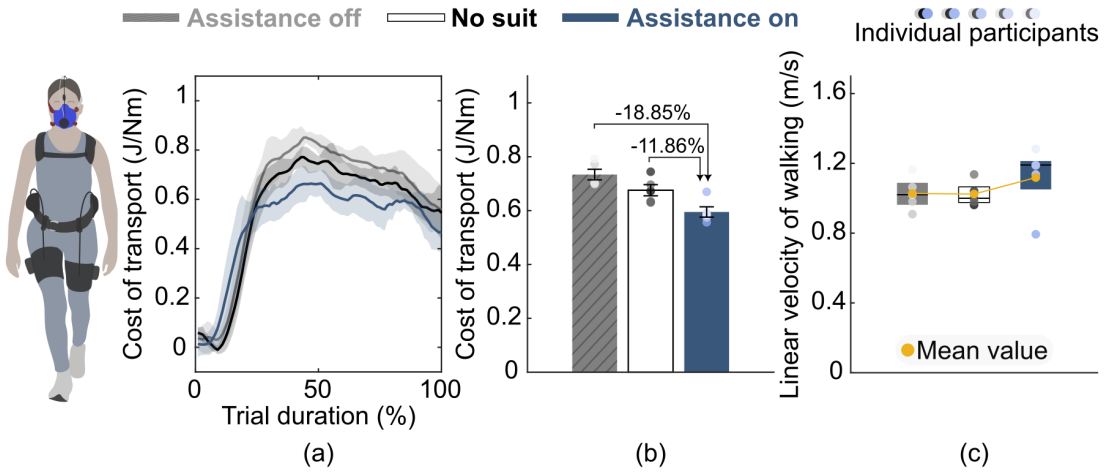


Figure A.5. Cost of transport results for five young adults. (a, b) Comparison of metabolic outcomes among the *assistance off* (grey), *no suit* (white), and *assistance on* (navy) conditions. (c) Linear velocity of walking. Timeseries are displayed as mean and standard deviation (shaded area). Individual participants results are shown as dot plots, while bars (mean±s.e.m) and boxplots indicate group results. In boxplots, box bounds indicate the lower and upper quartiles (25th and 75th percentiles respectively), the black line is the median and the orange circle is the mean.

Efficacy study with older adults

Within the main study presented in Chapter 7, a subgroup consisting of four older adults (with an average age of 73.50 ± 6.14 years, height 181.00 ± 10.23 cm, and weight 79.75 ± 13.72 kg) undertook an additional trial by walking the outdoor path without utilizing the soft robotic shorts. Here again, the objective was to demonstrate the minimal metabolic impact resulting from the device's additional weight. The comparison results of this third condition, known as the *no suit* condition, in relation to both the *assistance off* and *assistance on* conditions, are illustrated in Fig. A.6. Due to the limited sample size, no statistical analysis was performed on this comparison. Nevertheless, it is evident that the *assistance on* condition exhibits the lowest trend in comparison to both *no suit* and *assistance off*, reporting cost of transport reductions of $11.27 \pm 5.26\%$ and $12.86 \pm 5.10\%$ respectively.

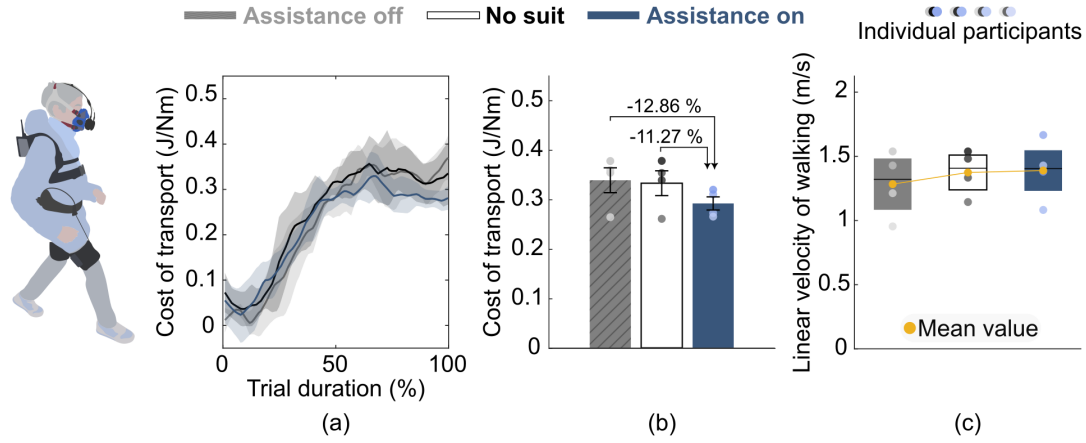


Figure A.6. Cost of transport results for four older adults. (a, b) Comparison of metabolic outcomes among the *assistance off* (grey), *no suit* (white), and *assistance on* (navy) conditions. (c) Linear velocity of walking. Timeseries are displayed as mean and standard deviation (shaded area). Individual participants results are shown as dot plots, while bars (mean±s.e.m) and boxplots indicate group results. In boxplots, box bounds indicate the lower and upper quartiles (25th and 75th percentiles respectively), the black line is the median and the orange circle is the mean.

Bibliography

[1] D. A. Winter, *Biomechanics and motor control of human movement*. John wiley & sons, 2009.

[2] R. M. Enoka, *Neuromechanics of human movement*. Human kinetics, 2008.

[3] H. Song, H. Park, and S. Park, "A springy pendulum could describe the swing leg kinetics of human walking," *Journal of biomechanics*, vol. 49, no. 9, pp. 1504–1509, 2016.

[4] N. Rashevsky, "A note on energy expenditure in walking on level ground and uphill," *The bulletin of mathematical biophysics*, vol. 24, pp. 217–227, 1962.

[5] D. C. Batman, "Hippocrates:'walking is man's best medicine!'," pp. 320–322, 2012.

[6] K. W. Choi, C.-Y. Chen, M. B. Stein, Y. C. Klimentidis, M.-J. Wang, K. C. Koenen, J. W. Smoller *et al.*, "Assessment of bidirectional relationships between physical activity and depression among adults: a 2-sample mendelian randomization study," *JAMA psychiatry*, vol. 76, no. 4, pp. 399–408, 2019.

[7] Z. Ungvari, V. Fazekas-Pongor, A. Csiszar, and S. K. Kunutsor, "The multifaceted benefits of walking for healthy aging: from blue zones to molecular mechanisms," *GeroScience*, pp. 1–29, 2023.

[8] S.-J. Cheng, Y.-R. Yang, F.-Y. Cheng, I.-H. Chen, and R.-Y. Wang, "The changes of muscle strength and functional activities during aging in male and female populations," *International Journal of Gerontology*, vol. 8, no. 4, pp. 197–202, 2014.

[9] J. D. Ortega and C. T. Farley, "Effects of aging on mechanical efficiency and muscle activation during level and uphill walking," *Journal of Electromyography and Kinesiology*, vol. 25, no. 1, pp. 193–198, 2015.

[10] H. B. Menz, S. R. Lord, and R. C. Fitzpatrick, "Age-related differences in walking stability," *Age and ageing*, vol. 32, no. 2, pp. 137–142, 2003.

[11] A. B.-v. Der Wiel, J. Gussekloo, A. J. De Craen, E. Van Exel, B. R. Bloem, and R. G. Westendorp, "Common chronic diseases and general impairments as determinants of walking disability in the oldest-old population," *Journal of the American Geriatrics Society*, vol. 50, no. 8, pp. 1405–1410, 2002.

[12] "World population prospects 2022: Summary of results," *United Nations*, 2022.

[13] H. Kawamoto and Y. Sankai, "Power assist system hal-3 for gait disorder person," in *International Conference on Computers for Handicapped Persons*. Springer, 2002, pp. 196–203.

[14] J. Kim, G. Lee, R. Heimgartner, D. Arumukhom Revi, N. Karavas, D. Nathanson, I. Galiana, A. Eckert-Erdheim, P. Murphy, D. Perry *et al.*, "Reducing the metabolic rate of walking and running with a versatile, portable exosuit," *Science*, vol. 365, no. 6454, pp. 668–672, 2019.

[15] L. M. Mooney, E. J. Rouse, and H. M. Herr, "Autonomous exoskeleton reduces metabolic cost of human walking during load carriage," *Journal of neuroengineering and rehabilitation*, vol. 11, pp. 1–11, 2014.

[16] A. Kapsalyamov, P. K. Jamwal, S. Hussain, and M. H. Ghayesh, "State of the art lower limb robotic exoskeletons for elderly assistance," *IEEE Access*, vol. 7, pp. 95 075–95 086, 2019.

[17] E. Martini, S. Crea, A. Parri, L. Bastiani, U. Faraguna, Z. McKinney, R. Molino-Lova, L. Pratali, and N. Vitiello, "Gait training using a robotic hip exoskeleton improves metabolic gait efficiency in the elderly," *Scientific reports*, vol. 9, no. 1, p. 7157, 2019.

[18] H.-J. Lee, S. Lee, W. H. Chang, K. Seo, Y. Shim, B.-O. Choi, G.-H. Ryu, and Y.-H. Kim, "A wearable hip assist robot can improve gait function and cardiopulmonary metabolic efficiency in elderly adults," *IEEE transactions on neural systems and rehabilitation engineering*, vol. 25, no. 9, pp. 1549–1557, 2017.

[19] N. Yagn, "Apparatus for facilitating walking, running, and jumping." *US Patent*, 440, 584, (406), 1890.

[20] C. L. Kelley, "Pedomotor," *US Patent*, 1, 308, 675 filed April 24, 1917 and issued July 1, 1919.

[21] R. S. Mosher, "From handiman to hardiman," 1967. 9, 10.

[22] S. Zaroodny, "Bumpusher-a powered aid locomotion," *Army, Aberdeen Proving Ground, Ballistic Research Laboratories, Technical Note*, vol. 1524, p. 40, 1963.

[23] "The wrong trousers," *BFI*, 1993.

[24] M. Xiloyannis, R. Alicea, A.-M. Georgarakis, F. L. Haufe, P. Wolf, L. Masia, and R. Riener, "Soft robotic suits: State of the art, core technologies, and open challenges," *IEEE Transactions on Robotics*, 2021.

[25] J. Jansen, "Phase i report: Darpa exoskeleton program," Oak Ridge National Lab.(ORNL), Oak Ridge, TN (United States), Tech. Rep., 2004.

[26] H. Kazerooni and R. Steger, "The berkeley lower extremity exoskeleton," 2006.

[27] A. B. Zoss, H. Kazerooni, and A. Chu, "Biomechanical design of the berkeley lower extremity exoskeleton (bleex)," *IEEE/ASME Transactions on mechatronics*, vol. 11, no. 2, pp. 128–138, 2006.

[28] C. Siviy, L. M. Baker, B. T. Quinlivan, F. Porciuncula, K. Swaminathan, L. N. Awad, and C. J. Walsh, "Opportunities and challenges in the development of exoskeletons for locomotor assistance," *Nature Biomedical Engineering*, vol. 7, no. 4, pp. 456–472, 2023.

[29] G. Colombo, M. Joerg, R. Schreier, V. Dietz *et al.*, "Treadmill training of paraplegic patients using a robotic orthosis," *Journal of rehabilitation research and development*, vol. 37, no. 6, pp. 693–700, 2000.

[30] K. Suzuki, G. Mito, H. Kawamoto, Y. Hasegawa, and Y. Sankai, "Intention-based walking support for paraplegia patients with robot suit hal," *Advanced Robotics*, vol. 21, no. 12, pp. 1441–1469, 2007.

[31] H. Shimada, Y. Kimura, T. Suzuki, T. Hirata, M. Sugiura, Y. Endo, K. Yasuhara, K. Shimada, K. Kikuchi, M. Hashimoto *et al.*, "The use of positron

emission tomography and fluorodeoxyglucose for functional imaging of muscular activity during exercise with a stride assistance system," *IEEE Transactions on Neural Systems and Rehabilitation Engineering*, vol. 15, no. 3, pp. 442–448, 2007.

[32] A. Esquenazi, M. Talaty, A. Packel, and M. Saulino, "The rewalk powered exoskeleton to restore ambulatory function to individuals with thoracic-level motor-complete spinal cord injury," *American journal of physical medicine & rehabilitation*, vol. 91, no. 11, pp. 911–921, 2012.

[33] K. A. Strausser, T. A. Swift, A. B. Zoss, H. Kazerooni, and B. C. Bennett, "Mobile exoskeleton for spinal cord injury: Development and testing," in *Dynamic Systems and Control Conference*, vol. 54761, 2011, pp. 419–425.

[34] K. Seo, S. Hyung, B. K. Choi, Y. Lee, and Y. Shim, "A new adaptive frequency oscillator for gait assistance," in *2015 IEEE International Conference on Robotics and Automation (ICRA)*. IEEE, 2015, pp. 5565–5571.

[35] J. Zhang, P. Fiers, K. A. Witte, R. W. Jackson, K. L. Poggensee, C. G. Atkeson, and S. H. Collins, "Human-in-the-loop optimization of exoskeleton assistance during walking," *Science*, vol. 356, no. 6344, pp. 1280–1284, 2017.

[36] M. K. Ishmael, D. Archangeli, and T. Lenzi, "A powered hip exoskeleton with high torque density for walking, running, and stair ascent," *IEEE/ASME Transactions on Mechatronics*, vol. 27, no. 6, pp. 4561–4572, 2022.

[37] A. T. Asbeck, R. J. Dyer, A. F. Larusson, and C. J. Walsh, "Biologically-inspired soft exosuit," in *2013 IEEE 13th International Conference on Rehabilitation Robotics (ICORR)*. IEEE, 2013, pp. 1–8.

[38] M. Wehner, B. Quinlivan, P. M. Aubin, E. Martinez-Villalpando, M. Baumann, L. Stirling, K. Holt, R. Wood, and C. Walsh, "A lightweight soft exosuit for gait assistance," in *2013 IEEE international conference on robotics and automation*. IEEE, 2013, pp. 3362–3369.

[39] Y.-L. Park, B.-r. Chen, N. O. Pérez-Arancibia, D. Young, L. Stirling, R. J. Wood, E. C. Goldfield, and R. Nagpal, "Design and control of a bio-inspired soft wearable robotic device for ankle–foot rehabilitation," *Bioinspiration & biomimetics*, vol. 9, no. 1, p. 016007, 2014.

[40] L. N. Awad, J. Bae, K. O'donnell, S. M. De Rossi, K. Hendron, L. H. Sloot, P. Kudzia, S. Allen, K. G. Holt, T. D. Ellis *et al.*, "A soft robotic exosuit improves walking in patients after stroke," *Science translational medicine*, vol. 9, no. 400, p. eaai9084, 2017.

[41] K. Schmidt, J. E. Duarte, M. Grimmer, A. Sancho-Puchades, H. Wei, C. S. Easthope, and R. Riener, "The myosuit: Bi-articular anti-gravity exosuit that reduces hip extensor activity in sitting transfers," *Frontiers in neurorobotics*, vol. 11, p. 57, 2017.

[42] G. Lee, J. Kim, F. Panizzolo, Y. M. Zhou, L. Baker, I. Galiana, P. Malcolm, and C. Walsh, "Reducing the metabolic cost of running with a tethered soft exosuit," *Science Robotics*, vol. 2, no. 6, p. eaan6708, 2017.

[43] L. N. Awad, A. Esquenazi, G. E. Francisco, K. J. Nolan, and A. Jayaraman, "The rewalk restore™ soft robotic exosuit: a multi-site clinical trial of the safety, reliability, and feasibility of exosuit-augmented post-stroke gait rehabilitation," *Journal of neuroengineering and rehabilitation*, vol. 17, pp. 1–11, 2020.

[44] J. Chung, R. Heimgartner, C. T. O'Neill, N. S. Phipps, and C. J. Walsh, "Exoboot, a soft inflatable robotic boot to assist ankle during walking: Design, characterization and preliminary tests," in *2018 7th ieee international conference on biomedical robotics and biomechatronics (biorob)*. IEEE, 2018, pp. 509–516.

[45] J. Moon, K. Nam, J. Ryu, Y. Kim, J. Yun, S. Yang, J. Yang, and G. Lee, "Reducing sprint time with exosuit assistance in the real world," *Science Robotics*, vol. 8, no. 82, p. eadf5611, 2023.

[46] C. J. Walsh, D. Paluska, K. Pasch, W. Grand, A. Valiente, and H. Herr, "Development of a lightweight, underactuated exoskeleton for load-carrying augmentation," in *Proceedings 2006 IEEE International Conference on Robotics and Automation, 2006. ICRA 2006.* IEEE, 2006, pp. 3485–3491.

[47] C. J. Walsh, K. Pasch, and H. Herr, "An autonomous, underactuated exoskeleton for load-carrying augmentation," in *2006 IEEE/RSJ International Conference on Intelligent Robots and Systems*. IEEE, 2006, pp. 1410–1415.

[48] C. J. Walsh, "Biomimetic design for an under-actuated leg exoskeleton for load-carrying augmentation," Ph.D. dissertation, Massachusetts Institute of Technology, 2006.

[49] M. Xiloyannis, E. Annese, M. Canesi, A. Kodiyan, A. Bicchi, S. Micera, A. Ajoudani, and L. Masia, "Design and validation of a modular one-to-many actuator for a soft wearable exosuit," *Frontiers in neurorobotics*, vol. 13, p. 39, 2019.

[50] F. L. Haufe, A. M. Kober, K. Schmidt, A. Sancho-Puchades, J. E. Duarte, P. Wolf, and R. Riener, "User-driven walking assistance: first experimental results using the myosuit," in *2019 IEEE 16th International Conference on Rehabilitation Robotics (ICORR)*. IEEE, 2019, pp. 944–949.

[51] F. L. Haufe, K. Schmidt, J. E. Duarte, P. Wolf, R. Riener, and M. Xiloyannis, "Activity-based training with the myosuit: a safety and feasibility study across diverse gait disorders," *Journal of neuroengineering and rehabilitation*, vol. 17, pp. 1–11, 2020.

[52] P. Slade, M. J. Kochenderfer, S. L. Delp, and S. H. Collins, "Personalizing exoskeleton assistance while walking in the real world," *Nature*, vol. 610, no. 7931, pp. 277–282, 2022.

[53] D. D. Molinaro, I. Kang, and A. J. Young, "Estimating human joint moments unifies exoskeleton control, reducing user effort," *Science Robotics*, vol. 9, no. 88, p. eadi8852, 2024.

[54] C. M. Thalman, J. Hsu, L. Snyder, and P. Polygerinos, "Design of a soft ankle-foot orthosis exosuit for foot drop assistance," in *2019 International Conference on Robotics and Automation (ICRA)*. IEEE, 2019, pp. 8436–8442.

[55] K. Gui, U.-X. Tan, H. Liu, and D. Zhang, "Electromyography-driven progressive assist-as-needed control for lower limb exoskeleton," *IEEE Transactions on Medical Robotics and Bionics*, vol. 2, no. 1, pp. 50–58, 2020.

[56] A. T. Asbeck, K. Schmidt, and C. J. Walsh, "Soft exosuit for hip assistance," *Robotics and Autonomous Systems*, vol. 73, pp. 102–110, 2015.

[57] N. Rydell, "Biomechanics of the hip-joint," *Clinical Orthopaedics and Related Research®*, vol. 92, pp. 6–15, 1973.

[58] R. L. Marsh, D. J. Ellerby, J. A. Carr, H. T. Henry, and C. I. Buchanan, "Partitioning the energetics of walking and running: swinging the limbs is expensive," *Science*, vol. 303, no. 5654, pp. 80–83, 2004.

[59] L. N. Jessup, L. A. Kelly, A. G. Cresswell, and G. A. Lichtwark, "It is not just the work you do, but how you do it: The metabolic cost of walking uphill and downhill with varying grades," *Journal of Applied Physiology*, 2023.

[60] J. R. Franz and R. Kram, "Advanced age and the mechanics of uphill walking: a joint-level, inverse dynamic analysis," *Gait & posture*, vol. 39, no. 1, pp. 135–140, 2014.

[61] J. M. Donelan, R. Kram, and A. D. Kuo, "Mechanical work for step-to-step transitions is a major determinant of the metabolic cost of human walking," *Journal of Experimental Biology*, vol. 205, no. 23, pp. 3717–3727, 2002.

[62] J. S. Gottschall and R. Kram, "Energy cost and muscular activity required for leg swing during walking," *Journal of Applied Physiology*, vol. 99, no. 1, pp. 23–30, 2005.

[63] B. H. Goodpaster, S. W. Park, T. B. Harris, S. B. Kritchevsky, M. Nevitt, A. V. Schwartz, E. M. Simonsick, F. A. Tylavsky, M. Visser, and A. B. Newman, "The loss of skeletal muscle strength, mass, and quality in older adults: the health, aging and body composition study," *The Journals of Gerontology Series A: Biological Sciences and Medical Sciences*, vol. 61, no. 10, pp. 1059–1064, 2006.

[64] O. S. Mian, J. M. Thom, L. P. Ardigo, M. V. Narici, and A. E. Minetti, "Metabolic cost, mechanical work, and efficiency during walking in young and older men," *Acta physiologica*, vol. 186, no. 2, pp. 127–139, 2006.

[65] D. S. Peterson and P. E. Martin, "Effects of age and walking speed on coactivation and cost of walking in healthy adults," *Gait & posture*, vol. 31, no. 3, pp. 355–359, 2010.

[66] R. C. Browning, J. R. Modica, R. Kram, and A. Goswami, "The effects of adding mass to the legs on the energetics and biomechanics of walking," *Medicine & Science in Sports & Exercise*, vol. 39, no. 3, pp. 515–525, 2007.

[67] F. A. Panizzolo, I. Galiana, A. T. Asbeck, C. Siviy, K. Schmidt, K. G. Holt, and C. J. Walsh, "A biologically-inspired multi-joint soft exosuit that can

reduce the energy cost of loaded walking," *Journal of neuroengineering and rehabilitation*, vol. 13, no. 1, pp. 1–14, 2016.

[68] E. Tricomi, M. Mossini, F. Missiroli, N. Lotti, X. Zhang, M. Xiloyannis, L. Roveda, and L. Masia, "Environment-based assistance modulation for a hip exosuit via computer vision," *IEEE Robotics and Automation Letters*, vol. 8, no. 5, pp. 2550–2557, 2023.

[69] Y. Ding, M. Kim, S. Kuindersma, and C. J. Walsh, "Human-in-the-loop optimization of hip assistance with a soft exosuit during walking," *Science robotics*, vol. 3, no. 15, p. eaar5438, 2018.

[70] N. Lotti, M. Xiloyannis, G. Durandau, E. Galofaro, V. Sanguineti, L. Masia, and M. Sartori, "Adaptive model-based myoelectric control for a soft wearable arm exosuit: A new generation of wearable robot control," *IEEE Robotics & Automation Magazine*, vol. 27, no. 1, pp. 43–53, 2020.

[71] M. Sierotowicz, N. Lotti, L. Nell, F. Missiroli, R. Alicea, X. Zhang, M. Xiloyannis, R. Rupp, E. Papp, J. Krzywinski *et al.*, "Emg-driven machine learning control of a soft glove for grasping assistance and rehabilitation," *IEEE Robotics and Automation Letters*, vol. 7, no. 2, pp. 1566–1573, 2022.

[72] N. Li, Y. Yang, G. Li, T. Yang, Y. Wang, W. Chen, P. Yu, X. Xue, C. Zhang, W. Wang *et al.*, "Multi-sensor fusion-based mirror adaptive assist-as-needed control strategy of a soft exoskeleton for upper limb rehabilitation," *IEEE Transactions on Automation Science and Engineering*, vol. 21, no. 1, pp. 475–487, 2022.

[73] R. Baud, A. R. Manzoori, A. Ijspeert, and M. Bouri, "Review of control strategies for lower-limb exoskeletons to assist gait," *Journal of NeuroEngineering and Rehabilitation*, vol. 18, pp. 1–34, 2021.

[74] D. Quintero, D. J. Villarreal, D. J. Lambert, S. Kapp, and R. D. Gregg, "Continuous-phase control of a powered knee–ankle prosthesis: Amputee experiments across speeds and inclines," *IEEE Transactions on Robotics*, vol. 34, no. 3, pp. 686–701, 2018.

[75] S. Mohammed, A. Same, L. Oukhellou, K. Kong, W. Huo, and Y. Amirat, "Recognition of gait cycle phases using wearable sensors," *Robotics and Autonomous Systems*, vol. 75, pp. 50–59, 2016.

[76] T. Igami, Y. Akiyama, S. Okamoto, and Y. Yamada, "Development of adaptive gait assist algorithm using ground reaction force," in *Workshop on Robot Control (WROCO 2019), Daejeon, Korea*, 2019.

[77] E. M. McCain, T. J. Dick, T. N. Giest, R. W. Nuckols, M. D. Lewek, K. R. Saul, and G. S. Sawicki, "Mechanics and energetics of post-stroke walking aided by a powered ankle exoskeleton with speed-adaptive myoelectric control," *Journal of neuroengineering and rehabilitation*, vol. 16, no. 1, pp. 1–12, 2019.

[78] L. Grazi, S. Crea, A. Parri, R. Molino Lova, S. Micera, and N. Vitiello, "Gastrocnemius myoelectric control of a robotic hip exoskeleton can reduce the user's lower-limb muscle activities at push off," *Frontiers in neuroscience*, vol. 12, p. 71, 2018.

[79] T. Yan, A. Parri, V. R. Garate, M. Cempini, R. Ronsse, and N. Vitiello, "An oscillator-based smooth real-time estimate of gait phase for wearable robotics," *Autonomous Robots*, vol. 41, no. 3, pp. 759–774, 2017.

[80] L. Righetti, J. Buchli, and A. J. Ijspeert, "Dynamic hebbian learning in adaptive frequency oscillators," *Physica D: Nonlinear Phenomena*, vol. 216, no. 2, pp. 269–281, 2006.

[81] ——, "Adaptive frequency oscillators and applications," *The Open Cybernetics & Systemics Journal*, vol. 3, no. 1, 2009.

[82] H. J. Hermens, B. Freriks, C. Disselhorst-Klug, and G. Rau, "Development of recommendations for semg sensors and sensor placement procedures," *Journal of electromyography and Kinesiology*, vol. 10, no. 5, pp. 361–374, 2000.

[83] C. L. Dembia, A. Silder, T. K. Uchida, J. L. Hicks, and S. L. Delp, "Simulating ideal assistive devices to reduce the metabolic cost of walking with heavy loads," *PloS one*, vol. 12, no. 7, p. e0180320, 2017.

[84] F. A. Panizzolo, E. Annese, A. Paoli, and G. Marcolin, "A single assistive profile applied by a passive hip flexion device can reduce the energy cost of walking in older adults," *Applied Sciences*, vol. 11, no. 6, p. 2851, 2021.

[85] I. Kang, D. D. Molinaro, S. Duggal, Y. Chen, P. Kunapuli, and A. J. Young, "Real-time gait phase estimation for robotic hip exoskeleton control during

multimodal locomotion," *IEEE Robotics and Automation Letters*, vol. 6, no. 2, pp. 3491–3497, 2021.

[86] F. Weigand, J. Zeiss, M. Grimmer, and U. Konigorski, "A novel approach for gait phase estimation for different locomotion modes using kinematic shank information," *IFAC-PapersOnLine*, vol. 53, no. 2, pp. 8697–8703, 2020.

[87] S. Pasinetti, A. Fornaser, M. Lancini, M. De Cecco, and G. Sansoni, "Assisted gait phase estimation through an embedded depth camera using modified random forest algorithm classification," *IEEE Sensors Journal*, vol. 20, no. 6, pp. 3343–3355, 2019.

[88] O. Sagi and L. Rokach, "Ensemble learning: A survey," *Wiley Interdisciplinary Reviews: Data Mining and Knowledge Discovery*, vol. 8, no. 4, p. e1249, 2018.

[89] Z.-H. Zhou, "Ensemble learning," in *Machine learning*. Springer, 2021, pp. 181–210.

[90] M. Su, Z. Zhang, Y. Zhu, and D. Zha, "Data-driven natural gas spot price forecasting with least squares regression boosting algorithm," *Energies*, vol. 12, no. 6, p. 1094, 2019.

[91] S. Parchekhari, A. Nakhaee, and A. Kadkhodaie, "A new model for permeability estimation in carbonate reservoirs by using nmr t2 distribution and lsboost ensemble technique," *Journal of Petroleum Science and Technology*, vol. 10, no. 4, pp. 20–29, 2020.

[92] A. Thongsook, T. Nunthawarasilp, P. Kraypet, J. Lim, and N. Ruangpayoongsak, "C4.5 decision tree against neural network on gait phase recognition for lower limp exoskeleton," in *2019 First International Symposium on Instrumentation, Control, Artificial Intelligence, and Robotics (ICA-SYMP)*, 2019, pp. 69–72.

[93] D. Barber, *Bayesian reasoning and machine learning*. Cambridge University Press, 2012.

[94] I. Kang, P. Kunapuli, and A. J. Young, "Real-time neural network-based gait phase estimation using a robotic hip exoskeleton," *IEEE Transactions on Medical Robotics and Bionics*, vol. 2, no. 1, pp. 28–37, 2019.

[95] A. G. González, J. Rodrıguez, X. Sagartzazu, A. Schumacher, and I. Isasa, "Multiple coherence method in time domain for the analysis of the transmission paths of noise and vibrations with non stationary signals," *Proceedings of ISMA 2010*, 2010.

[96] F. Peronnet, D. Massicotte *et al.*, "Table of nonprotein respiratory quotient: an update," *Can J Sport Sci*, vol. 16, no. 1, pp. 23–29, 1991.

[97] F. A. Panizzolo, G. M. Freisinger, N. Karavas, A. M. Eckert-Erdheim, C. Siviy, A. Long, R. A. Zifchock, M. E. LaFiandra, and C. J. Walsh, "Metabolic cost adaptations during training with a soft exosuit assisting the hip joint," *Scientific reports*, vol. 9, no. 1, pp. 1–10, 2019.

[98] Y. Ding, I. Galiana, A. T. Asbeck, S. M. M. De Rossi, J. Bae, T. R. T. Santos, V. L. De Araujo, S. Lee, K. G. Holt, and C. Walsh, "Biomechanical and physiological evaluation of multi-joint assistance with soft exosuits," *IEEE Transactions on Neural Systems and Rehabilitation Engineering*, vol. 25, no. 2, pp. 119–130, 2016.

[99] L. Chen, C. Chen, Z. Wang, X. Ye, Y. Liu, and X. Wu, "A novel lightweight wearable soft exosuit for reducing the metabolic rate and muscle fatigue," *Biosensors*, vol. 11, no. 7, p. 215, 2021.

[100] G. Courtine and M. Schieppati, "Human walking along a curved path. i. body trajectory, segment orientation and the effect of vision," *European Journal of Neuroscience*, vol. 18, no. 1, pp. 177–190, 2003.

[101] Y. Koren, R. Mairon, I. Sofer, Y. Parmet, O. Ben-Shahar, and S. Bar-Haim, "Vision, cognition, and walking stability in young adults," *Scientific reports*, vol. 12, no. 1, pp. 1–10, 2022.

[102] Y. Qian, Y. Wang, C. Chen, J. Xiong, Y. Leng, H. Yu, and C. Fu, "Predictive locomotion mode recognition and accurate gait phase estimation for hip exoskeleton on various terrains," *IEEE Robotics and Automation Letters*, vol. 7, no. 3, pp. 6439–6446, 2022.

[103] A. J. Young and D. P. Ferris, "State of the art and future directions for lower limb robotic exoskeletons," *IEEE Transactions on Neural Systems and Rehabilitation Engineering*, vol. 25, no. 2, pp. 171–182, 2016.

[104] B. T. Quinlivan, S. Lee, P. Malcolm, D. M. Rossi, M. Grimmer, C. Siviy, N. Karavas, D. Wagner, A. Asbeck, I. Galiana *et al.*, "Assistance magnitude versus metabolic cost reductions for a tethered multiarticular soft exosuit," *Science robotics*, vol. 2, no. 2, p. eaah4416, 2017.

[105] K. Scherpereel, D. Molinaro, O. Inan, M. Shepherd, and A. Young, "A human lower-limb biomechanics and wearable sensors dataset during cyclic and non-cyclic activities," *Scientific Data*, vol. 10, no. 1, p. 924, 2023.

[106] L. Gionfrida, D. Kim, D. Scaramuzza, D. Farina, and R. D. Howe, "Wearable robots for the real world need vision," *Science Robotics*, vol. 9, no. 90, p. eadj8812, 2024.

[107] Z. Fu, A. Kumar, A. Agarwal, H. Qi, J. Malik, and D. Pathak, "Coupling vision and proprioception for navigation of legged robots," in *Proceedings of the IEEE/CVF Conference on Computer Vision and Pattern Recognition*, 2022, pp. 17 273–17 283.

[108] D. Kim, D. Carballo, J. Di Carlo, B. Katz, G. Bledt, B. Lim, and S. Kim, "Vision aided dynamic exploration of unstructured terrain with a small-scale quadruped robot," in *2020 IEEE International Conference on Robotics and Automation (ICRA)*. IEEE, 2020, pp. 2464–2470.

[109] B. Laschowski, W. McNally, A. Wong, and J. McPhee, "Computer vision and deep learning for environment-adaptive control of robotic lower-limb exoskeletons," in *2021 43rd Annual International Conference of the IEEE Engineering in Medicine & Biology Society (EMBC)*. IEEE, 2021, pp. 4631–4635.

[110] ——, "Environment classification for robotic leg prostheses and exoskeletons using deep convolutional neural networks," *Frontiers in Neurorobotics*, vol. 15, p. 730965, 2022.

[111] N. E. Krausz, T. Lenzi, and L. J. Hargrove, "Depth sensing for improved control of lower limb prostheses," *IEEE Transactions on Biomedical Engineering*, vol. 62, no. 11, pp. 2576–2587, 2015.

[112] A. Kadambi, C. de Melo, C.-J. Hsieh, M. Srivastava, and S. Soatto, "Incorporating physics into data-driven computer vision," *Nature Machine Intelligence*, pp. 1–9, 2023.

[113] J. A. Hesch, G. L. Mariottini, and S. I. Roumeliotis, "Descending-stair detection, approach, and traversal with an autonomous tracked vehicle," in *2010 IEEE/RSJ International Conference on Intelligent Robots and Systems*. IEEE, 2010, pp. 5525–5531.

[114] A. Albert, M. Suppa, and W. Gerth, "Detection of stair dimensions for the path planning of a bipedal robot," in *2001 IEEE/ASME International Conference on Advanced Intelligent Mechatronics. Proceedings (Cat. No. 01TH8556)*, vol. 2. IEEE, 2001, pp. 1291–1296.

[115] B. Laschowski, W. McNally, A. Wong, and J. McPhee, "Exonet database: Wearable camera images of human locomotion environments," *Frontiers in Robotics and AI*, vol. 7, p. 562061, 2020.

[116] A. Pérez-Yus, G. López-Nicolás, and J. J. Guerrero, "Detection and modelling of staircases using a wearable depth sensor," in *Computer Vision-ECCV 2014 Workshops: Zurich, Switzerland, September 6-7 and 12, 2014, Proceedings, Part III 13*. Springer, 2015, pp. 449–463.

[117] A. Perez-Yus, D. Gutierrez-Gomez, G. Lopez-Nicolas, and J. J. Guerrero, "Stairs detection with odometry-aided traversal from a wearable RGB-D camera," *Computer Vision and Image Understanding*, vol. 154, pp. 192–205, 2017.

[118] X.-F. Han, J. S. Jin, M.-J. Wang, W. Jiang, L. Gao, and L. Xiao, "A review of algorithms for filtering the 3d point cloud," *Signal Processing: Image Communication*, vol. 57, pp. 103–112, 2017.

[119] M. A. Fischler and R. C. Bolles, "Random sample consensus: a paradigm for model fitting with applications to image analysis and automated cartography," *Communications of the ACM*, vol. 24, no. 6, pp. 381–395, 1981.

[120] R. Adams and L. Bischof, "Seeded region growing," *IEEE Transactions on pattern analysis and machine intelligence*, vol. 16, no. 6, pp. 641–647, 1994.

[121] U. B. Code, "International building code," *International Code Council, USA*, 1997.

[122] K. He and J. Sun, "Computing nearest-neighbor fields via propagation-assisted kd-trees," in *2012 IEEE Conference on Computer Vision and Pattern Recognition*. IEEE, 2012, pp. 111–118.

[123] R. Riener, M. Rabuffetti, and C. Frigo, "Stair ascent and descent at different inclinations," *Gait & posture*, vol. 15, no. 1, pp. 32–44, 2002.

[124] E. Tricomi, N. Lotti, F. Missiroli, X. Zhang, M. Xiloyannis, T. Muller, S. Crea, E. Papp, J. Krzywinski, N. Vitiello *et al.*, "Underactuated soft hip exosuit based on adaptive oscillators to assist human locomotion," *IEEE Robotics and Automation Letters*, 2021.

[125] X. Zhang, E. Tricomi, F. Missiroli, N. Lotti, C. Bokranz, D. Nicklas, and L. Masia, "Enhancing gait assistance control robustness of a hip exosuit by means of machine learning," *IEEE Robotics and Automation Letters*, vol. 7, no. 3, pp. 7566–7573, 2022.

[126] S. Balasubramanian, A. Melendez-Calderon, A. Roby-Brami, and E. Burdet, "On the analysis of movement smoothness," *Journal of neuroengineering and rehabilitation*, vol. 12, no. 1, pp. 1–11, 2015.

[127] S. Kipp, W. C. Byrnes, and R. Kram, "Calculating metabolic energy expenditure across a wide range of exercise intensities: the equation matters," *Applied Physiology, Nutrition, and Metabolism*, vol. 43, no. 6, pp. 639–642, 2018.

[128] J. C. Selinger and J. M. Donelan, "Estimating instantaneous energetic cost during non-steady-state gait," *Journal of Applied Physiology*, vol. 117, no. 11, pp. 1406–1415, 2014.

[129] F. L. Haufe, A. M. Kober, P. Wolf, R. Riener, and M. Xiloyannis, "Learning to walk with a wearable robot in 880 simple steps: a pilot study on motor adaptation," *Journal of neuroengineering and rehabilitation*, vol. 18, pp. 1–14, 2021.

[130] K. Zhang, C. Xiong, W. Zhang, H. Liu, D. Lai, Y. Rong, and C. Fu, "Environmental features recognition for lower limb prostheses toward predictive walking," *IEEE transactions on neural systems and rehabilitation engineering*, vol. 27, no. 3, pp. 465–476, 2019.

[131] K. Zhang, J. Luo, W. Xiao, W. Zhang, H. Liu, J. Zhu, Z. Lu, Y. Rong, C. W. de Silva, and C. Fu, "A subvision system for enhancing the environmental adaptability of the powered transfemoral prosthesis," *IEEE transactions on cybernetics*, vol. 51, no. 6, pp. 3285–3297, 2020.

[132] A. G. Kurbis, B. Laschowski, and A. Mihailidis, "Stair recognition for robotic exoskeleton control using computer vision and deep learning," in *2022 International Conference on Rehabilitation Robotics (ICORR)*. IEEE, 2022, pp. 1–6.

[133] A. Leroux, J. Fung, and H. Barbeau, "Postural adaptation to walking on inclined surfaces: I. normal strategies," *Gait & posture*, vol. 15, no. 1, pp. 64–74, 2002.

[134] J. Joseph and R. Watson, "Telemetering electromyography of muscles used in walking up and down stairs," *The Journal of bone and joint surgery. British volume*, vol. 49, no. 4, pp. 774–780, 1967.

[135] D. P. Ferris, "The exoskeletons are here," *Journal of neuroEngineering and rehabilitation*, vol. 6, no. 1, pp. 1–3, 2009.

[136] H. Herr, "Exoskeletons and orthoses: classification, design challenges and future directions," *Journal of neuroengineering and rehabilitation*, vol. 6, pp. 1–9, 2009.

[137] R. L. Medrano, G. C. Thomas, C. G. Keais, E. J. Rouse, and R. D. Gregg, "Real-time gait phase and task estimation for controlling a powered ankle exoskeleton on extremely uneven terrain," *IEEE Transactions on Robotics*, 2023.

[138] D. Torricelli, C. Rodriguez-Guerrero, J. F. Veneman, S. Crea, K. Briem, B. Lenggenhager, and P. Beckerle, "Benchmarking wearable robots: challenges and recommendations from functional, user experience, and methodological perspectives," *Frontiers in Robotics and AI*, p. 168, 2020.

[139] E. R. Westervelt, J. W. Grizzle, C. Chevallereau, J. H. Choi, and B. Morris, "Feedback control of dynamic bipedal robot locomotion," 2018.

[140] D. J. Villarreal, H. A. Poonawala, and R. D. Gregg, "A robust parameterization of human gait patterns across phase-shifting perturbations," *IEEE Transactions on Neural Systems and Rehabilitation Engineering*, vol. 25, no. 3, pp. 265–278, 2016.

[141] D. Quintero, D. J. Lambert, D. J. Villarreal, and R. D. Gregg, "Real-time continuous gait phase and speed estimation from a single sensor," in *2017*

IEEE Conference on Control Technology and Applications (CCTA). IEEE, 2017, pp. 847–852.

[142] G. Welch, G. Bishop *et al.*, "An introduction to the kalman filter," 1995.

[143] M. Kuster, S. Sakurai, and G. Wood, "Kinematic and kinetic comparison of downhill and level walking," *Clinical biomechanics*, vol. 10, no. 2, pp. 79–84, 1995.

[144] H. J. Ralston, "Energy-speed relation and optimal speed during level walking," *Internationale Zeitschrift für Angewandte Physiologie Einschliesslich Arbeitsphysiologie*, vol. 17, no. 4, pp. 277–283, 1958.

[145] A. Tapal, E. Oren, R. Dar, and B. Eitam, "The sense of agency scale: A measure of consciously perceived control over one's mind, body, and the immediate environment," *Frontiers in psychology*, vol. 8, p. 1552, 2017.

[146] F. L. Haufe, E. G. Duroyon, P. Wolf, R. Riener, and M. Xiloyannis, "Outside testing of wearable robots for gait assistance shows a higher metabolic benefit than testing on treadmills," *Scientific reports*, vol. 11, no. 1, p. 14833, 2021.

[147] J. Kim, B. T. Quinlivan, L.-A. Deprey, D. Arumukhom Revi, A. Eckert-Erdheim, P. Murphy, D. Orzel, and C. J. Walsh, "Reducing the energy cost of walking with low assistance levels through optimized hip flexion assistance from a soft exosuit," *Scientific reports*, vol. 12, no. 1, p. 11004, 2022.

[148] P. W. Franks, G. M. Bryan, R. M. Martin, R. Reyes, A. C. Lakmazaheri, and S. H. Collins, "Comparing optimized exoskeleton assistance of the hip, knee, and ankle in single and multi-joint configurations," *Wearable Technologies*, vol. 2, p. e16, 2021.

[149] V. Chambon, N. Sidarus, and P. Haggard, "From action intentions to action effects: how does the sense of agency come about?" *Frontiers in human neuroscience*, vol. 8, p. 320, 2014.

[150] R. L. Medrano, G. C. Thomas, and E. J. Rouse, "Can humans perceive the metabolic benefit provided by augmentative exoskeletons?" *Journal of NeuroEngineering and Rehabilitation*, vol. 19, no. 1, p. 26, 2022.

[151] G. S. Sawicki and D. P. Ferris, "Mechanics and energetics of level walking with powered ankle exoskeletons," *Journal of Experimental Biology*, vol. 211, no. 9, pp. 1402–1413, 2008.

[152] P. Sorrentino and N. Thompson, *Youth*, 2016.

[153] T. Hortobágyi, C. Mizelle, S. Beam, and P. DeVita, "Old adults perform activities of daily living near their maximal capabilities," *The Journals of Gerontology Series A: Biological Sciences and Medical Sciences*, vol. 58, no. 5, pp. M453–M460, 2003.

[154] G. Ercolini, E. Trigili, A. Baldoni, S. Crea, and N. Vitiello, "A novel generation of ergonomic upper-limb wearable robots: Design challenges and solutions," *Robotica*, vol. 37, no. 12, pp. 2056–2072, 2019.

[155] G. S. Sawicki, O. N. Beck, I. Kang, and A. J. Young, "The exoskeleton expansion: improving walking and running economy," *Journal of neuroengineering and rehabilitation*, vol. 17, no. 1, pp. 1–9, 2020.

[156] J. Löloff, M. Theisen, A. Mertens, and J. Funke, "Human-machine symbiosis: ambivalent intuitions regarding gain and loss of personal control explain acceptance of smart mobility aids," *Behaviour & Information Technology*, pp. 1–9, 2023.

[157] D. Park and K.-J. Cho, "Development and evaluation of a soft wearable weight support device for reducing muscle fatigue on shoulder," *PloS one*, vol. 12, no. 3, p. e0173730, 2017.

[158] X. Zhang, E. Tricomi, F. Missiroli, N. Lotti, and L. Masia, "Real-time assistive control via imu locomotion mode detection in a soft exosuit: An effective approach to enhance walking metabolic efficiency," *IEEE/ASME Transactions on Mechatronics*, 2023.

[159] C. Basla, I. Hungerbühler, J. T. Meyer, P. Wolf, R. Riener, and M. Xiloyannis, "Usability of an exosuit in domestic and community environments," *Journal of NeuroEngineering and Rehabilitation*, vol. 19, no. 1, p. 131, 2022.

[160] U. Dapp, C. E. Minder, S. Golgert, B. Klugmann, L. Neumann, and W. von Renteln-Kruse, "The inter-relationship between depressed mood, functional decline and disability over a 10-year observational period within the longitudinal urban cohort ageing study (lucas)," *J Epidemiol Community Health*, vol. 75, no. 5, pp. 450–457, 2021.